‘*In Silico* Design & Chemical Synthesis of Diazenyl Photoswitches for the Regulation of *Trypanosoma Cruzi* *trans*-Sialidase Activity’

Sebastiaan van Elst, Erianna I. Alvarado-Melendez, Tom Wennekes - Department of Chemical Biology and Drug Discovery – Debye Institute for Nanomaterial Science, Utrecht University, 6624138

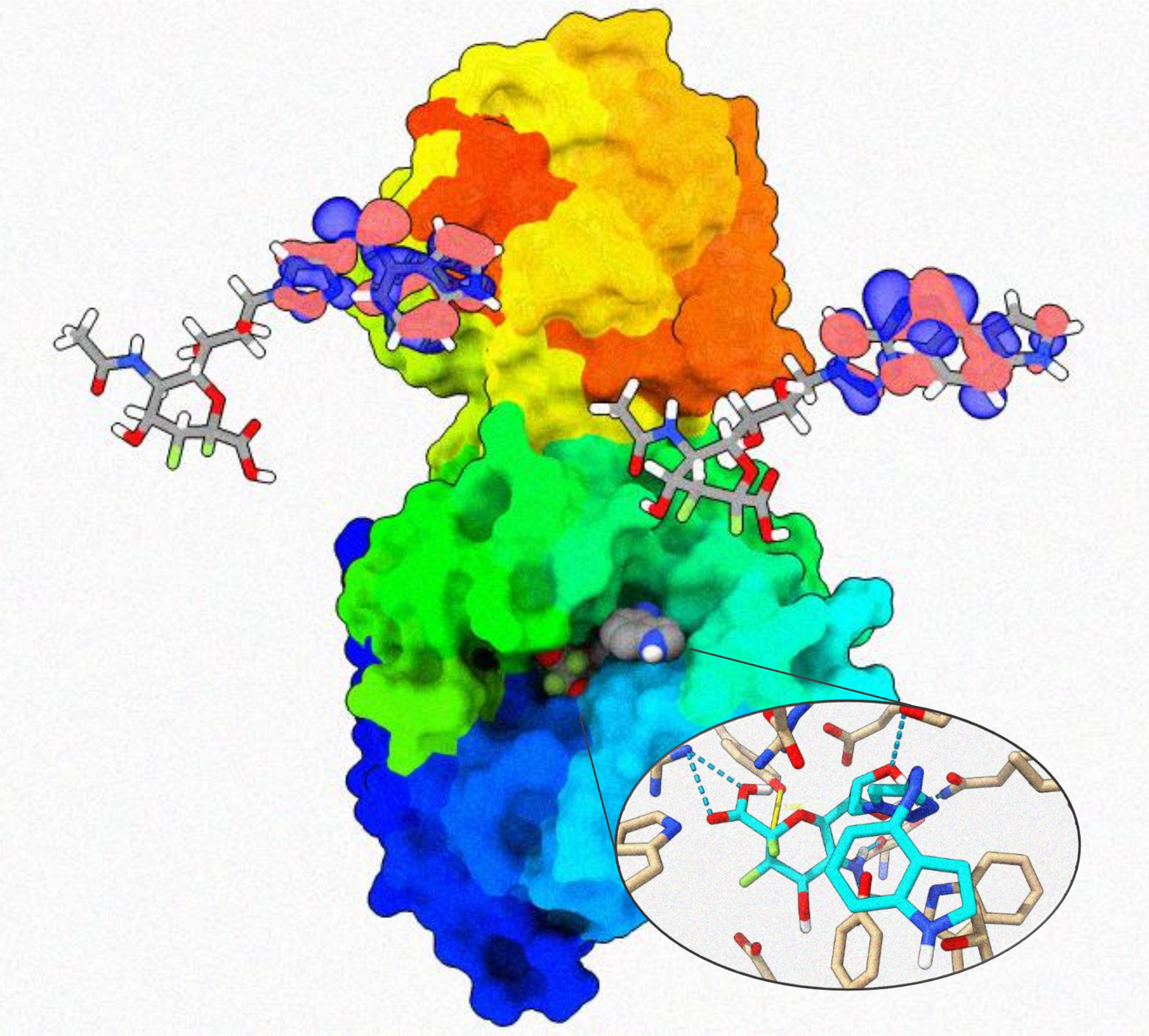

Front cover: *depiction of the Trypanosoma cruzi trans-sialidase with a designed photoswitchable 2,3-difluorosialic acid inhibitor docked in the active site. The HOMO and LUMO of the inhibitor is displayed in front of the enzyme-substrate complex.*

Abstract

In this work, the in silico design of photo regulatory probes for the T. cruzi trans-sialidase and the progress on the synthesis thereof is reported. Photoswitchable inhibitors have become of interest to medicinal chemists due to the bio-orthogonal properties of visible light. Docking studies and (TD-)DFT calculations were performed to predict probe affinities and their photophysical properties. For the synthesis of the candidates, a modular approach was designed in which the glycan derivatives and photoswitches were synthesized independently.

1. Introduction

Over the recent decades, sialidases have gained more attention due to their role as virulence factors in the pathogenesis for various diseases.[5] In the early 1990's it was observed for *Trypanosoma cruzi,* that the sialic acid transferase pathway predominated the hydrolase activity, but questions remained about the origins of this phenomenon.[1] It was not until the 2000's that the team of Amaya et al.[2][3] isolated the *Trypanosoma cruzi* trans-sialidase intermediates and investigated the mechanistic pathways involved. It was concluded that the Tyr342 residue acts as a catalytic nucleophile in a simple ping-pong double displacement mechanism.[2] The isolated intermediate, characterized by x-ray crystallography, is depicted in fig. 1(a-b). The enzyme's active site warps the leaving group at the anomeric carbon in a pseudo-axial position, easing the desired protonation by the Asp59 residue. The Glu230 residue is in close proximity with the Tyr342 residue, and can act as a base catalyst. It is believed that it deprotonates the phenol moiety on tyrosine and regenerates through protonation of the phenol or another suitable nucleophile. The activated Tyr342 residue will then attack the anomeric carbon atom, forming the covalent intermediate and expelling the leaving group, see fig. 2. The rate of hydrolysis, and therefore the lifetime of the covalent intermediate, is dependent on the electronic properties of the substrate and the interaction strength with local residues. It was therefore proposed that lifetimes could be increased by fluorinating C3 of sialic acid, due to the inductive effects destabilizing the oxocarbenium transition state.[2][3][6] Trapping of the intermediate can be achieved by introducing a suitable

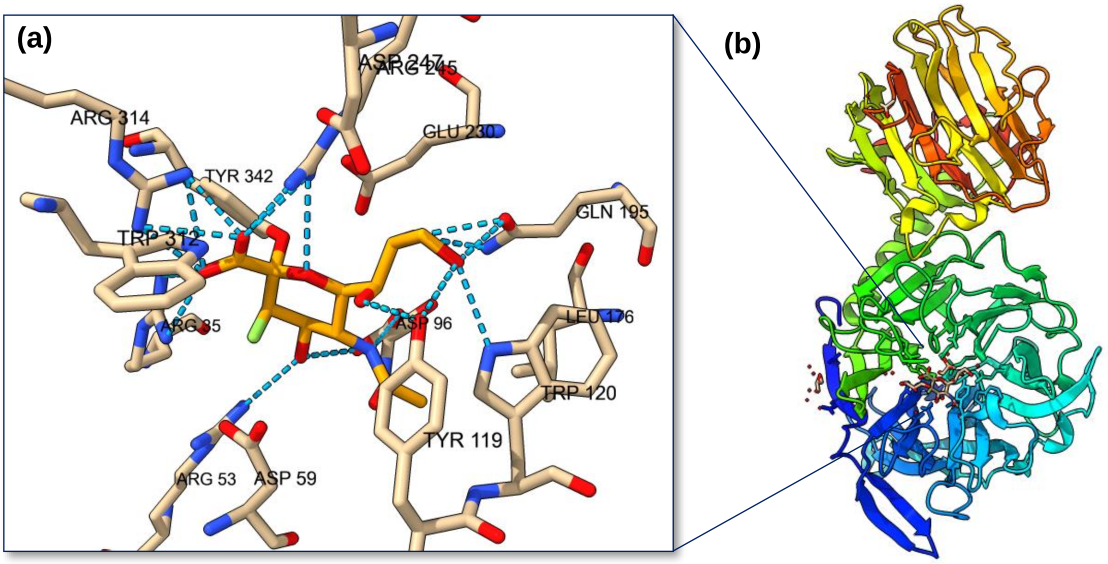

Figure 1: ***(a)*** *Crystallographic structure of the covalent sialic acid intermediate with the Tyr342 residue[3] [PDB: 2AH2] (Visualization performed in ChimeraX[4])* ***(b)*** *Secondary structure of Trypanosoma cruzi Trans-Sialidase*

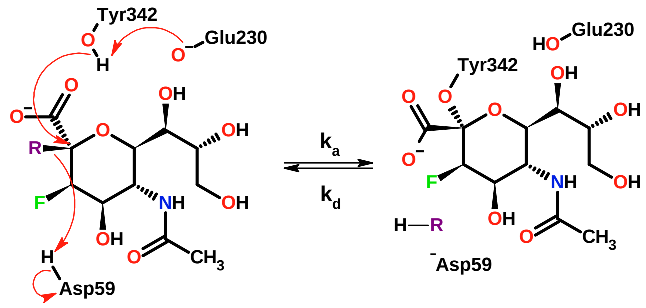

Figure 2: "Ping-pong-like mechanism of inhibition proposed by Amaya et al.[2][6]

leaving group at the anomeric carbon.[6] Since then, multiple iterations of the fluorinated sialic acid probes have been designed with inhibition constants ranging up to the subnanomolar range.[7] One probe of particular interest; 9-azido-2,3-difluorosialic acid, is shown in fig 3. The high affinity makes it an excellent inhibitor for bacterial- and recombinant human sialidases,[7] and can also be used for fluorescent imaging studies due to its orthogonal reactivity.[8] The azido moiety allows for late stage functionalization [fig. 3(a)] via click chemistry, by reduction of the azide followed by amine coupling and much more. Because of these properties, the team at the CBDD research group was interested in using the 9-azido moiety for modification with diazenyl based photo-switches.

1.1 Photoinduced Isomerization

Molecular machines have gained massive interest in recent years, due to their applications in material science, pharmaceutics and catalysis.[11][12] Azo-aryl derivatives are among the oldest known conjugates that possess the ability to isomerize along the sp^2 N=N double bond under the influence of light.[13] The result is the occurrence of a thermally stable trans (E) isomer and a meta-stable cis (Z) isomer, see figure 4.[14]

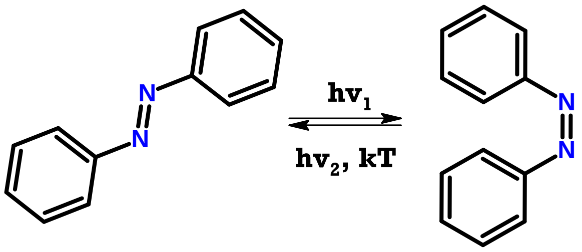

Figure 4: Photoinduced isomerization of azo-benzene around the sp^2 *N=N double bond.*

For azobenzene, E → Z isomerization can be induced by irradiation with a wavelength of 320 nm, while reversal can be achieved at 450 nm or by thermal relaxation.[11] Remarkable features of azobenzene and its derivatives are the high quantum yields, great photo-stability and (tunable) half-life times. The underlying mechanism of isomerization is still not entirely agreed upon in the scientific community, owing its thanks to the timescales at which interconversions occur.[15] Advances in *femtosecond time-resolved photo-electron spectroscopy*, allowed for the elucidation of relaxation pathways and is described in (*Schultz et al., 2002*).[15] Another powerful tool, which will be used extensively in this paper, is density functional theory (DFT).

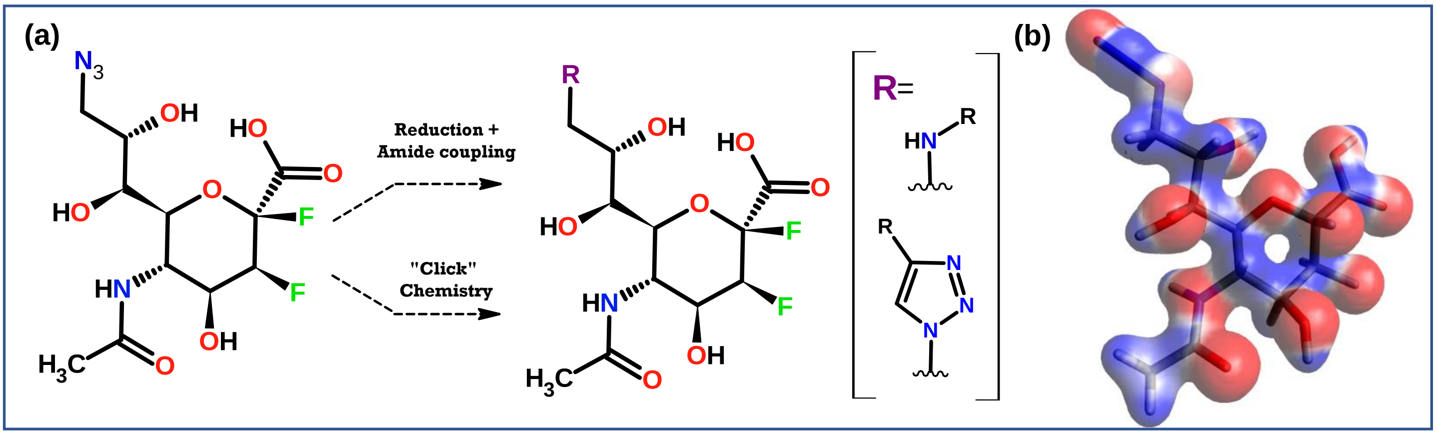

Figure 3: ***(a)*** *"9-azido-2,3-difluorosialic acid probe*[7] *and late stage functionalization pathway via 'click'-chemistry and amine coupling.* ***(b)*** *Electron density Isosurface of 9-azido-2,3-difluorosialic acid colored by ESP calculated at the B3LYP-level in ORCA.*[9][10]

1.2 Electronic Transitions of Photoisomerization

To understand the mechanism of photo-induced isomerization (PII), let's first examine the fundamental mechanisms in azobenzene. As mentioned before, many questions remain about the exact mechanism of PII and a simplified attempt will be made here. DFT and molecular orbital (MO) theory will be of central importance and will lay the foundation for the discussion. Depicted in fig. 5 are the MO's and corresponding relative orbital energies calculated for E/Z azobenzene using the BP86 def2-SVP def2/J basis sets in ORCA.[9] When performing the geometry optimization, one might find a multitude of conformers that are energetically accessible and this is where the first discrepancies arise. Empirical and theoretical data on excitation energies indicates significant deviations among researchers.[15][16][17] A justification for the toy-models used will be provided in the discussion. Assuming we have a viable model, see fig. 5, three distinct electronic transitions can be identified for each stereoisomer. Starting at the E-isomer, which in this model possesses C_2-symmetry, the S_1 excitation level corresponds to the $n \rightarrow \pi^*$ transition. The transition is symmetry forbidden and possesses weak oscillator strengths (A → B).[18] According to this geometry two nearly degenerate S_2 excitations are found next, corresponding to the $\pi \rightarrow \pi^*$ transition which is symmetry allowed and responsible for the E→Z PII.[11-18] After absorption of the photon, an exciton-hole pair is formed, which via rotation and/or inversion relaxes back to the cis isomer, where it is metastable as mentioned before.[17] In the case of Z-azobenzene,

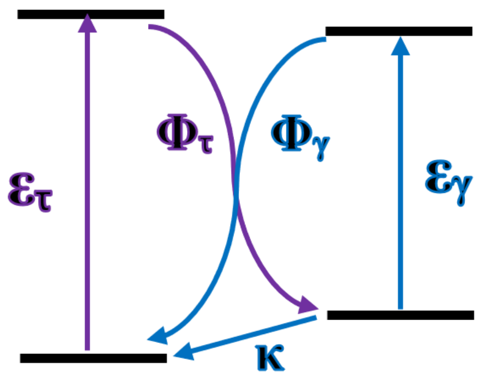

Figure 6: *Inspired from (Yager et al., 2006).[14] State model with parameters ε (the extinction coefficient), Φ (the quantum yield) and κ (rate of thermal relaxation).*

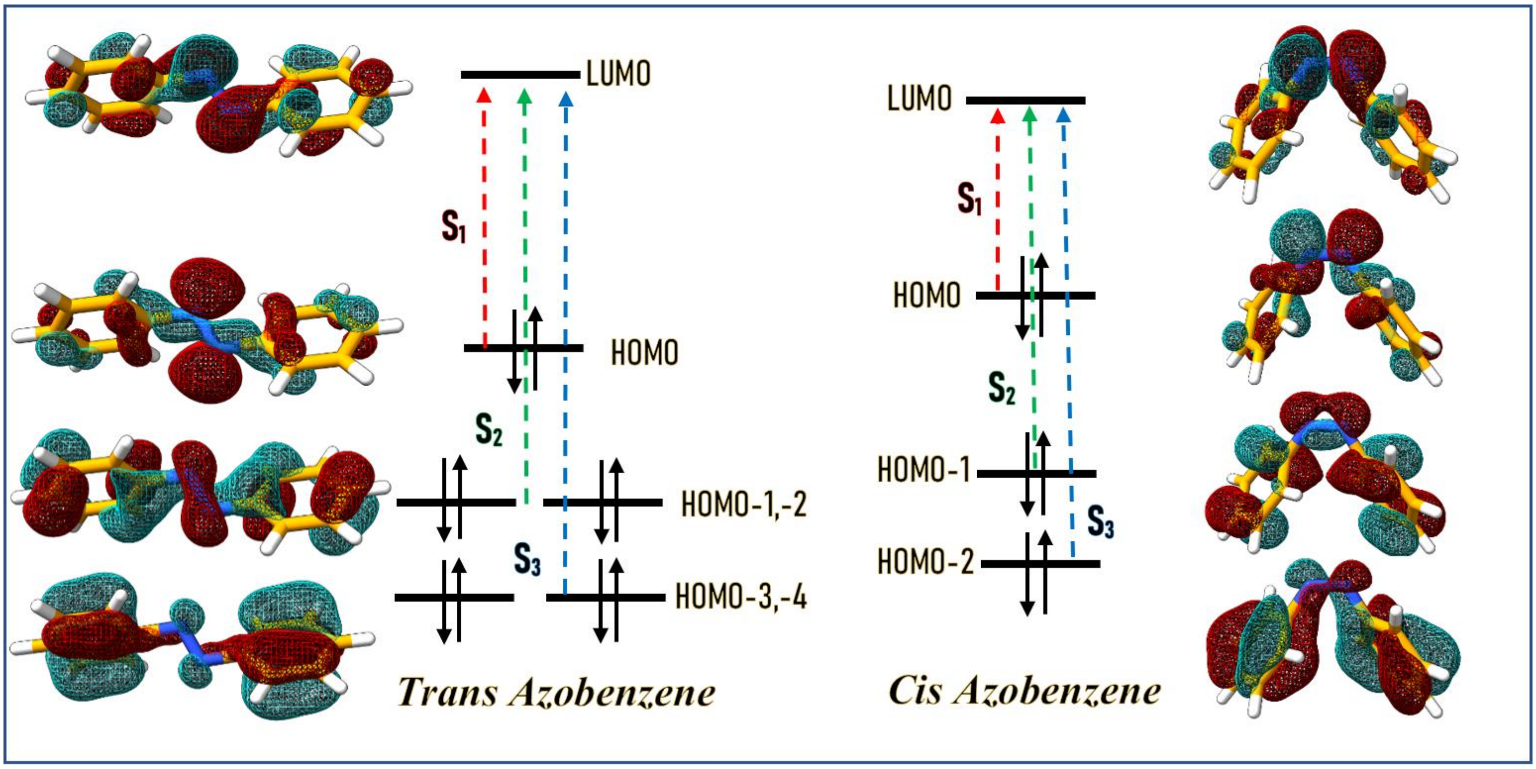

Figure 5: *Molecular Orbital Isosurface and relative orbital level energies calculated at the (TDDFT) BP86-level in ORCA and visualized in ChimeraX.[9][10] On the left and right are the energy levels depicted for the E and Z-azobenzene respectively. The principal electronic transitions are shown along the colored arrows and are denoted S1 (red), S2 (green) and S3 (blue).*

the situation is moderately different; the HOMO is now that of a π* orbital. The S_1 excitation therefore corresponds to that of a π* → π* transition, which in principle is quasi allowed but very poorly described in literature. The fact that the HOMO in the ground state configuration of the Z-conformer is that of a π* orbital could contribute to the tendency for thermal relaxation to the E-conformation, and might be an interesting topic for future research. The second excitation energy, S_2, corresponds to the familiar π → π* transition. This is symmetry allowed and responsible for the PII process which in this case relaxes back to the stable E-isomer. The decrease in bandgap causes a red-shift, and excitation is generally achieved at longer wavelengths of light than for the Z isomer. This holds true for virtually all photoswitches.[11-19] The exact rotation/inversion mechanism will be outside the scope of this review and more details can be found in the references.[15][19] A simplified state model for the PII process is illustrated in fig. 6.[14] Along the purple and blue lines the process of E→Z and Z→E isomerization is shown respectively. The extinction coefficient (ε), the quantum yield (Φ) and the rate of thermal relaxation (κ) provide key insights into the photo-switching-performance which can all be determined by simple UV/VIS- and nuclear magnetic resonance (NMR) spectroscopy.

1.3 Alteration of Spectral Properties for Azo-chromophores

The spectral behavior, i.e. the UV/VIS-absorption properties, of azo containing chromophores can be altered by changing the local substituents on the aromatic moieties. Electron withdrawing and/or donating groups affect the electronic environment of the photo-switch, thereby in turn changing the band gap for the π → π* transition. Based on its photophysical properties, the azo chromophores are divided into three subcategories, namely the azobenzene type, the amino azobenzene type and the pseudo-stilbene type.[14][20][21] For azo-benzene type photoswitches the π → π* transition is located in the UV/blue-region. The simplest example is depicted in fig. 7(a). Alkyl, aryl, halide, nitro and carboxylic acid derivatives are among the many moieties with which this spectral behavior is obtained. Half-life times of the Z-isomer are in the order of hours to days.[14][22] Amino azobenzene types, are characterized by π → π* transitions in the violet-blue region of the spectrum. The requirement for this type

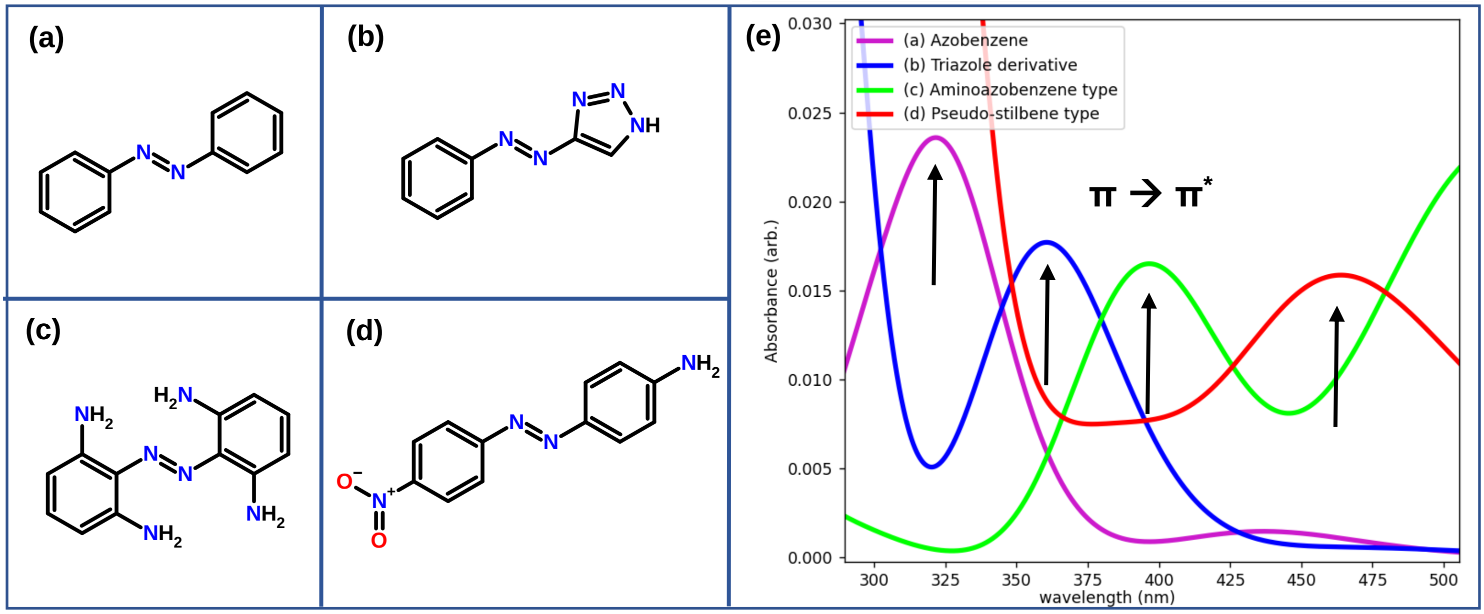

*Figure 7: **(a)** Azobenzene **(b)** Example of heterocyclic triazole derivative **(c)** Example of an aminoazobenzene like photoswitch **(d)** Example of a pseudo-stilbene like photoswitch **(e)** Simulated UV/VIS-spectra from the transition velocity dipole moment of the compounds (a-d). Calculations performed with TD-DFT at the BP86-level.[9][10] The π → π* transition for each derivative is accentuated with the arrows.*

of spectral behavior is the presence of an amino- or hydroxy group in the ortho and/or para position of the azo-moiety. A hypothetical example is depicted in fig. 7(c). Half-life times of the (Z)-isomer are usually on the order of milliseconds to seconds which make them less desirable as photoswitches.[14][21] The final category, the pseudo-stilbene type, is characterized by the broadest absorption bands which are redshifted and can span over the entire range of the VIS spectrum. These spectral properties are attributed to the push and pull inductive effect when an EDG and EWG are placed on the para positions of the azo-moiety.[23] A typical example is depicted in fig. 7(d). One must take great care in changing substitution patterns on pseudo-stilbenes, due to a potential loss of the desired spectral properties and this should be studied case by case. Other modifications that can be used to alter the spectral properties of the photoswitch, besides substitutions on the ring, is the use of heterocyclic aromatic rings. A typical example of this is depicted in fig. 7(b). The effect of changing the ring is usually not profound enough to get its own classification, however the $\pi \rightarrow \pi^*$ transition generally shifts to longer wavelengths. This can be exploited to fine-tune the desired UV/VIS-absorption properties. Half-life times of the Z-isomer are also greatly increased from days to years.[24] Another interesting property of the heterocycles is a decoupling effect of the photoswitch from the substituents on the ring. This results in a quenched contribution of the local substituents on the $\pi \rightarrow \pi^*$ transition, which might be utilized when one desires to maintain the initial excitation wavelengths while altering the structure of a target molecule. A summary of the substitution effects on the spectral properties is provided in fig. 7(e), which is computed with the aid of TD-DFT.[9] The relative absorption intensities have been modified for illustrative purposes. From the azobenzene type to the pseudo-stilbene type, a narrowing of the $\pi \rightarrow \pi^*$ bandgap is observed, resulting in excitation at longer wavelengths and generally broader absorption bands. The effect of exchanging a phenyl ring by a triazole ring is depicted as well, in which a redshift with respect to the parent molecule is observed. These substitution effects are great tools for chemists and material scientist to tweak the bandgaps from the UV to the near-IR to adhere to the intended application.

1.4 Photoswitches in Chemical Biology

Photoswitches have become increasingly more attractive to the field of chemical biology due to their ability to spatially control atoms on the nanometer scale while using non-invasive techniques like light. The previously described E/Z-isomerization mechanism can be seen as an *on*-and-*off* switch in which one of the isomers gains a certain activity while the other yields the initial unperturbed state. Subjects where this has been applied include the photocontrol of peptide conformers, the spatial control of nucleic acids, the control over receptor and channel activity and the photo regulation of enzymatic activity.[25-28] Two examples of these applications are depicted in fig. 8. Bear in mind that the *on*-and-*off* states are not necessarily the Z- and E-conformers respectively, and therefore care should be taken in designing a photoswitch for a particular application. The *on*-and-*off* states are entirely determined by the geometry of the system and sometimes no difference in activity is observed between the stereoisomers. Modelling and docking studies provide helpful tools to gain insight into the governing structure-activity relationships and form the foundation for designing the molecular switch. In most designs, the Z-conformer is preferred to be the *on*-state, due to the photo-stationary-state's preference (at ambient light and temperature) for the thermodynamically favorable E-species.

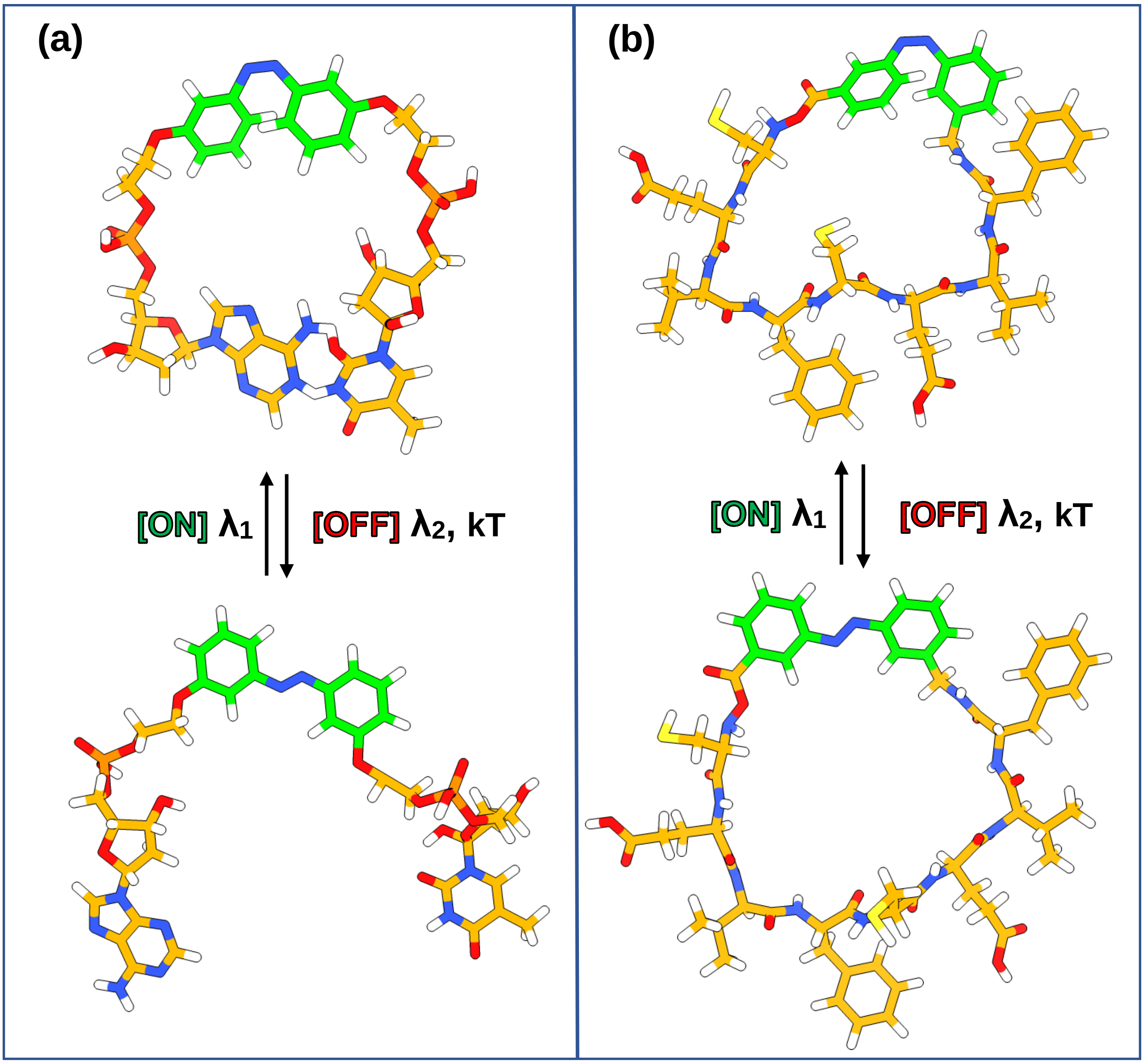

Figure 8: **Photoswitching units are highlighted in lime** ***(a)*** *Toy-model of two nucleic acid strands, bearing a single adenine (A) and thymine (T), tethered by an azobenzene photoswitching unit. In the (E)-conformer the base pairs are in the OFF state. In the (Z)-conformer the moieties pair to the ON-state.* ***(b)*** *Example for the photocontrol of peptides using azobenzene-structures. Switching from E→Z accompanies a conformational change which can alter the activity of the peptide.*

This will result in the stationary mode of the photoswitch being the *off*-state which can be turned on at will by irradiation with the appropriate wavelengths. Another important reason to design the Z-isomer as the *on*-state is its metastability. As mentioned before, the Z-isomer is metastable and will thermally relax back to the E-isomer over time. This would mean that if the Z-conformer was the *off*-state, the photoswitch would automatically turn on over time, decreasing the amount of control one has over the system. In some applications this might be desirable, when slow release of active states over time is required, however for most medicinal applications it is displeasing. Another important requirement for biological systems, is for the operating wavelengths to be between the VIS-IR range. UV radiation can damage the organics and would therefore be undesirable. The final consideration, which is easily overlooked, is the solubility associated with azo containing chromophores. Biological systems operate in aqueous media necessitating solubility of the photoswitch in polar -

solvents, and can be accomplished by changing substitution patterns on the chromophore systems. Taking these aspects into consideration, the Wennekes lab at the research group CBDD was interested in modifying carbohydrate based probes, like 9-azido-2,3-difluorsialic acid, with a photoswitch to regulate the activity of some common enzyme targets. Modelling- and docking studies were employed to identify potential targets in which the desired *on*-and-*off* behavior could be observed, and a small library of potential photo-switchable inhibitors was created. The before mentioned *T. cruzi* trans-sialidase, was one of those candidates which *in silico* indicated to allow for the photo-regulation of enzyme activity. More details can be found in the discussion.

1.5 Mechanism of photo regulation in T. cruzi trans-sialidases

Several approaches exist with which photo regulation of enzymatic activity can be achieved and are described in more detail in (Szymánski et al.).[27] This work will concern itself with the incorporation of a photoswitchable moiety on a known effector, namely the 9-azido-2,3-difluoro-sialic acid probe. As can be seen in the crystal structure of *T. cruzi* trans-sialidase shown in fig. 9(a), a pocket of free volume is located at the C9-terminus of the sialic acid probe. This should in theory allow for modification of the probe with an azo containing photoswitch at the C9-position without too much loss of inhibitory activity. The goal is then to design a photoswitch which fits neatly in the active site while occurring as the Z-isomer, and is too big to fit into the pocket while occurring as the E-isomer. This would result in the desired *on*-and-*off* behavior which can be regulated with light. The intended process of the photo regulation of enzymatic activity is schematically depicted in fig 9(b). On the top left is shown the unbound enzyme which can catalyze the conversion of the native substrate. The free volume around the C9 position is depicted in such a manner to illustrate the effect of isomerization in the active site. The probe with the photo-switch in its E-conformer is of incompatible geometry with the shape of the active site. Therefore the native substrates will have a greater affinity for the enzyme and thus will not lead to a decrease in activity of the trans sialidase. This is, however, the idealized case because in reality the E-conformer will

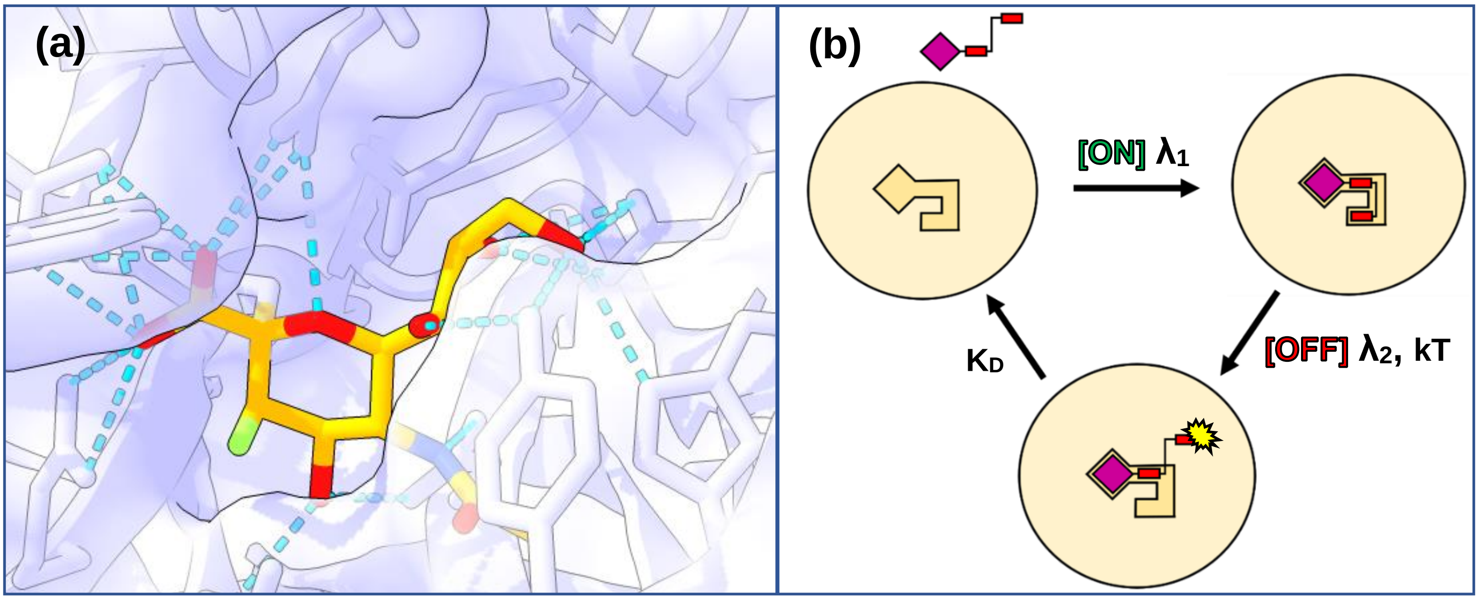

Figure 9: (a) *X-ray structure of 2,3-difluorosialic acid covalently bound to the Tyr342 residue in the active site of T. cruzi trans-sialidase PDB: 2AH2. The pocket of the active site has an opening around the C9 of the carbohydrate, allowing for derivatization of the probe.* ***(b)*** *Schematic representation for the mechanism of photo regulation in T. cruzi trans sialidases. Starting in the stationary off-state on the top-left, activation can be achieved at λ_1 where the inhibition takes place. Irradiation with λ_2 results in PII to the E-state which due to steric clash with the enzyme allows for hydrolysis of the anomeric position (K_D) and results in the unbound off-state.*

possess some inhibitory activity. The main boundary condition is that the inhibition constant of the E-conformer is at least way above that of the native substrates so that enzymatic activity approximates that of the unperturbed system. Irradiation of the photoswitch with λ_1 result in E → Z isomerization, see fig. 9(b) top right. The E-isomer fits neatly in the active site, which will result in the attack of the Tyr342 residue on the anomeric carbon atom, expelling the fluorine leaving group. For the Z-conformer to alter the enzymatic activity, the first boundary condition is that the affinity of the Z-conformer well exceeds that of the native substrate, so virtually all Tyr342 residues are bound to the modified probes. The second boundary condition is for the rate of hydrolysis and the rate of thermal relaxation of the *on*-state to be in a practical time-frame. Too rapid hydrolysis of the probe may result in an increase of enzyme activity over time, while too short half-life times of the Z-isomer result in the photoswitch turning off. These parameters are difficult to accurately predict *in silico* and should therefore be determined experimentally. When one pleases to turn the inhibitor off, irradiation of the system with λ_2 will result in the situation depicted in fig. 9(b) at the bottom right. The Z→E isomerization will induce an intense steric clash between the modified probe and the local residues creating an energetically unfavorable situation. This will in turn result in oscillations around the covalent bond between the probe and Tyr342 residue, which will ultimately lead to hydrolysis of the covalent intermediate and regeneration of the free enzyme, see fig. 9(b) bottom left. The rate of hydrolysis after irradiation with λ_2 is demarcated as K_D and should be quantified *in vitro*.

2. Results & Discussion

2.1 Computational Studies

2.1.1 Computational methods for docking studies

X-ray crystallographic data on enzyme structures was in all cases obtained from the PDB. The main crystal structure used in this work is that of 2AH2 - T. cruzi in complex with 2,3-difluorosialic acid.[3] The Autodock 4.2 program was used to perform all enzyme preparations and docking calculations.[29] Ligand structures were optimized with the MMF94s molecular force field in AutodockTools4 and Avogadro.[10][29] Enzyme structures were prepared by deleting all non-standard ligands, water and inorganic species. All non-polar hydrogen atoms were merged and the corresponding Gasteiger charges were computed. The grid map was prepared by centering the grid box in the active site on the Tyr342 residue and the desired map types were selected based on the moieties of the probes. The most universal grid contains 98 x 94 x 80 points in the x, y, z dimensions respectively for a total number of 761805 grid points. For the preparation of the docking parameter file the number of active torsions and torsional degrees of freedom in the ligands was selected accordingly with a randomized initial position and initial dihedral offset. Docking was performed non-covalently with rigid residues. The search algorithm was set to the genetic algorithm (GA) parameters with a maximum number of GA runs between 40 – 100, a population size of 150 and a maximum number of evaluations of 2500000. All other parameters were kept standardized. Docking results were analyzed and grouped in AutodockTools4 and visualized in Chimera X.[4][29]

2.1.2 Design and screening of the photoswitchable probes

The general docking method of the designed probes in this work was based on a mimetic approach. Getting reliable docking energies and conformations is often difficult, so by mimicking the known conformation of the 2,3-difluoro-sialic acid probe in the active site (as elucidated by X-ray crystallography), one should in theory obtain more accurate results. The design of the photoswitchable probes themselves is an iterative process and requires some creative thinking. There are no general successful guidelines for designing the probes and it usually comes down to a symmetry and geometry problem. The starting point from which modifications were applied was designed by (E. Alvarez Melendez†) and is depicted in table 1 (entry code = $\xi_{\alpha\varepsilon}$). From that point, over 44 photoswitch-containing-probes were designed, which were all modelled separately for the E- and Z-isomers. The performance of the photoswitch was scored on the estimated inhibition constant, the estimated free energy of binding, the clustering of energetically favorable conformations, the distance between the anomeric carbon with respect to the Tyr342 residue and the difference in predicted activity between the *on*-and-*off* states. The top 5 most promising candidates are depicted in table 1. The best photoswitching unit designed in this work, denoted $\boldsymbol{\Omega}_{\alpha\varepsilon}$, has the tightest fit in the trans-sialidase (Ts) active site with a predicted inhibition constant of 51,7 picomolar. When switched to the trans conformation, the estimated free energy of binding climbs to positive values where inhibition is virtually impossible. The synthesis of this particular probe however, is quite challenging and was therefore not realistic for the time-frame of this work. Because of this, efforts have been made to

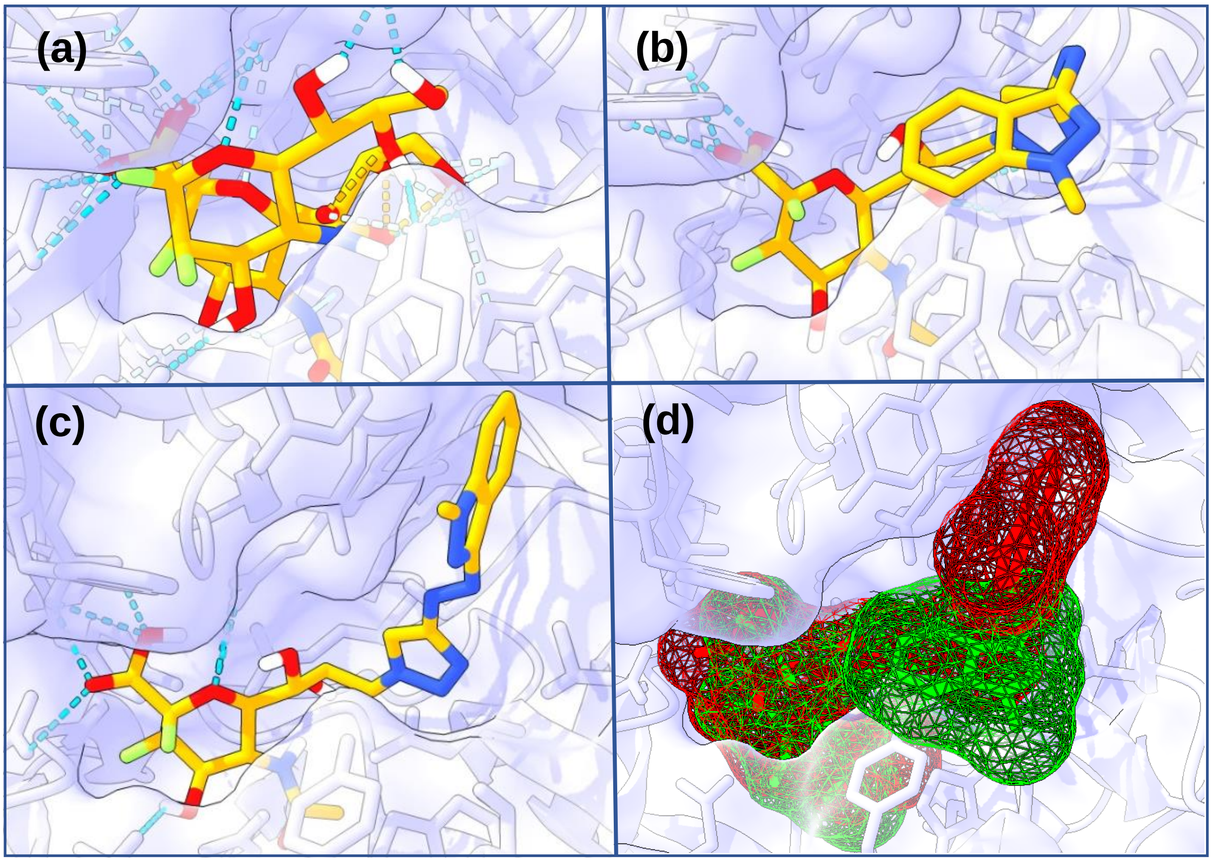

Figure 10: ***(a)*** *In silico estimated average conformer of 2,3-difluorosialic acid in the T. cruzi Ts active site, superimposed with the experimental crystal structure.* ***(b)*** *Calculated docking conformer of Z-*$\boldsymbol{\Gamma}_{\alpha\varepsilon}$ ***(c)*** *Calculated docking conformer of E-*$\boldsymbol{\Gamma}_{\alpha\varepsilon}$ ***(d)*** *Illustration on-and off behavior of the Z / E-conformer for* $\boldsymbol{\Gamma}_{\alpha\varepsilon}$*. The meshed surfaces are color coded green for the on-state and red for the off-state.*

Entry	***Chemical Structure of the Photoswitch moiety in the Z-configuration***	***Est. Free Energy of binding Z-isomer***	***Est. Inhibition constant Z- isomer***	***Est. Free Energy of binding E-isomer***	***Est. Inhibition constant E-isomer***	***Potency as a measure of the K_i E/Z-ratio***
$\Omega_{\alpha\varepsilon}$	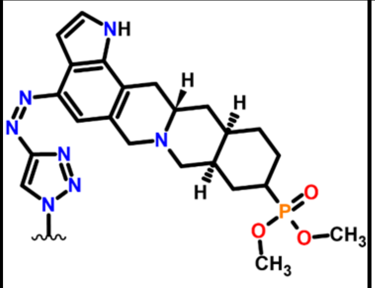	-14,04 kcal/mol	51,7 pM	+8,10 kcal/mol	N/A	N/A
$\Gamma_{\alpha\varepsilon}$	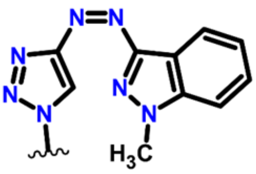	-10,77 kcal/mol	12,66 nM	-4,24 kcal/mol	776,51 μM	61335,7
$\Delta_{\alpha\varepsilon}$	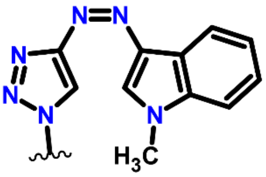	-10,09 kcal/mol	40,1 nM	≥ -5,16 kcal/mol	≥ 165,66 μM	4131,17
$\Lambda_{\alpha\varepsilon}$	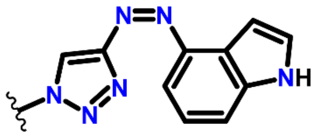	-9,92 kcal/mol	53,9 nM	-4,85 kcal/mol	280,80 μM	5209,64
$\xi_{\alpha\varepsilon}$	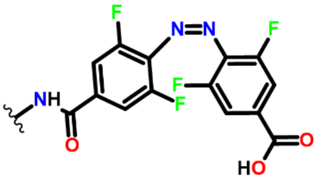	-6,19 kcal/mol	28,84 μM	≥-9,15 kcal/mol	≥196,97 nM	0,007

Table 1: *The top 5 promising photoswitch modifications to the 2,3-difluorosialic acid probe in the C9 position. The in silico predicted performance is ranked from top to bottom by the free energy of binding and the inhibition constants for the Z and E conformers. The relative performance is given in the far-right column as a function of the $K_i(E)/K_i(Z)$.*

to synthesize the remaining photo-switchable probes. Moreover in the synthesis methodology. The structures of these targets are less bulky, see tab. 1, which causes their *off*-state to maintain some activity. The boundary condition, as mentioned in the introduction, was that the inhibition constant of the E-conformer is way above that of the native substrate. Therefore a control was performed by docking the 2,3-difluorosialic acid probe to the *T. Cruzi* Ts using the same docking parameters as for the inhibitors. An average *in silico* predicted conformer, superimposed with its experimental covalent intermediate's counterpart is shown in fig. 10 (a). The estimated inhibition constant of the native inhibitor was calculated to be between 55,03 – 262,94 μM in 7 separate experiments consisting of 100 runs. Then, after applying the boundary condition to the designed probes, three distinct situations were established. $\Omega_{\alpha\varepsilon}$ and $\Gamma_{\alpha\varepsilon}$ lie well above the estimated native working concentration, see tab. 1, and therefore pass the first requirement for the desired behavior. $\Delta_{\alpha\varepsilon}$ and $\Lambda_{\alpha\varepsilon}$ lie in the danger zone where, depending on the absolute native inhibition constant, the E-conformer may show *off*-behavior or will compete with the native inhibitor. And finally, for entry $\xi_{\alpha\varepsilon}$ an entirely different behavior is observed where the E-conformer has a higher affinity then the Z-isomer. This is not necessarily a problem, however the Z-conformer's estimated inhibition constant lies way below that of the predicted working concentration and is therefore the least promising of all candidates. The first boundary condition for the Z-conformer was for the est. inhibition constant to lie way below that of the native working concentration. From tab. 1 it can be deduced that all designs, even $\xi_{\alpha\varepsilon}$ if the E-conformer is seen as the *on*-state, pass this requirement. The final boundary condition for the Z-isomer was for the rate of hydrolysis and the rate of thermal relaxation to be of operable time spans. Because it is extremely difficult to accurately predict these combined properties, designs like $\Omega_{\alpha\varepsilon}$, $\Delta_{\alpha\varepsilon}$ and $\Lambda_{\alpha\varepsilon}$ which have not been synthesized before pose a possible risk. This does however not exclude them for possessing the desired operable half-life times, there is just a lack of data. $\Gamma_{\alpha\varepsilon}$ and $\xi_{\alpha\varepsilon}$ are designs which have already been reported in literature and have been known to possess half-life times of thermal relaxation on the order of days. Due to the before mentioned boundary conditions, $\xi_{\alpha\varepsilon}$ will be kept out of the discussion. The synthesis and photophysical characterization of a $\Gamma_{\alpha\varepsilon}$ type derivative is reported in (D. Fang et al.) and was of great help for this work.[24] The team found for $\Gamma_{\alpha\varepsilon}$ derivatised with an alkyl side chain a half-life time for the Z-isomer of 1,5 days. This is well within the range for the application as a photoswitchable inhibitor and thereby made $\Gamma_{\alpha\varepsilon}$ the most promising candidate of all the designs presented. The predicted docking geometries of the Z- and E-conformers are shown in fig. 10(b-c) respectively. The Z-isomer is *in silico* predicted to be $\sim 61\cdot 10^3$ times more active, while possessing the correct geometry in the *T. cruzi* Ts active site, than the E-isomer which would effectively lead to the desired *on*-and-*off* behavior. In the trans conformer in fig. 10(c), the energetically disfavored arrangement of the aromatic rings on the photoswitch is adopted. This distortion is predicted to stem from steric clash with the Tyr248 residue and Asp247 backbone. These residues hinder the Z→E relaxation process and are hoped to force the probe out of the active site. The photo regulation process is illustrated further in fig. 10(d) where both the conformers are superimposed and mapped according to their molecular surface. In the *on*-state (green), the photoswitch neatly warps around the pocket allowing for inhibition, while in the *off*-state (red) the aromatic moieties experience steric clashes with the molecular surface of the enzyme. All these considerations combined made entry $\Gamma_{\alpha\varepsilon}$ the main focus of this work, but moreover in the synthesis methodology.

2.1.3 Methods for quantum chemical calculations

All molecular models and cartesian coordinate files were prepared in the Avogadro program.[9] For the evaluation of photophysical properties, a multitude of geometries were created by inducing guided torsion while applying the MMF94s force field with a molecular dynamics (300 K) search algorithm. For the quantum chemical calculations, the ORCA 4.0 software and Multiwfn program were used in all cases.[9][30] (TD-)DFT calculations were done with the aid of ORCA. Single point energy optimizations were computed at the B3LYP level using the RIJCOSX auxiliary basis set. [B3LYP RIJCOSX SP def2-SVP]. TD-DFT calculations, for the prediction of excited states, were performed at the BP86 level. [BP86 def2-SVP def2/J]. This is not the highest quality DFT functional available, however when dealing with reasonable amounts of conformers, larger basis sets become computationally expensive. MO's and UV/VIS-spectra were visualized in ChimeraX using the quantum chemistry SEQCROW 1.8 plug-in.[31][32] Topological analysis, electron localization functionals (ELF), exciton-hole pair calculations and natural transition orbitals (NTO's) were computed and visualized in the Multiwfn program.[30]

2.1.4 Prediction of electronic structure and photophysical properties

For the *in silico* screening of the desired photoswitchable behavior, TD-DFT calculations were employed as a qualitative analysis. To keep this part of the discussion intelligible, only the most promising candidate ($\Gamma_{\alpha\varepsilon}$) is briefly reviewed. As mentioned, a multitude of conformers might be energetically accessible at room temperature which can all contribute to the UV/VIS-absorption properties. Therefore multiple runs were performed on both the Z- and E isomer while making some minor alterations in the input geometry. The final conformers, as calculated by DFT (BP86), are depicted in fig. 11(a-b). The pyranose conformers of the sialic acid derivatives were superimposed and estimated to adopt a $^{3,O}B$-conformation for both the Z- and E-isomer. The CNNC dihedral angel of the E-isomer was estimated to range between 176,4-179,2° and that of the E-isomer between 0,5-7,3°. Additional data on the excited state calculations is supplied in the appendix. The UV/VIS spectrum was then computed from the transition electric dipole moments of the lowest energy conformations, see fig. 11(c). It was estimated that E→Z PII could be achieved at 350-400 nm ($\pi \rightarrow \pi^*$), while Z→E PII could be achieved at 450-600 nm. Surprisingly the calculations on the Z→E PII process seem to indicate that these excitations occur from orbitals of n- and π^*-symmetry, instead of the usual $\pi \rightarrow \pi^*$ transition. This might be an interesting topic for further research, as the orbital transitions of Z→E PII is poorly

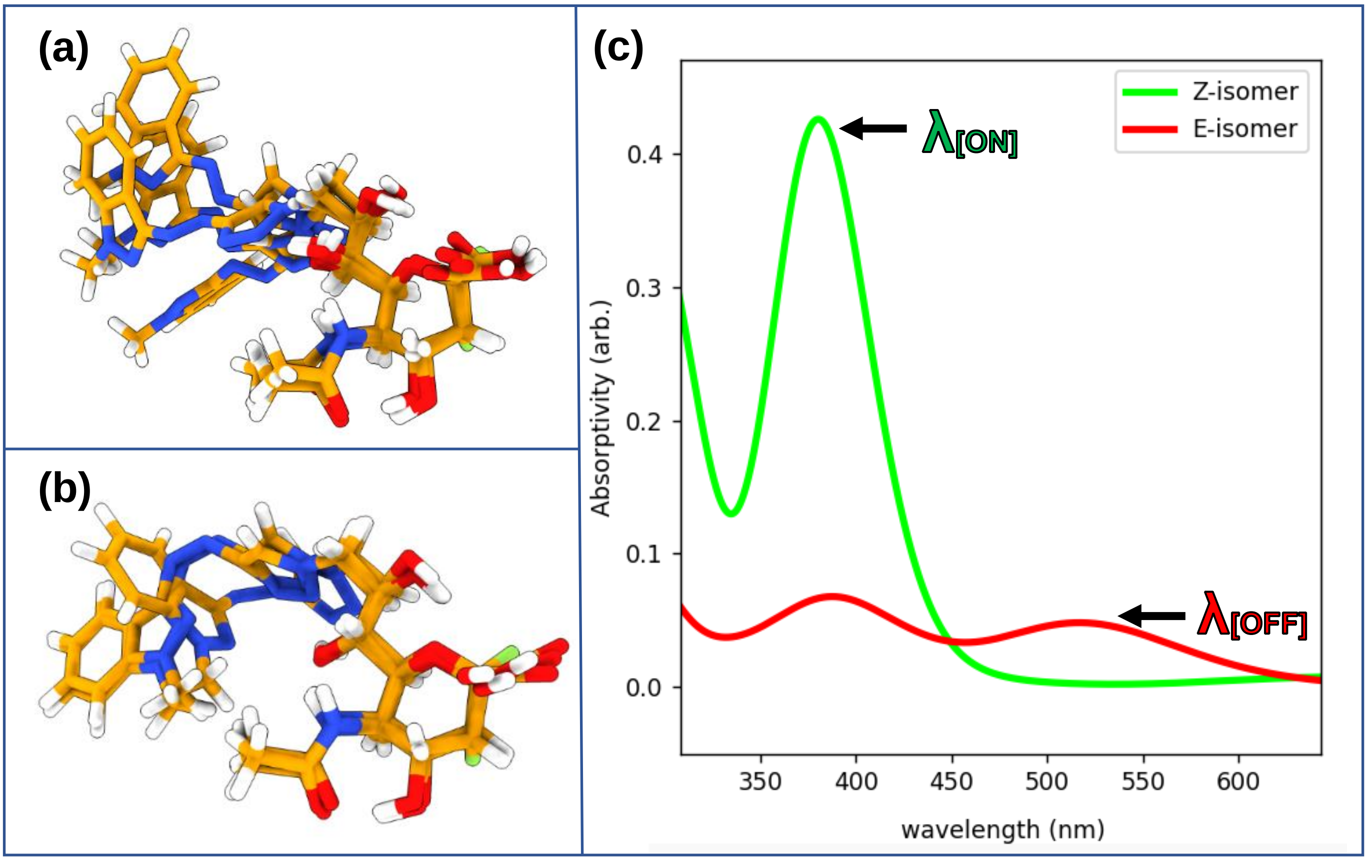

Figure 11: ***(a)*** *Superimposed calculated conformers of E-$\Gamma_{\alpha\varepsilon}$ at the BP86-level* ***(b)*** *Superimposed calculated conformers of Z-$\Gamma_{\alpha\varepsilon}$.* ***(c)*** *UV/VIS-spectra of E/Z-$\Gamma_{\alpha\varepsilon}$ computed from the transition electric dipole moments at the BP86 level of theory. The operating wavelengths of photoisomerization are highlighted by the arrows.*

described in literature. To compare the *in silico* predictions with the nearest experimental evidence, the work of (D. Fang et al.) was used in which an alkylated azo containing triazole-indazole photoswitch is reported. The team achieved the highest E→Z photoconversion at 395 nm (85%) and for Z→E at 532 nm (>98%).[24] The calculated spectrum in fig. 11(c) shows good correlation with the overall spectral characteristics for both the wavelengths and intensities. This all combined was a first indication that the desired photoswitch properties could be conserved for $\Gamma_{\alpha\varepsilon}$.

2.2 Synthesis Methodology

2.2.1 General synthesis strategy of the photoswitchable probes

For the synthesis of the potential candidates, a modular approach was constructed in which the 9-azido-2,3-difluorosialic acid probe and the photoswitch derivative were synthesized independently, see scheme 1.

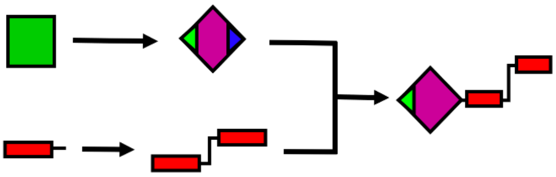

Scheme 1: *General synthesis approach of the photoswitchable 2,3-difluorosialic acid inhibitors.*

The synthesis of the 9-azido-2,3-difluoro-sialic acid probe has already been thoroughly described in literature and typically consists of 7 to 9 steps. The synthesis of the photoswitch candidates was less straightforward and consisted of 3 to 4 steps per design. When the probes and photoswitches had been synthesized the goal was to couple them via either a 1,3-dipolar [2+3] cycloaddition or by reducing the azide on the probe followed by amide coupling. The coupling strategy utilizing click chemistry seemed to be the most promising due it's widely promoted *simplicity* and orthogonal reactivity.

2.2.2 Synthesis of 9-azido-2,3-difluoro-sialic acid

For the synthesis of the 9-azido-2,3-difluorosialic acid probes, two main routes were constructed based on the approach of (W., Li et al.), see scheme 2.[7] The first route was from the original paper [scheme 2(a→d*→g)] in which, starting from ManNAc, the desired glycan derivatives could be obtained in 9 steps. The route affords in theory four distinct stereoisomers which were to be used in structure-activity studies during the *in vitro* assays. In the first step a regio-selective tosylation is performed followed by immediate acetylation of the sugar, see scheme 2(a-b*). The acetylation allows for relatively easy purification of the glycan, but causes some problems in the subsequent introduction of the azido moiety, scheme 2(c*). Due to the poor solubility in polar solvents, caused by the protecting groups, the azidofication had to be performed in apolar media. The authors circumvent this issue by the use of TMS-N_3, however in this work solely NaN_3 was used. The reaction was therefore performed in DMF and yields were around 35%. To obtain the desired intermediate S2, see scheme 2, an additional deprotection step had to be performed which all combined made the synthesis route less appealing. Because of this a second route was constructed as depicted in scheme 2(a-g). In the first step, ManNAc was tosylated with TsCl in pyridine like before, however no subsequent acetylation was performed. This had the advantage that the azidofication could be performed in polar media like water : acetone mixtures and no further deprotection step had to be done shortening the total synthesis to 7 steps. The downside to this method however, was that the purification of S1 was rather troublesome and the intermediate remained contaminated with pyridinium p-toluenesulfonate and

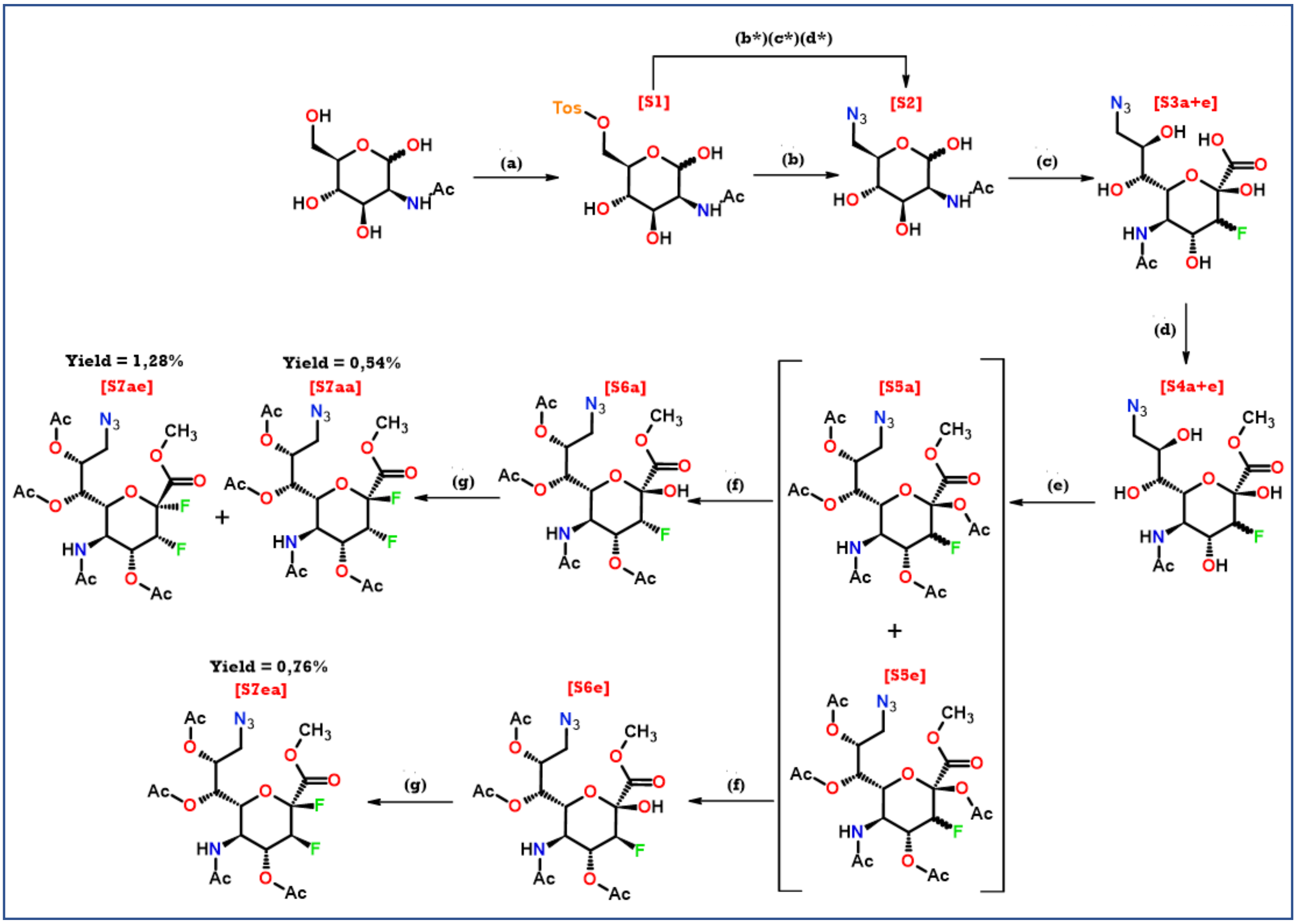

Scheme 2: ***(a)*** *with TsCl in pyridine at 0°C→RT, 1,5 days.* ***(b)*** *with NaN_3 in acetone/water, Δ, 26 h.* ***(b*)*** *with Ac_2O in pyridine at RT, 2,5 h.* ***(c*)*** *with NaN_3 in DMF, Δ, 14 h.* ***(d*)*** *with NaOMe in MeOH at 0°C, 2 h.* ***(c)*** *with 3-fluoropyruvic acid sodium salt, Neu5Ac aldolase in an aq. 0,05 M KPO_4 buffer, 5-6 days.* ***(d)*** *with Amberlite® IR 120-H in MeOH at RT, 8h.* ***(e)*** *with Ac_2O in pyridine at RT, 14 h. Racemic resolution by flash column chromatography* ***(f)*** *with hydrazine acetate in DCM/MeOH at 0°C, 6h.* ***(g)*** *with DAST in dry DCM at -30°C, 1h. Resolution by flash column chromatography.*

p-toluenesulfonic acid until acetylation in later steps. This difference in purity is illustrated in the ^{1}H-NMR spectra of S1, S2 and their acetylated counterparts (S1*,S2*) which can be found in the appendix. The azidofication in a polar solvent system, scheme 2(b), seemed to work smoothly as TLC indicated full conversion to S2. However, the work-up was again troublesome due to the low affinity of the unprotected glycan for organic solvents, decreasing the yield to 42%. Taking both methods pros and cons into consideration, the recommended path of action would be to first tosylate the ManNAc followed by acetylation, as this allows for purification of the product. Then, subsequent deprotection followed by azidofication in polar solvents should yield S2 in relatively clean fashion. In the next step, scheme 2(c), a chemo-enzymatic conversion of S2 by Neu5Ac aldolase is employed to form the desired 9-azido-sialic acid derivative (S3a+e). 3-fluoropyruvic acid is fed as a substrate as to regioselectively incorporate the fluoro-moiety on the 3-position of the sialic acid derivative. The Neu5Ac aldolase initially showed great stereoselectivity towards the desired *manno*-conformer (F3 axial), graph 1, with a composition of ~87,5 % axial after 1 day. Over the course of 6 days this decreased to ~77% which was attributed to the denaturation of the

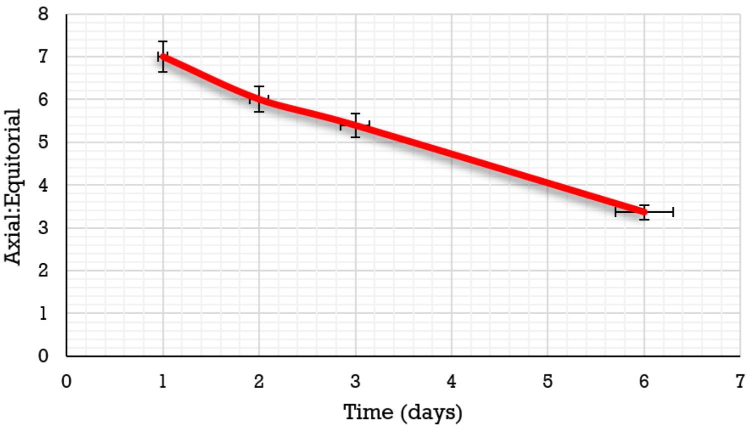

Graph 1: *Ratio (F3) axial over equatorial as a function of the reaction time. Relative conformer abundance was determined by ^{19}F-NMR.*

enzyme over time. This induces small perturbations in the overall active site geometry which is accompanied by a loss in stereoselectivity. Another important feature of the chemoenzymatic synthesis was the evolution of acidic species. The enzymatic catalysis worked best in mildly basic conditions so this necessitated the use of a buffer system. The yields of the chemoenzymatic synthesis were pushed to near quantitative values by maintaining the pH between 7-8 during the reaction. This afforded S3 as an mixture of epimers (axial : equatorial) which in this phase were inseparable by chromatography. Therefore, the carboxylic acid at C1 was esterified to its methylated counterpart [scheme 2(d)] using amberlite resin, followed by peracetylation with Ac_2O in pyridine [scheme 2(e)]. The acetylation of the sialic acid derivatives to S5a and S5e increased the difference in retention indexes to 10 – 15 %. This in turn allowed for the separation of the epimers by flash column chromatography using a gradient of EtOAc and PE which is described in more detail in the experimental section. Separation of the epimers past this stage becomes increasingly more difficult so it is strongly recommended to perform the racemic resolution at this stage of the synthesis. S5a was determined to have a diastereomeric excess (d.e.) of 94% while S5e had a d.e. of 99%, as measured by ^{19}F-NMR. Both diastereomers were under investigation due to their - potentially divergent hydrolysis rates for *T. cruzi* Ts species, so both conformers were further modified. To introduce the fluorine atom on the anomeric carbon, a regioselective deacetylation had to be performed first. This was accomplished by reacting S5a and S5e with hydrazine acetate separately in a DCM : MeOH solvent mixture, scheme 2(f). The hydrazine acetate reacted exclusively with the anomeric acetyl protected hydroxy group allowing the use of a relatively large excess of reagent. The yields of the anomeric deprotection to S6a and S6e were 80% and 65% respectively. The significant difference is likely due to losses in the work-up process, as TLC indicated full conversion. The final step in the synthesis of the 9-azido-2,3-difluoro-sialic acid probe was the fluorination of the anomeric position, see scheme 2(g). The results of the fluorination for both epimers were mechanistically pretty exciting and will therefore be discussed in a bit more detail. The suspected mechanistic pathways of the fluorination using DAST is shown in scheme 3. The team of (W., Li et al.) found for the 9-azido probe that after the enzymatic step, the anomeric hydroxy group adapted solely the axial position as depicted in scheme 2 [S4-S6]. This was confirmed in this work by ^{19}F/^{1}H-NMR as both S6a and S6e were obtained as **β**-anomers. This would imply that if the fluorination using DAST only proceeds via the S_N2 mechanism, as depicted in scheme 3, the anomeric fluoride would exclusively adopt the equatorial position. However when performing the reaction on S6a, both fluorinated anomers were formed. This indicated that the resonance pathway to the oxocarbenium transition state, see scheme 3, might play a role as the sp^2-like conformation allows for attack on either side of the anomeric carbon atom. However, when performing the fluorination on S6e, only the formation of the **α**-anomer was observed, which indicated the S_N2 mechanism was the

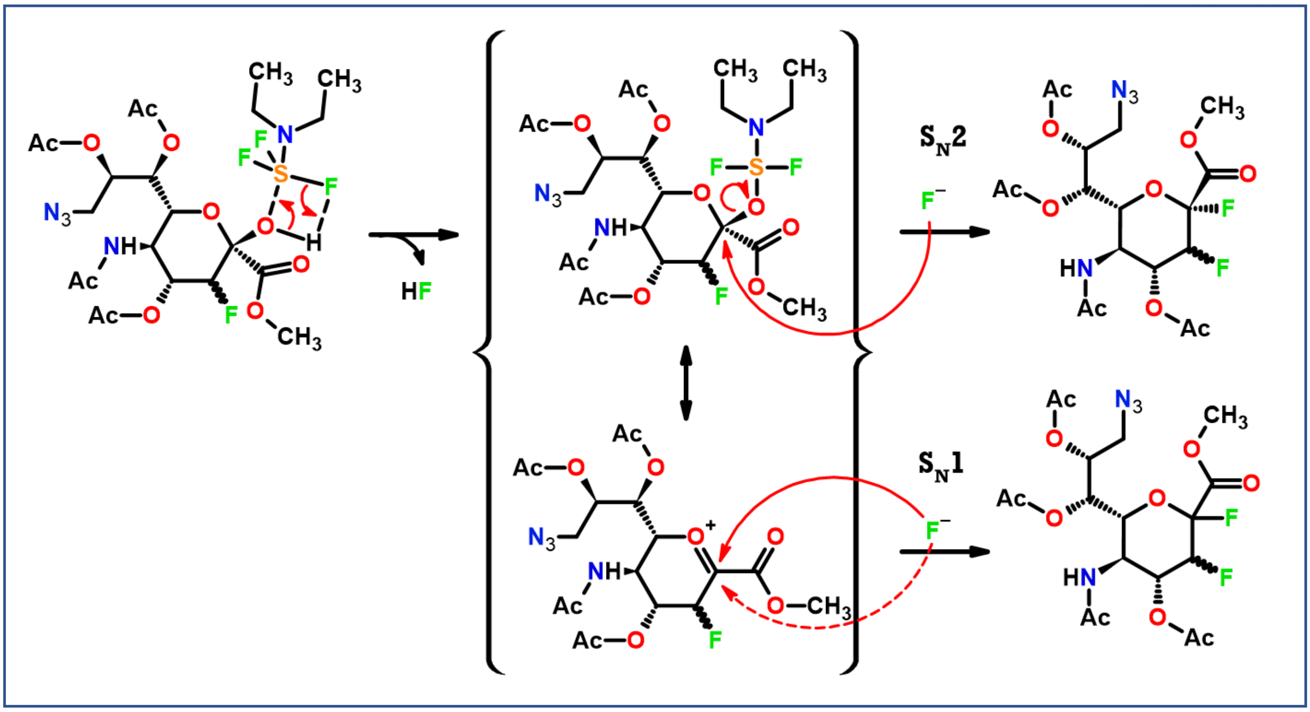

Scheme 3: Proposed mechanistic pathways for the fluorination. In the early reaction coordinate DAST arranges in a planar fashion with anomeric hydroxy group.[33] This is followed by elimination of HF which yields the DASD-β-O-sialic acid conformer as shown in the brackets. The fluorination can then proceed via the S_N2 mechanism, which is accompanied by an inversion of stereochemistry yielding the α-anomer. In the second pathway, DASD-β-O-sialic acid rearranges to the oxocarbenium transition state followed by a S_N1 attack, which is accompanied by a loss of stereospecificity.

dominant reaction pathway. To explain these results, conformers of S6a and S6e were constructed to quantify the effect of alternating the F3 position on the stability of the oxocarbenium state. The epimers were both subjected to a single point energy calculation at the B3LYP level of theory, after which the ELF maps were plotted in Multiwfn.[30] The plane was then mapped around the fluorine (C3) and the pyranose oxygen atom to illustrate the difference in the electronic environment for S6a-e. The ELF-maps are shown in fig. 12(a-b). After careful evaluation, it was proposed that the results could be reconciled by the through-space electrostatic stabilization of the incipient oxocarbenium state by the axial fluorine atom. This is described in more detail in (Miljković, M. et al.).[34] As depicted in fig. 12(a), the axial fluorine atom is in close proximity with the anomeric centre which allows it to donate electron density to the oxocarbenium transition state (TS), in turn stabilizing it. If the fluorine is in the equatorial position, see fig. 12(b), it points away from the anomeric center, which disables it from mitigating the charge build-up in the oxocarbenium TS, even destabilizing it. This explains why S6e only afforded the α-anomer via the S_N2 mechanism, while S6a affords a mixture of anomers through both the S_N1 and S_N2 pathway. This has implications for the hydrolysis rates in *T. Cruzi* Ts species as well, as the probe with F3 in the equatorial position is destabilizing the TS more intensely. The exact kinetics were to be determined by the *in vitro* assays. To conclude, the ratio of S7ae : S7aa for the fluorination of S6a was determined to be 2,5 : 1 which were separable by flash column chromatography. The starting material S6a had a d.e. of 94% however, which caused the S7aa probe to be contaminated with ~30% S7ea. These were inseparable by chromatography and kept as such. The fluorination of S6e afforded solely S7ea. The overall yields to the desired probes were 1,28% for S7ae, 0,54 % for S7aa and 0,76% for S7ea, as shown in scheme 2.

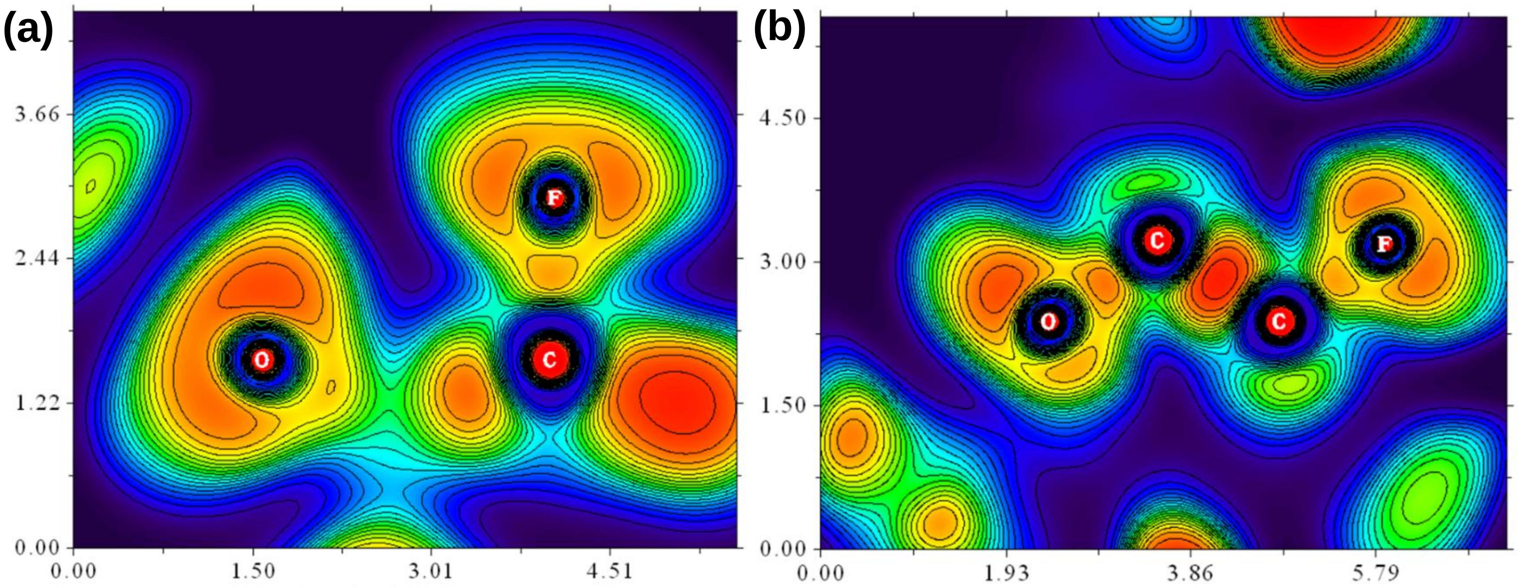

Figure 12: *Lengths in Angstrom (Å)* ***(a)*** *Electron localization function (ELF) map of S6a calculated at the B3LYP-level (DFT). The fluorine in the (C3) axial position is in close proximity with the anomeric center.* ***(b)*** *ELF-map of S6e (DFT-B3LYP) in which the fluorine points away of the anomeric center.*

2.2.3 Synthesis of the photoswitches

The synthesis of the 'clickable' photoswitches was based on the protocol described in (D. Fang et al.) and is shown for Γ in scheme 4.[24] Designs like Λ, Δ and Γ were to be made following this approach. However after multiple tests, the indole based photoswitch systems seemed to be sensitive to most reaction conditions, with the formation of many side products. Therefore the synthesis of the indole-based designs were placed on hold while the more promising candidates were synthesized first. The indazole design, Γ, was known to be made following this strategy and was therefore prioritized. The building block E1 was synthesized from 2-fluorobenzonitrile according to the procedure of (Liu, H.-J., et al.).[35] 2-fluorobenzonitrile was refluxed with methylhydrazine in ethanol, for a total yield of 49%, scheme 4(a). The aminoindazole, E1, was then converted to its corresponding diazonium salt, E2, via treatment with BF$_3$·Et$_2$O and t-BuONO in THF, scheme 4(b). The diazonium salt is poorly soluble in THF and could therefore be purified by filtration. The final step, scheme 4(c), was the coupling to the TIPS protected photoswitch. This was done by deprotonating TIPSA *in situ* using n-BuLi followed by the addition of the n-BuLi solution to E2 in THF at -78°C. The mixture was then slowly warmed to RT over the course of 45 minutes. It was found that the

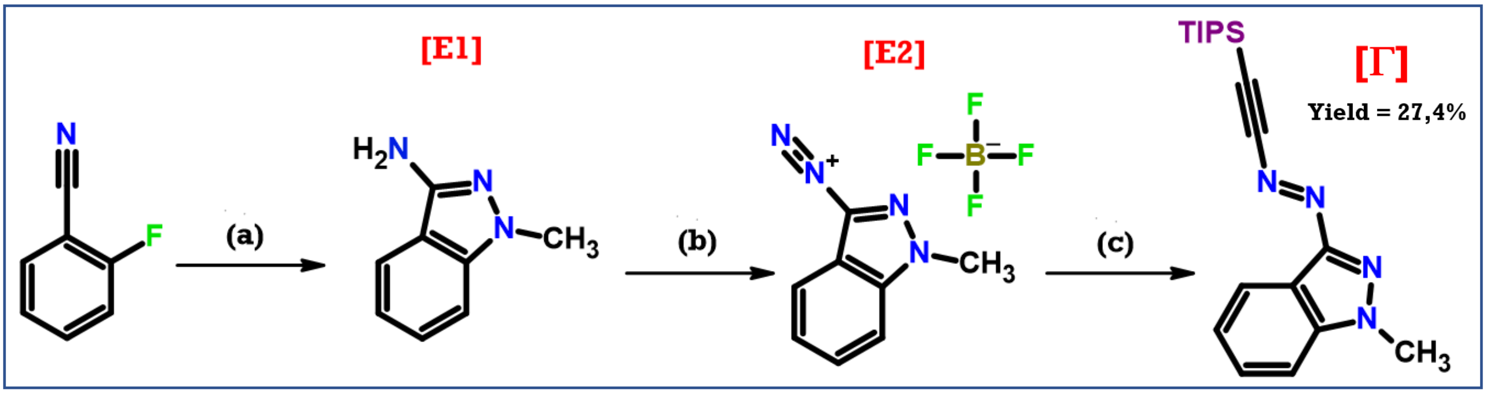

Scheme 4: ***(a)*** *with methylhydrazine in EtOH, Δ, for 9h.* ***(b)*** *with BF$_3$·Et$_2$O and t-BuONO in THF at 0°C for 30 min.* ***(c)*** *first TIPSA and n-BuLi in THF at 0°C for 30 min., then with E2 in THF at -78°C → RT, 45 min – 1h.*

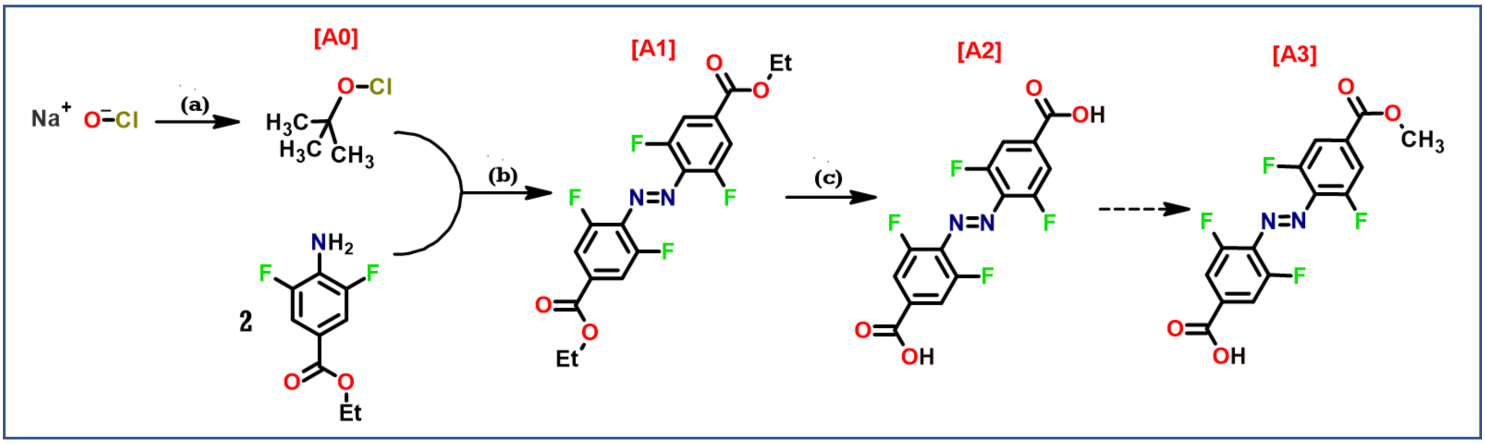

***Scheme 5: (a)** with acetic acid and tert-butanol at RT for 5 min. **(b)** with sodium iodide in diethyl ether at RT for 16 h. **(c)** with a 1M aqueous sodium hydroxide solution in THF at RT for 4 h.*

success of the reaction depended strongly on the rate of warming and the exposure to light, with the best result being obtained at heating rates of ~2,2 °C/min and the lights turned off. Another interesting characteristic of the reaction was that when step (c) in scheme 4 was performed in the dark, solely the (E)-isomer was formed as confirmed by ^{1}H-NMR spectroscopy. The yield over the last two steps, scheme 4(b-c), was determined to be 56% for a total yield of 27,4% starting from 2-fluorobenzonitrile. The synthesis procedure could be optimized, as the authors of the original papers describe higher yields for the same process.[24][35] However due to time constraints, no efforts on this had been made. The final photoswitch discussed here, A3 in scheme 5, was meant to be employed in an amide-type coupling strategy to the glycan probe. The probe was estimated from the *in silico* calculations to lie outside the desired photo regulatory working range. However, as a control of the *ab initio* methods, it was decided to still pursue the synthesis of the target. Tert-butyl hypochlorite [A0] was freshly prepared by the reaction of sodium hypochlorite with acetic acid and tert-butanol, scheme 5(a). The ethyl-4-amino-3,5-difluoro-benzoate was already prepared previously by (E. Alvarez Melendez†). The first step was the coupling to the azo-benzene-like chromophore as depicted in scheme 5(b). This was done by treating the monomer with the freshly prepared tert-butyl hypochlorite solution and sodium iodide in diethyl ether. The reaction was performed with the lights turned off as to minimize E → Z isomerization. This afforded [A1] in 70% yield which was determined to possess a E:Z ratio of 7,3 : 1. To remove the ethyl protecting groups on the carboxylic acid moieties, [A1] was dissolved in THF and deprotected using a 1M aq. NaOH solution. [A2] was obtained in quantitative yields with an E:Z ratio of 2,7 : 1. The final step to the desired probe was the regioselective protection of [A2] as depicted in scheme 5. However, due to time constrains no progress on this had been made since, and this might be an interesting topic for future research.

2.2.4 Efforts on coupling via 1,3-dipolar [2+3] cycloaddition

The functionalization of the 9-azido-probe via click-chemistry was supposed to be a convenient method of coupling the glycan to the photoswitch, however this turned out to be the bottle-neck of the entire project. The general conditions tried in this work are shown in scheme 6(a-h). The conditions described in (D. Fang et al.) were tried first in which Cu(II)SO$_4$ is reduced *in situ* by sodium ascorbate to the active Cu(I) species.

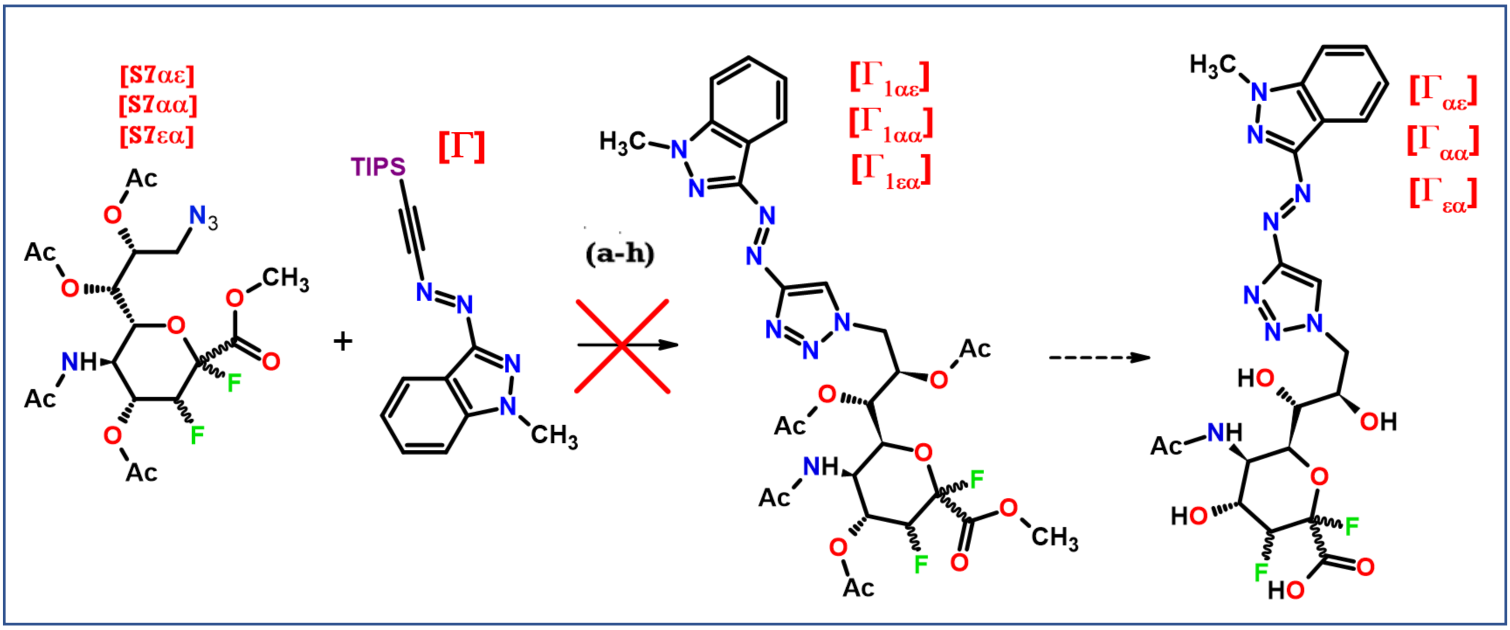

Scheme 6: ***(a)*** *with $Cu(II)SO_4$, NaAsc, TBAF in $THF:H_2O$ (5:1).* ***(b)*** *with $Cu(II)SO_4 \cdot 5H_2O$, NaAsc, TBAF in DMF.* ***(c)*** *with $Cu(II)SO_4 \cdot 5H_2O$, NaAsc, TBAF in $DMF:H_2O$ (10:1)* ***(d)*** *with $Cu(II)SO_4 \cdot 5H_2O$, NaAsc, TBAF in THF:MeOH (9:2)* ***(e)*** *with $Cu(II)SO_4 \cdot 5H_2O$, NaAsc, TBAF in THF H_2O (1:1)* ***(f)*** *with $Cu(II)SO_4 \cdot 5H_2O$, NaAsc, TBAF, TEA in $THF:H_2O$ (5:3)* ***(g)*** *with Cu(I)I, AgF, DIPEA,TBAF in DMF* ***(h)*** *with Cu(I)I, TBAI, AgF in $THF:H_2O$ (3:1).*

The reaction was performed in a $THF:H_2O$ mixture (5:1) with the use of TBAF as a desilylation agent. However, after multiple attempts it was concluded that the conditions were insufficient for the coupling of the glycan based azido-moieties and therefore new conditions had to be found. Because of this, solvent compositions and concentrations of reactant/reagent species were varied systematically and attempted on multiple glycan probes. This part of the optimization process is signified by steps (a-f) in scheme 6. After numerous trials in different solvent systems, the initial conditions were used while altering the $THF:H_2O$ ratio to 1:1, scheme 6(e), and increasing the TBAF content to 3 equivalents. This attempt was performed on S7ea first and seemed to produce the desired click-product as indicated by a singlet around 8,08 ppm in the ^{1}H-NMR spectrum. The spectra of this attempt are provided in the appendix ($\Gamma_{1\varepsilon\alpha}$). However, reproducing the results using the exact same conditions proved to be difficult as the reaction did not proceed in further attempts on multiple probes. To identify the problems within the method, several different approaches were constructed. The first obvious problem was that the generation and life-times of active Cu(I) species was sub-optimal, causing the apparent discrepancies. Therefore the coupling was attempted by using copper(I)iodide so that the catalyst was active from the start. The conditions tried are depicted in scheme 6(g-h), but did not yield significantly different results. This indicated that the anomalies were not necessarily caused by the catalyst but rather by the probes themselves. The second possible problem was that the desilylation of the TIPS group caused the bottle-neck. Therefore it was attempted to deprotect the photoswitch to its corresponding alkyne. Three different desilylation agents, namely TBAF, K_2CO_3 and AgF, were used to deprotect the photoswitch however to no avail. This strongly suggested that the irreproducibility and discrepancies of the click reaction were related to the deprotection of the photoswitch module. Sadly due to time constraints, this part was not optimized and the 1,3-dipolar [2+3] cyclo-addition was therefore not successful. To exclude

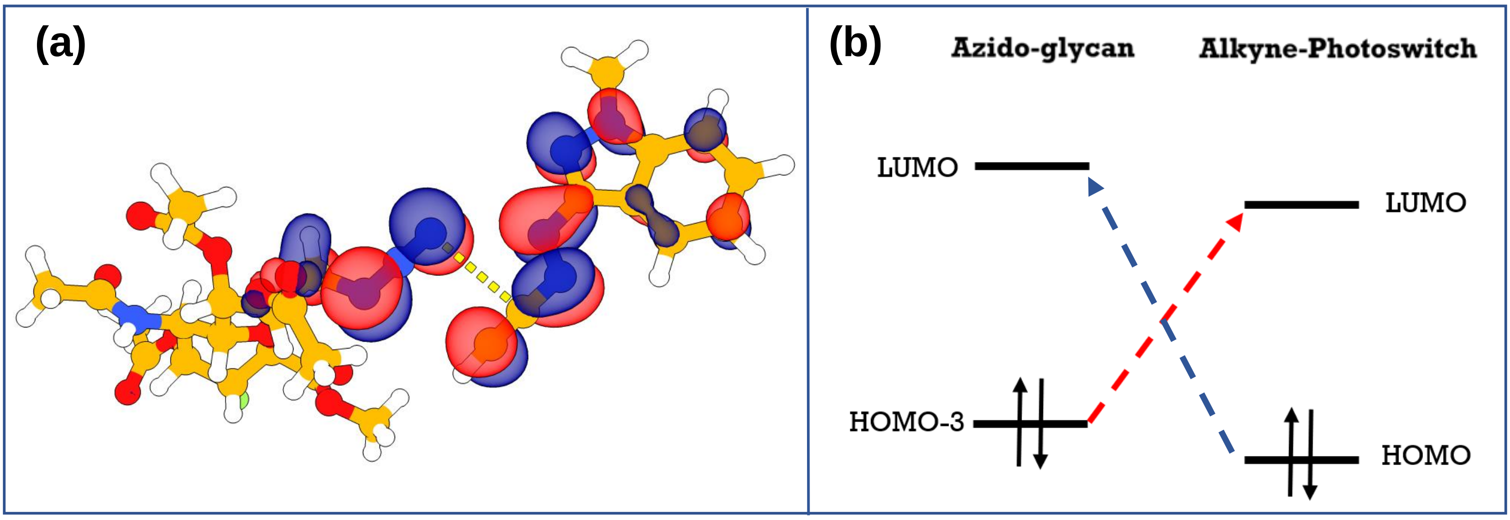

Figure 13: (a) *DFT models (calculated at the B3LYP-level with a RIJCOSX auxiliary basis set) of S7ae and the TIPS-deprotected photoswitch (Γ) module. The iso-surfaces of the HOMO-3 of the azido-glycan and the LUMO of the alkyne photoswitch are depicted in which the constructive overlap of orbitals can be seen.* ***(b)*** *MO-diagram for the 1,3-dipolar cycloaddition in which the HOMO-3 of the azido-glycan attacks the LUMO of the alkyne-photoswitch (red arrow), or the HOMO of the alkyne attacks the LUMO of the azido-glycan (blue arrow).*

any mechanistic reasons complicating the copper click-reaction, DFT models of the photoswitch- and glycan modules were constructed and are presented in fig. 13. After the single-point energy calculations it was concluded that the 1,3-dipolar cycloaddition proceeds through a HOMO-LUMO controlled dipole, which is signified by a similar HOMO-LUMO gap as depicted in fig. 13(b).[36] The calculations predict a slight preference for the attack of the HOMO(-3) of the azide on the LUMO of the alkyne for which the respective orbital symmetries are depicted in fig. 13(a). In conclusion, the DFT-models seem to indicate that the unsuccessful click-coupling was not due to mechanistic considerations but rather due to difficulties of generating the TIPS-deprotected alkyne *in situ*. Therefore it is strongly recommended for future research, that suitable conditions are found so that the photo regulatory effect of the designs on *T. Cruzi* Ts species can be studied in more detail.

4. Conclusions

In summary, the *in silico* design and the synthesis of photoswitchable inhibitors for the regulation of *Trypanosoma cruzi* trans-sialidase species is described in this work. The estimation on relative active site affinities for *on*-and-*off* states was performed by means of docking studies in Autodock4.2. The most promising candidate, $\Gamma_{\alpha\varepsilon}$, was estimated to possess inhibition constants of 12,66 nM and 776,51 µM in the Z- and E-isomeric states respectively. To *ab initio* screen if the desired photophysical properties were conserved after linking the photoswitches to the glycans, (TD-)DFT calculations were performed which predicted estimated operating wavelengths to range between 350-400 nm and 450-600 nm for the E- and Z-isomers of $\Gamma_{\alpha\varepsilon}$ respectively. For the synthesis of the photoswitchable glycans, a modular approach was designed in which the 9-azido-2,3-difluorosialic acid was obtained between 7-9 steps and the photoswitches were obtained in 3-4 steps. The synthesis of the modified glycans yielded S7ae in 1,78%-, S7aa in 0,54%- and S7ea in 0,76% yield. The synthesis of the photoswitch afforded Γ in 27,4% yield. The final 1,3-dipolar cycloaddition proved to be unsuccessful after numerous attempts, which was attributed to the difficult desilylation of the TIPS protected alkyne.

4. Experimental Section

4.1 Synthesis of 9-Azido-5-Acetyl-2,3-Difluorosialic acid Probes

[S1] *2-Acetamido -2-deoxy-6-tosyl-D-mannopyranose*

A solution of TsCl (4,74 g, 24,9 mmol, 1,10 eq) in pyridine (23 ml) was added dropwise in an hour to a solution of N-acetyl-D-mannosamine (5 g, 22,6 mmol) in pyridine (70 ml) at 0°C under N_2. The solution was left overnight (0°C→RT) with stirring. The next morning, TLC (DCM :MeOH=8:2) indicated the presence of starting material so 0,1 eq. (0,43 g) of TsCl in 2 ml pyridine was added dropwise every half hour. After 5 times of addition, the amount of TsCl was increased to 0,2 eq. per half hour. This was performed 4 times after which TLC (DCM:MeOH=8:2) showed full conversion. The reaction mixture was quenched with 120 ml MeOH, the solvents co-evaporated with toluene and dried in vacuo. The crude was dry-loaded onto silica and flash column chromatography (DCM:MeOH =9,5:0,5→9:1) afforded 8,02 g of S1 as a yellowish foam (21,3 mmol, 94 %) complexed with pyridinium p-toluene sulfonate (5,92 g) which was used in the next step as such. [α/β-anomer ratio= 1 : 0,41] *NMR α/β-mixture S1:* ^{1}H NMR (400 MHz, D_2O) δ 7.71 (dd, J = 8.4, 3.2 Hz, 2H), 7.35 (dd, J = 8.3, 3.4 Hz, 2H), 4.90 – 4.79 (m, 1H), 4.31 – 4.06 (m, 3H), 4.03 – 3.59 (m, 2H), 3.48 – 3.26 (m, 1H), 2.30 (d, J = 2.0 Hz, 3H), 1.91 (d, J = 15.9 Hz, 3H). *NMR pyridinium p-toluene sulfonate:* ^{1}H NMR (400 MHz, D_2O) δ 8.68 – 8.58 (m, 2H), 8.48 (tt, J = 8.0, 1.5 Hz, 1H), 7.93 (t, J = 7.0 Hz, 2H), 7.53 (d, J = 8.1 Hz, 2H), 7.20 (d, J = 7.9 Hz, 2H), 2.24 (s, 3H).

note: if there is p-toluene sulfonic acid present after the column→add toluene and a small amount of DCM → filter off the toluene and dry the residue in vacuo.

[S2] *2-Acetamido-6-azido-2,6-dideoxy-α-D-mannopyranose*

8,02 g of S1 (21,3 mmol) complexed with 5,92 g pyridinium p-toluene sulfonate was dissolved in a water : acetone mixture (50 ml : 150 ml) and placed under nitrogen. Then 5,7 g of sodium azide (87 mmol, 4,1 eq.) was carefully added and the mixture was refluxed (60 °C) with stirring. After 22 h , TLC (DCM:MeOH:EtOAc= 9 : 1 : 0,1) showed the presence of starting material so another 3 eq. NaN_3 (~4,2 g) was added in 4 h. After this time TLC indicated full conversion and the reaction mixture was co-evaporated to dryness with toluene/ acetronitrile in vacuo. The crude was then dryloaded onto silica and flash column chromatography (DCM:MeOH = 9,5:0,5 → 8:2) afforded 1,976 g of S2 as a white foam + 257 mg of a white yellowish foam. Combined yield of 2,23 g (~42%, 9,07 mmol). ^{1}H NMR (400 MHz, D_2O) δ 4.99 (s, 1H), 3.84 – 3.39 (m, 3H), 1.92 (dq, J = 7.2, 2.3 Hz, 3H), 4.35 – 4.19 (m, 1H), 4.18 – 4.07 (m, 1H), 3.94 – 3.84 (m, 1H).

[S3a+e] *5-Acetamido-9-azido-3,5,9-trideoxy-3-fluoro-D-erythro-α-L-manno-non-2-ulopyranosonic acid & Gluco-non-2- ulopyranosonic acid*

To a solution of S2 (1,976 g, 8 mmol) in aq. 0,05 M KPO_4 buffer (20 ml) was added 3-fluoropyruvic acid sodium salt (375 mg, 2,57 mmol, 0,32 eq), 1 ml of a 1 wt.% NaN_3 phosphate buffer and Neu5Ac aldolase (20 mg, 20 U/mg). The mixture was shaken for 7h at 37°C. Another 0,8 eq. fluoropyruvic acid (938 mg, 6,43 mmol) + 20 mg Neu5Ac Aldolase were added and the mixture was shaken over the weekend at 37°C. ^{19}F-NMR (10%-D_2O) indicated that the fluoropyruvic acid was still present and another 60 mg of Neu5Ac Aldolase was added over a period of 2,5 days. After this time, ^{19}F-NMR (10%-D_2O) + TLC (DCM:MeOH=9:1) indicated full consumption of the sugar. The mixture was diluted with 1,5 volumetric equivalents of EtOH, cooled at -20°C for 20 min and placed in the orbital shaker at

4500 RPM. The supernatant was removed, concentrated in vacuo and dry-loaded onto silica. Flash column chromatography (EtOAc : MeOH : H_2O : CH_3COOH = 7 : 2 : 0,9 : 0,1) followed by co-evaporation with toluene yielded 2,8 g of S3(a+e) as an off-white solid (8 mmol, quant.) with 3-fluoropyruvic acid stuck as an impurity (total mass = 3,3 g). The product was used as such in the next step. [*ratio ax. : eq. = 3,16*] ^{1}H NMR (400 MHz, D_2O) δ 5.45 – 4.86 (m, 1H), 4.55 – 4.31 (m, 1H), 4.29 – 3.94 (m, 2H), 3.92 – 3.80 (m, 1H), 3.80 – 3.49 (m, 2H), 3.41 – 3.24 (m, 1H), 1.94 – 1.80 (m, 3H). ^{19}F NMR (376 MHz, D_2O) δ -199.32 (dd, J = 49.6, 12.5 Hz, equatorial), -208.23 (dd, J = 49.4, 29.7 Hz, axial), -229.23 (t, J = 46.7 Hz).

[S4a+e] ***Methyl 5-acetamido-9-azido-3,5,9-trideoxy-3-fluoro-D-erythro-α-L-manno-non-2-ulopyranosonate & gluco-non-2-ulopyranosonate***

2,8 g of S3(a+e) (~8 mmol) was dissolved in 150 ml MeOH and ion exchange resin Amberlite® IR 120-H (6 g) was added under N2-atmosphere. After 8 h, TLC (DCM : MeOH= 8:2) showed full conversion. The mixture was filtered, the resin was washed with MeOH and the solvents evaporated in vacuo. This afforded 2,472 g of a reddish foam which was dry-loaded onto silica after which flash column chromatography (DCM: MeOH = 95 : 5 → 90 : 10) allowed for the separation of 1,435 g S4a+e (3,92 mmol) + 586 mg of a side product as off-white foams. [S4a+e] ^{1}H NMR (400 MHz, CD_3OD) δ 5.24 – 4.86 (m, 1H), 4.76 – 4.26 (m, 2H), 4.25 – 4.14 (m, 1H), 4.14 – 4.00 (m, 1H), 3.99 – 3.60 (m, 3H), 3.58 – 3.31 (m, 3H), 1.99 (d, J = 1.6 Hz, 3H). ^{19}F NMR (376 MHz, CD_3OD) δ -201.63 (dd, J = 49.4, 12.5 Hz, equatorial). -209.41 (dd, J = 49.5, 28.7 Hz, axial).

[S5a+e] ***Methyl 5-acetamido-2,4,7,8-tetra-O-acetyl-9-azido-3,5,9-trideoxy-3-fluoro-D-erythro-α-L-manno- non-2-ulopyranosonate & gluco-non-2-ulopyranosonate***

1,435 g of S4a+e (~3,92 mmol) was dissolved in pyridine (10 ml) and placed under N_2. Then Ac_2O (20 ml) was added and the mixture was stirred at RT overnight. After this time TLC (DCM:MeOH=9:1) indicated full conversion, the mixture was then poured into water and extracted with DCM (3x).The organic phase was dried over Na_2SO_4, filtered and co-evaporated with toluene. The crude was dissolved in DCM and filtered over silica (DCM:MeOH = 97:3) affording 1,49 g of a yellowish-white foam. The foam was dry-loaded onto silica and flash column chromatography (EtOAc : PE = 7 : 3 → 8:2) afforded 490 mg of S5a (0,92 mmol) as a white foam + 200 mg of S5e (0,37 mmol) as a white foam. [S5a] ^{1}H NMR (400 MHz, $CDCl_3$) δ 5.38 – 5.31 (m, 2H), 4.99 – 4.84 (m, 2H), 4.25 (q, *J* = 10.3 Hz, 1H), 4.19 – 4.12 (m, 1H), 3.87 (dd, *J* = 13.6, 2.7 Hz, 1H), 3.84 (s, 3H), 3.41 (dd, *J* = 13.4, 7.5 Hz, 1H), 2.18 (s, 3H), 2.17 (s, 3H), 2.10 (s, 3H), 2.07 (s, 3H), 1.90 (s, 3H). ^{19}F NMR (376 MHz, $CDCl_3$) δ -208.71 (dd, *J* = 49.2, 27.6 Hz). [S5e] ^{1}H NMR (400 MHz, $CDCl_3$) δ 5.47 – 5.35 (m, 2H), 4.85 (dt, *J* = 6.9, 3.0 Hz, 1H), 4.68 – 4.56 (m, 1H), 4.30 – 3.99 (m, 2H), 3.91 – 3.73 (m, 4H), 3.34 (dd, *J* = 13.7, 7.5 Hz, 1H), 2.24 (s, 3H), 2.16 – 2.15 (m, 3H), 2.08 (s, 3H), 2.07 (s, 3H), 1.89 (d, *J* = 7.2 Hz, 3H). ^{19}F NMR (376 MHz, $CDCl_3$) δ -199.26 (dd, *J* = 49.0, 12.1 Hz).

[S6a] ***Methyl 5-acetamido-4,7,8-tri-O-acetyl-9-azido-3,5,9-trideoxy-3-fluoro-D-erythro-α-L-manno-2-non-2-ulopyranosonate***

490 mg of S5a (0,92 mmol) was dissolved in dry DCM (4,3 ml), cooled in an ice bath and flushed with N_2. 385 mg hydrazine acetate (~4,19 mmol, 4,5 eq.) was then dissolved in MeOH (6,4 ml) and added dropwise to the solution. The mixture was stirred at 0°C for 6 h after which TLC (EtOAc) indicated full conversion. The solvents were then evaporated, the residue dissolved in EtOAc and washed with H_2O, a 1 M aq. HCl solution and a sat. $NaHCO_3$ solution. The organic layer was dried over Na_2SO_4 and evaporated to

completeness in vacuo. This afforded 360 mg of S6a (0,73 mmol) as a white foam which was used in the next step without further purification. ^{1}H NMR (400 MHz, $CDCl_3$) δ 5.61 – 5.40 (m, 1H), 5.29 (d, J = 5.7 Hz, 1H), 5.21 (ddd, J = 7.7, 4.9, 2.5 Hz, 1H), 4.99 – 4.78 (m, 1H), 4.31 (m, J = 7.9 Hz, 2H), 3.87 (s, 3H), 3.73 (dd, J = 13.5, 2.5 Hz, 1H), 3.41 (dd, J = 12.2, 7.1 Hz, 1H), 2.17 (s, 3H), 2.12 (s, 3H), 2.09 (s, 3H), 1.91 (s, 3H). ^{19}F NMR (376 MHz, $CDCl_3$) δ -205.51 (dd, J = 49.4, 27.9 Hz).

[S6e] *Methyl 5-acetamido-4,7,8-tri-O-acetyl-9-azido-3,5,9-trideoxy-3-fluoro-D-erythro-α-L-gluco-2-non-2-ulopyranosonate*

200 mg of S5e (0,37 mmol) was dissolved in dry DCM (1,8 ml), cooled in an ice bath and flushed with N_2. 158 mg hydrazine acetate (~1,72 mmol, 4,5 eq.) was then dissolved in MeOH (2,6 ml) and added dropwise to the solution. The mixture was stirred at 0°C for 7 h after which TLC (EtOAc:PE=7:3) indicated full conversion. The solvents were then evaporated, the residue dissolved in EtOAc and washed with H_2O, a 1 M aq. HCl solution and a sat. $NaHCO_3$ solution. The organic layer was dried over Na_2SO_4 and evaporated to completeness in vacuo. This afforded 120 mg of S6e (0,24 mmol) as a white foam which was used in the next step without further purification. ^{1}H NMR (400 MHz, $CDCl_3$) δ 5.39 (t, J = 10.1 Hz, 1H), 5.25 (dd, J = 7.2, 2.2 Hz, 1H), 5.14 (td, J = 7.1, 3.0 Hz, 1H), 4.97 – 4.80 (m, 1H), 4.39 – 4.20 (m, 1H), 4.15 (dd, J = 10.7, 2.2 Hz, 1H), 3.94 (s, 3H), 3.37 (dd, J = 16.5, 3.6 Hz, 1H), 3.28 (dd, J = 13.5, 7.0 Hz, 1H), 2.14 (s, 3H), 2.11 (s, 3H), 2.07 (s, 3H), 1.89 (s, 3H). ^{19}F NMR (376 MHz, $CDCl_3$) δ -199.07 (dd, J = 49.5, 11.8 Hz).

[S7ae+aa]*Methyl 5-acetamido-4,7,8-tri-O-acetyl-9-azido-2,3,5,9-tetradeoxy-3-fluoro-D-erythro-β-L-manno-non-2-ulopyranosylonate fluoride & -α-L-manno-non-2-ulopyranosylonate fluoride*

360 mg of S6a (0,73 mmol) was dissolved in 15 ml dry DCM, cooled to -30°C with a Dewar cooling assembly and placed under N_2. 0,14 ml DAST (1,02 mmol, 1,4 eq.) was then added dropwise and the mixture was stirred at this temperature for 1h. The reaction was then quenched by addition of MeOH (50,5 µL) and the mixture concentrated in vacuo. The residue was dissolved in DCM and washed with water, a 1M aq. HCl solution and a sat. aq. $NaHCO_3$ solution. The organic layer was dried over Na_2SO_4 and the solvents removed to dryness affording an off-white foam. The crude was dry-loaded onto silica and flash column chromatography (EtOAc:PE = 4:6 → 8:2) afforded 143 mg of S7ae (0,29 mmol, major) + 80,2 mg of an impure S7aa-S7ea mixture (~0,16 mmol) as white foams. [S7ae] ^{1}H NMR (400 MHz,$CDCl_3$) δ 5.39 (d, J = 9.5 Hz, 1H), 5.33 – 5.28 (m, 1H), 5.24 (td, J = 6.4, 2.8 Hz, 1H), 5.21 – 5.02 (m, 1H), 4.32 – 4.25 (m, 1H), 4.12 (q, J = 10.5 Hz, 1H), 3.91 (s, 3H), 3.67 (dd, J = 13.6, 2.9 Hz, 1H), 3.33 (dd, J = 13.6, 6.0 Hz, 1H), 2.18 (s, 3H), 2.13 (s, 3H), 2.11 (s, 3H), 1.92 (s, 3H).^{19}F NMR (376 MHz, $CDCl_3$) δ -123.31 (d, J = 11.2 Hz), -216.92 (ddd, J = 50.9, 26.3, 11.4 Hz). [S7aa+S7ea] ^{1}H NMR (400 MHz, $CDCl_3$) δ 5.48 – 5.40 (m, 1H), 5.36 – 5.30 (m, 1H), 5.24 – 5.04 (m, 2H), 4.28 (d, *J* = 10.7 Hz, 1H), 4.11 (q, *J* = 7.2 Hz, 1H), 3.89 (d, *J* = 1.4 Hz, 3H), 3.79 (dd, *J* = 13.6, 2.8 Hz, 1H), 3.37 (dd, *J* = 13.6, 6.8 Hz, 1H), 2.16 (s, 3H), 2.10 (s, 3H), 2.09 (s, 3H), 1.90 (s, 3H). ^{19}F NMR (376 MHz, $CDCl_3$) δ -118.00 (t, *J* = 13.7 Hz, S7ea), -122.07 (dd, *J* = 16.2, 3.1 Hz, S7aa), -199.63 (dt, *J* = 48.9, 14.1 Hz, S7ea), -206.52 – -206.85 (m,S7aa).

[S7ea] *Methyl 5-acetamido-4,7,8-tri-O-acetyl-9-azido-2,3,5,9-tetradeoxy-3-fluoro-D-erythro-α-L-gluco-non-2-ulopyranosylonate fluoride*

120 mg of S6e (0,24 mmol) was dissolved in 5 ml dry DCM, cooled to -30°C with a Dewar cooling assembly and placed under N_2. 0,05 ml DAST (0,34 mmol, 1,4 eq.) was then added and the mixture was stirred at this temperature for 40 min. The

reaction was then quenched by addition of MeOH (16,8 µL) and concentrated in vacuo. The residue was dissolved in DCM and washed with water, a 1M aq. HCl solution and a sat. aq. $NaHCO_3$ solution. The organic layer was dried over Na_2SO_4 and the solvents removed to dryness affording an off-white foam. The crude was dry-loaded onto silica and flash column chromatography (EtOAc:PE= 4:6→7:3) afforded 65 mg of S7ea (0,13 mmol) as a white foam. ^{1}H NMR (400 MHz, $CDCl_3$) δ 5.55 (dt, J = 14.9, 9.2 Hz, 1H), 5.41 (d, J = 10.0 Hz, 1H), 5.26 – 5.14 (m, 2H), 4.46 (d, J = 10.7 Hz, 1H), 4.36 (q, J = 10.3 Hz, 1H), 3.89 (s, 3H), 3.50 (dd, J = 13.4, 2.9 Hz, 1H), 3.31 (td, J = 14.1, 5.4 Hz, 1H), 2.15 (s, 3H), 2.09 (d, J = 1.7 Hz, 7H), 1.91 (s, 3H). ^{19}F NMR (376 MHz, $CDCl_3$) δ -118.00 (t, J = 13.7 Hz), -199.62 (dt, J = 48.7, 14.0 Hz).

4.2 Synthesis of 4-{(Z/E)-[4-(methoxycarbonyl)-2,6-difluorophenyl] -diazenyl}-3,5-difluorobenzoic acid

Tert-butyl hypochlorite

50 ml of a NaOCl solution (12% active chlorine) was placed under N_2 and cooled below 10°C with an ice bath. Then a solution of tert-butanol (3,7 ml) and acetic acid (2,5 ml) were added and the mixture was stirred intensively for 5 min. The mixture was placed in a separatory funnel, the aq. layer removed, washed with a 10% $NaHCO_3$ solution and water. The yellow liquid was used as such in the next step.

[A1] *Diethyl 4,4'-[(Z/E)-diazenediyl]bis(3,5-difluorobenzoate)*

This procedure was carried out in the absence of light

Ethyl 4-amino-3,5-difluorobenzoate (500 mg, 2,48 mmol) was dissolved in 15 ml dry Et_2O after which 758 mg NaI (5,06 mmol, 2,04 eq.) was added. The apparatus was flushed with N_2, 0,6 ml freshly prepared t-BuOCl (~2 eq.) was added and the mixture was stirred overnight. The next day, TLC (EtOAc:PE = 2:8) indicated that some starting material was still present so another 0,3 ml of t-BuOCl was added and the mixture was stirred for 1h. After this time TLC indicated full conversion, the reaction was quenched with 40 ml of a 1M $Na_2S_2O_3$ solution and the aq. phase was extracted twice with DCM. The org. phase was dried over Na_2SO_4 and concentrated in vacuo. The crude was dry-loaded onto silica after which flash column chromatography (DCM:PE=2:1) afforded 350 mg of A1 (1,74 mmol, 70%) as a red powder. [88% trans : 12% cis] [A1-cis] ^{1}H NMR (400 MHz, $CDCl_3$) δ 7.77 – 7.69 (m, 4H), 4.42 (q, J = 7.1 Hz, 4H), 1.41 (t, J = 7.1 Hz, 6H). ^{19}F NMR (376 MHz, $CDCl_3$) δ -119.54 (d, J = 8.8 Hz). (dd, J = 7.1, 2.4 Hz).[A1-trans] ^{1}H NMR (400 MHz, $CDCl_3$) δ 7.54 – 7.49 (m, 4H), 4.31 (q, J = 7.1 Hz, 4H), 1.35 (td, J = 7.2, 2.2 Hz, 6H). ^{19}F NMR (376 MHz, $CDCl_3$) δ -132.98.

[A2] *4,4'-[(Z/E)-diazenediyl]bis(3,5-difluorobenzoic acid)*

This procedure was carried out in the absence of light

350 mg of A1 (1,74 mmol) was dissolved in 16 ml THF and flushed with N_2, after which 4,2 ml of a 1 M aq. NaOH solution was added. The solution was stirred for 4 h when TLC (DCM:MeOH:TFA=9:0,9:0,1) showed full consumption of the starting material. The solution was neutralized with an aq. 1M HCl solution, extracted with EtOAc (3 x) and washed with a sat. aq. brine solution. The organic layer was then dried over Na_2SO_4 and the solvents evaporated in vacuo affording 120 mg of A2 as an red/orange solid. Therefore the aq. layer was co-evaporated with toluene in vacuo for a combined mass of 3 g A2 + residual salts as a orangish solid. The -

crude was dry-loaded onto silica, filtered over silica-gel (DCM:MeOH: TFA = 8 : 1,99 : 0,01) and the solvents removed in vacuo to afford 295 mg of A2 (~1,74 mmol) as a red/orange solid. The product contained EtOAc but was used as such in the next step. ^{1}H NMR (400 MHz, CD_3OD) δ 7.81 – 7.74 (m, 4H, trans), 7.59 (d, J = 7.7 Hz, 1H, cis). ^{19}F NMR (376 MHz, CD_3OD) δ -120.85 (d, J = 7.0 Hz, cis), -122.11 (d, J = 9.8 Hz, trans).

4.3 Synthesis of (E)-1-methyl-3-(((triisopropylsilyl)ethynyl)diazenyl)-1H-indazole

[E1] *3-Amino-1-methyl-1H-indazole*

A mixture of 1,08 ml 2-fluorobenzonitrile (10,0 mmol) and 2,8 ml methylhydrazine (50,0 mmol, 5 eq.) in EtOH (10.0 mL) was heated to reflux (70°C). After 9 h, the mixture was cooled to RT and then concentrated in vacuo. H_2O (10.0 mL) and EtOAc (20.0 mL) were added to the residue. The organic layer was washed with H_2O (10.0 mL), brine (10.0 mL), dried over Na_2SO_4, filtered, and concentrated in vacuo. The yellow crude solution was briefly cooled with liquid N_2, the solid was collected and washed with cooled PE. This process was repeated 3 times to afford 0,717 g E1 (4,9 mmol) as a yellow solid. ^{1}H NMR (400 MHz, $CDCl_3$) δ 7.52 (d, J = 8.1 Hz, 1H), 7.37 – 7.29 (m, 1H), 7.19 (dt, J = 8.5, 0.9 Hz, 1H), 7.00 (ddd, J = 7.8, 6.8, 0.9 Hz, 1H), 4.02 (s, 2H), 3.83 (s, 3H).

[E2] *1-(N-methyl-1H-indazole)diazonium tetrafluoroborate*

This procedure was carried out in the absence of light

300 mg of E1 (~2,0 mmol) was dissolved in dry THF (4 mL) and cooled with an ice bath to 0°C. Then, $BF_3{\cdot}Et_2O$ (0,2 ml, 2,4 mmol, 1,2 eq.) was added dropwise, after which 0,28 ml t-BuONO (2,4 mmol, 1,2 eq.) in THF (1,6 ml) was added dropwise and the mixture was stirred at 0°C for 30 min. The precipitate was collected, washed with excess Et_2O and dried in vacuum to obtain E2 which was used directly in the next step.

[Γ$_{\alpha\varepsilon}$] *(E)-1-methyl-3-(((triisopropylsilyl) ethynyl)diazenyl)-1H-indazole*

This procedure was carried out in the absence of light

0,44 ml TIPSA (2 mmol, 1 eq.) was dissolved in dry THF (6 ml), cooled to 0°C and placed under N_2. After inert conditions had been established, 0,8 ml n-BuLi in hexane (2,5 M, ~2,2 mmol, 1,1 eq.) was added dropwise. The reaction was stirred for 30 min at 0°C. In the meantime, E2 was suspended in dry THF (6 ml), cooled to -78°C with the Julabo FT903 cooling assembly and placed under N_2. After the 30 min mark the n-BuLi mixture was quickly transferred to the diazonium salt solution. The mixture was stirred for 15 min at -78°C after which it was allowed to reach RT (~2,2°C/min) (45 min). The reaction was quenched with a sat. aq. $NaHCO_3$ solution (4 ml) and extracted with EtOAc (3x 4 mL). The organic layer was washed with (8 ml) brine, dried over Na_2SO_4 and concentrated in vacuo. The crude was dry-loaded onto silica and flash column chromatography (PE:DCM = 4:1 → 1:1) afforded 383 mg of E3 as a red/orange solid (1,12 mmol). ^{1}H NMR (400 MHz, $CDCl_3$) δ 8.17 (dt, J = 8.1, 1.0 Hz, 1H), 7.48 (ddd, J = 8.4, 6.8, 1.1 Hz, 1H), 7.42 (dt, J = 8.4, 1.0 Hz, 1H), 7.34 (ddd, J = 8.0, 6.8, 1.1 Hz, 1H), 4.21 (s, 3H), 1.16 – 1.14 (m, 18H)

5. Appendix

5.1 Spectroscopic Data – Nuclear Magnetic Resonance (NMR) Spectroscopy

[S1] *2-Acetamido-2-deoxy-6-tosyl-D-mannopyranose + Pyridinium p-toluene sulfonate*

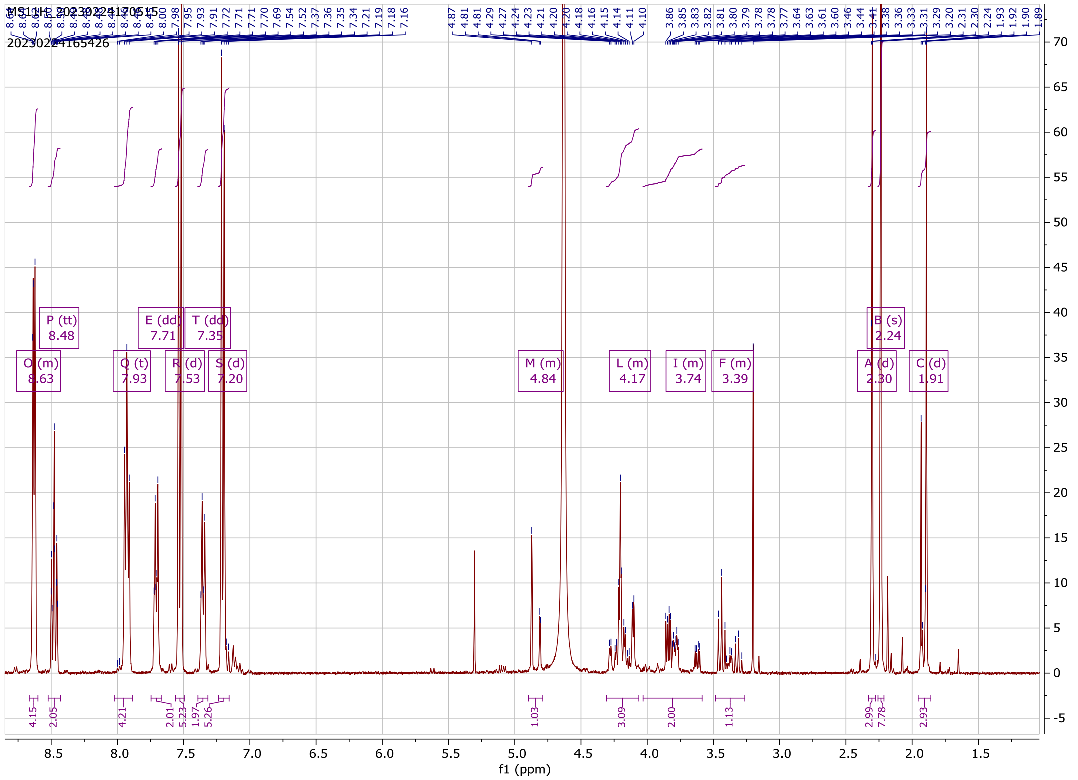

[S1*] *2-Acetamido-1,3,4-tri-O-acetyl-2-deoxy-6-tosyl-D-mannopyranose*

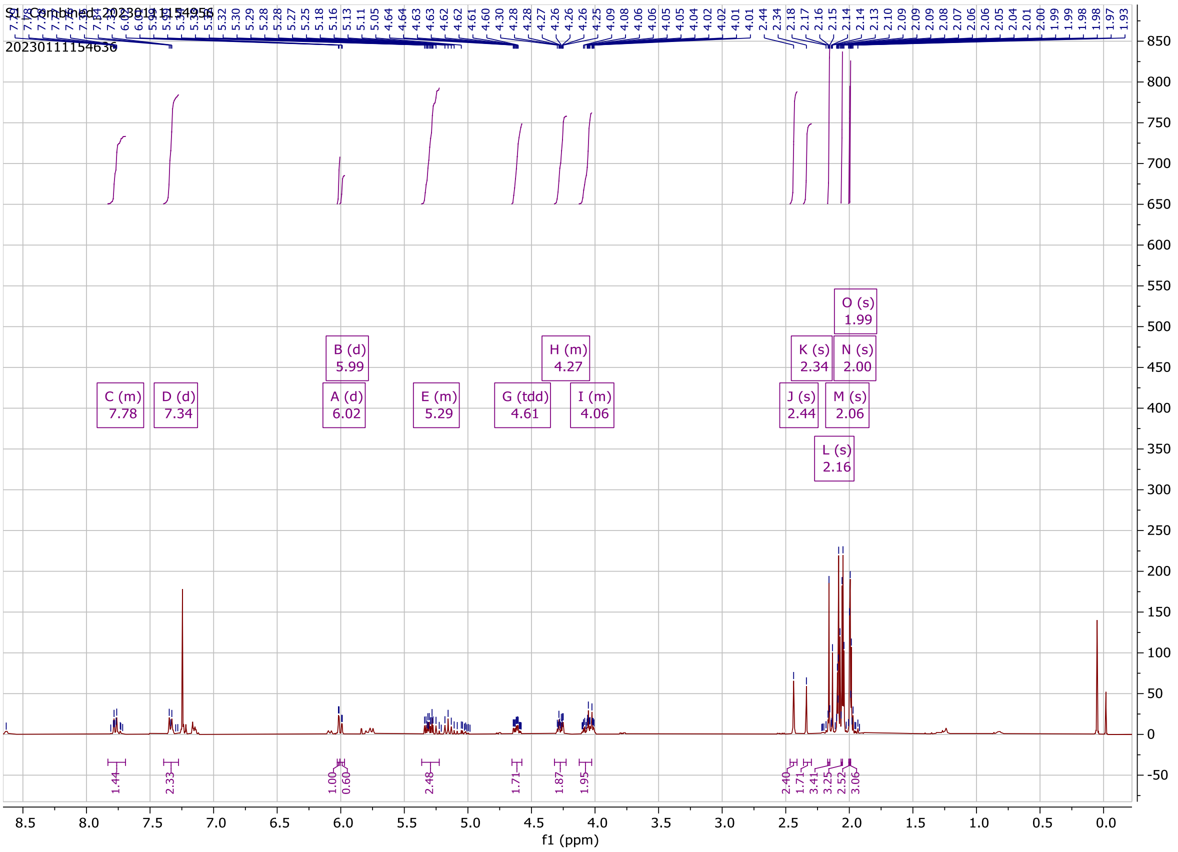

[S2] *2-Acetamido-6-azido-2,6-dideoxy-α-D-mannopyranose*

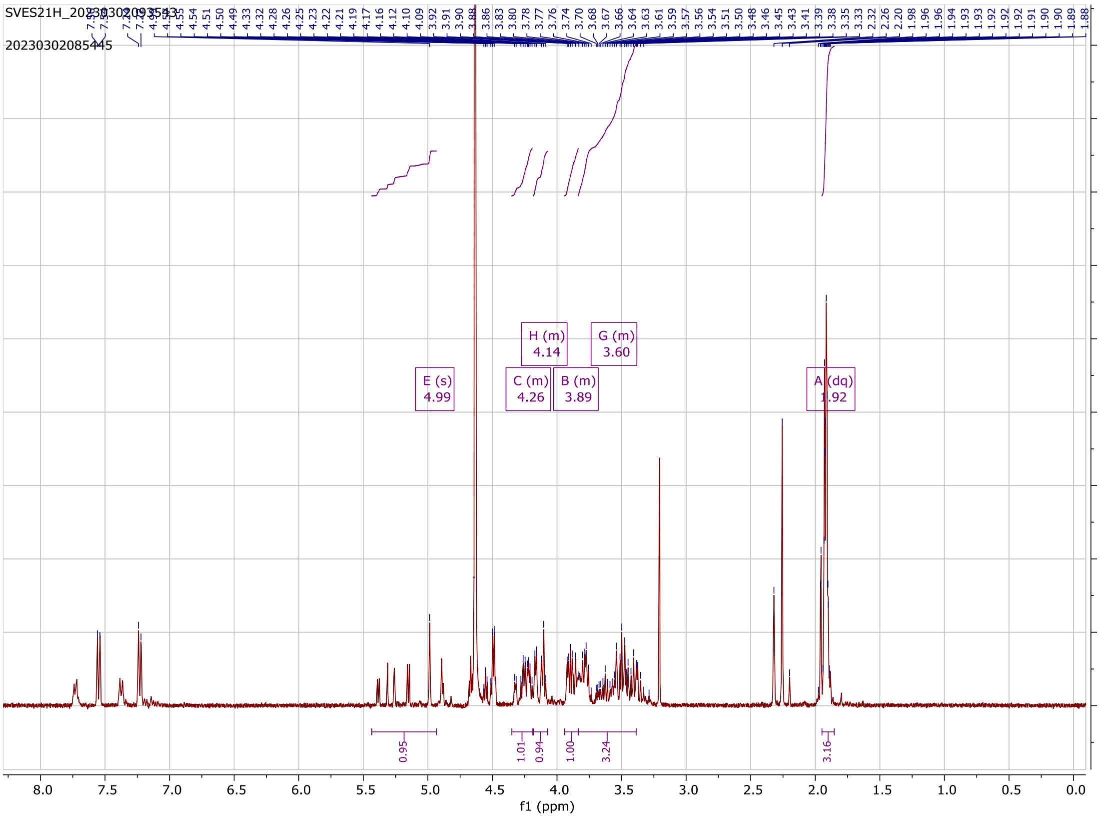

[S2*] *2-Acetamido-1,3,4-tri-O-acetyl-6-azido-2,6-dideoxy-D-mannopyranose*

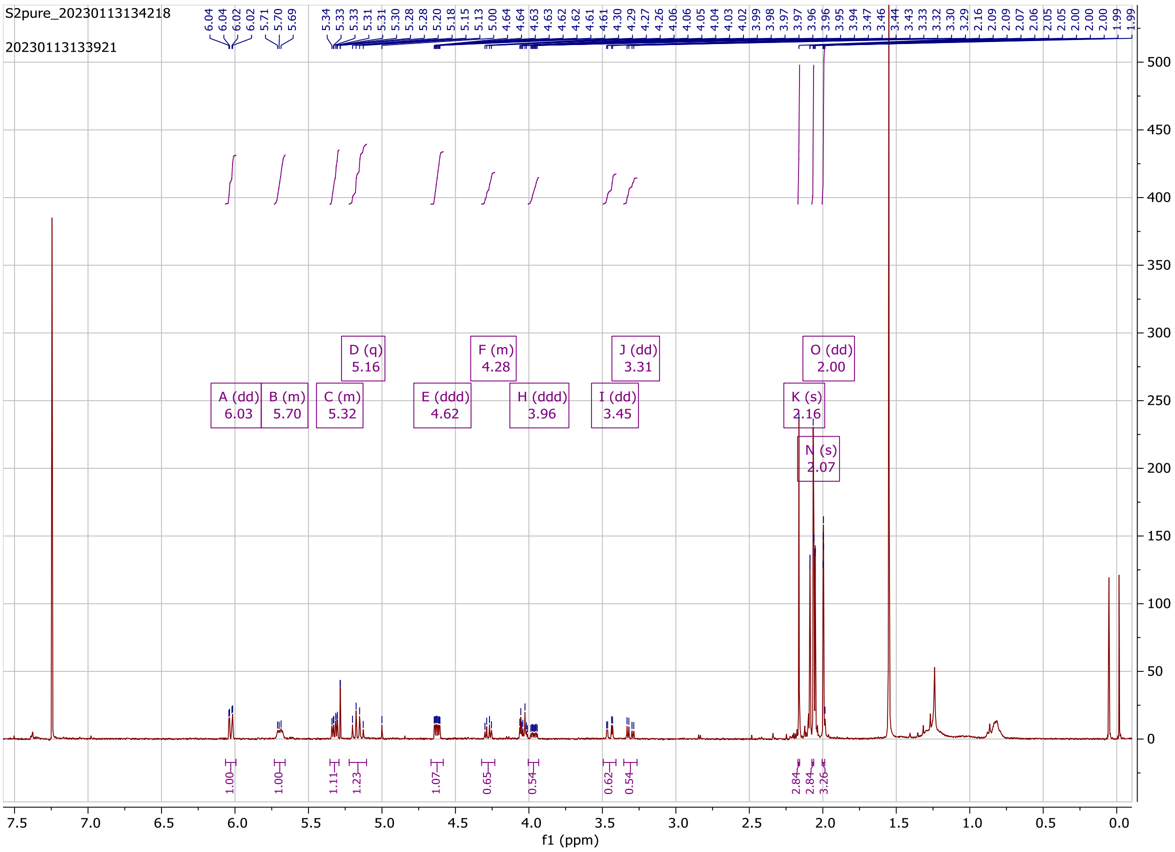

[S3a+e] *5-Acetamido-9-azido-3,5,9-trideoxy-3-fluoro-D-erythro-α-L-manno-non-2-ulopyranosonic acid & Gluco-non-2-ulopyranosonic acid*

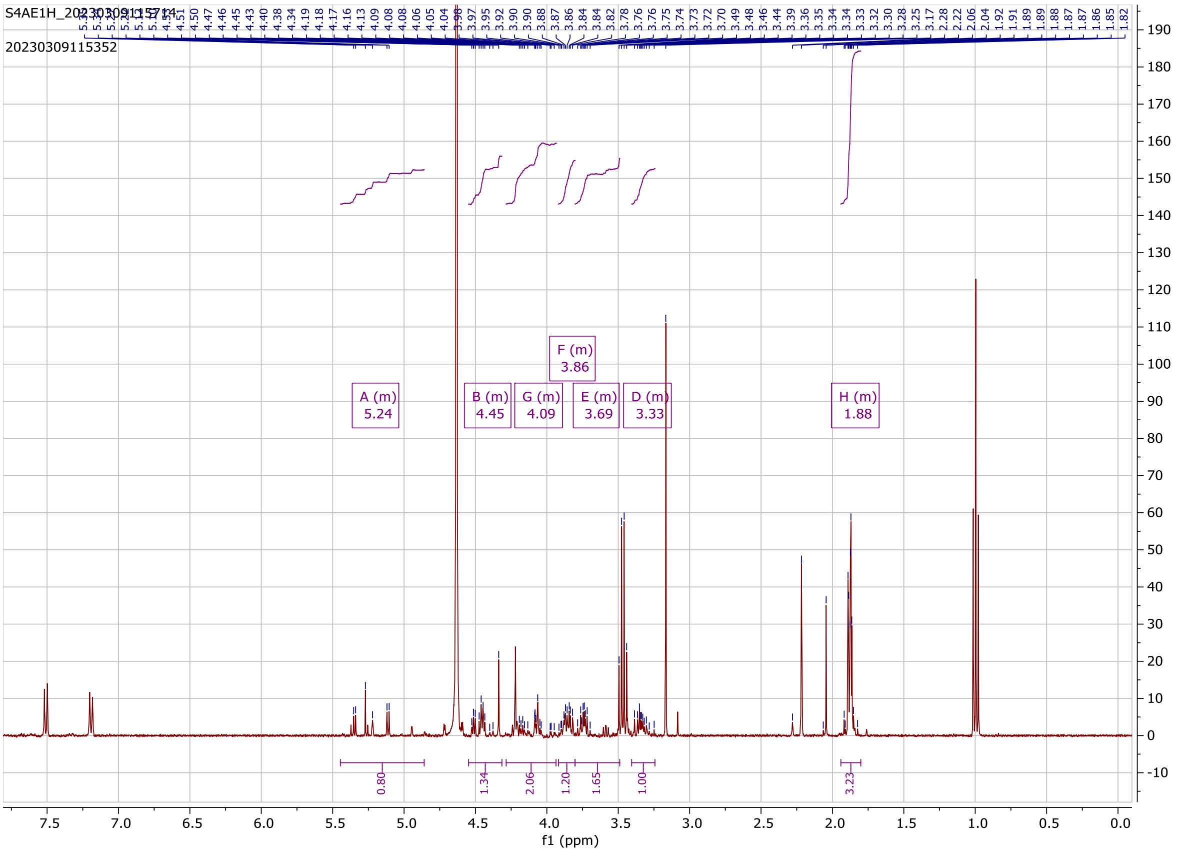

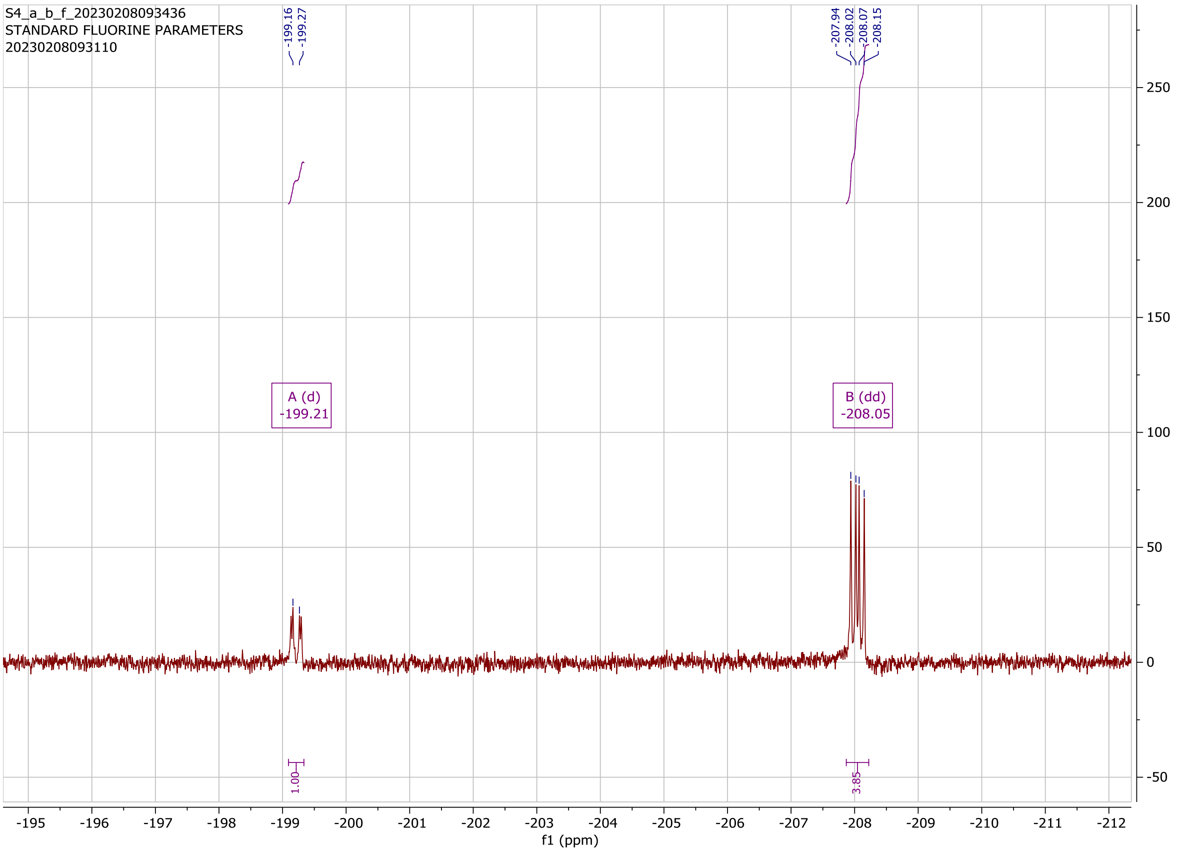

[S4a] ***Methyl 5-acetamido-9-azido-3,5,9-trideoxy-3-fluoro-D-erythro-α-L-manno-non-2-ulopyranosonate*** **&** **[4e]** ***gluco-non-2-ulopyranosonate***

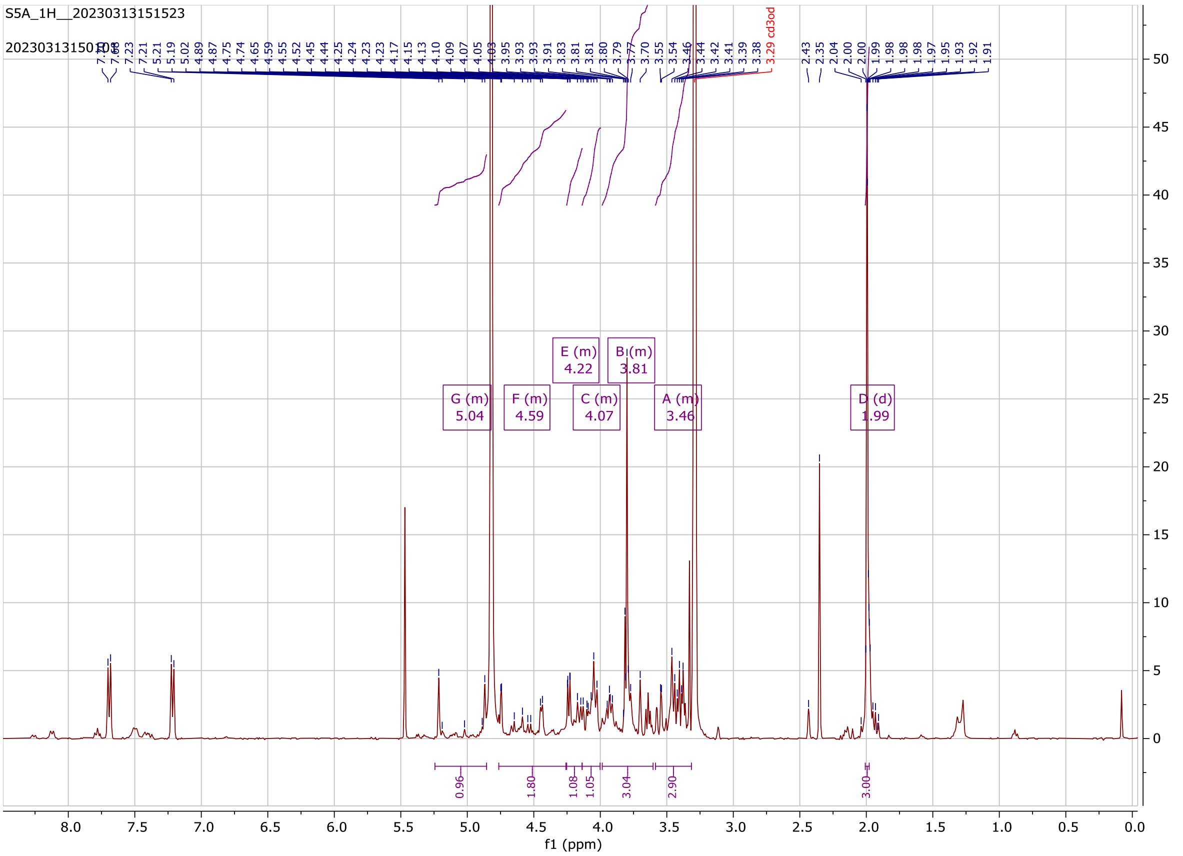

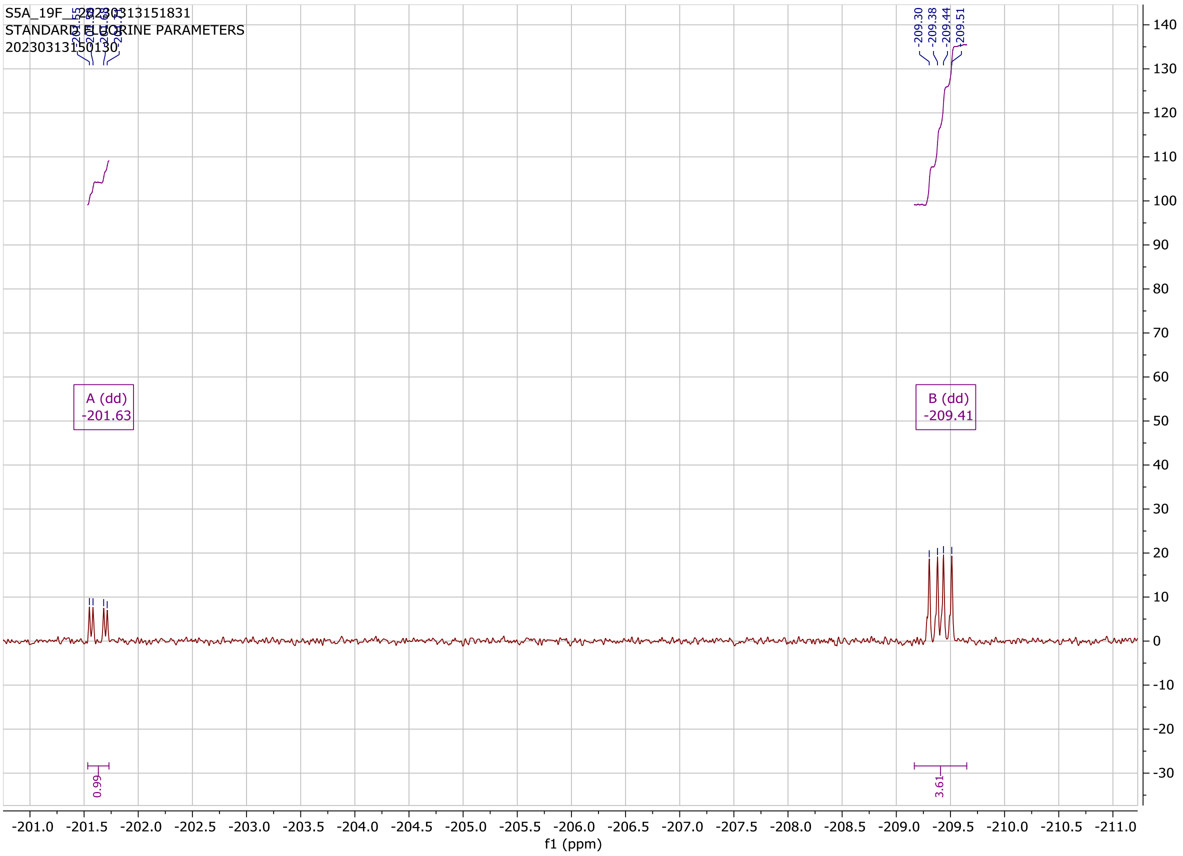

[S5a] *Methyl 5-acetamido-2,4,7,8-tetra-O-acetyl-9-azido-3,5,9-trideoxy-3-fluoro-D-erythro-α-L-manno-non-2-ulopyranosonate*

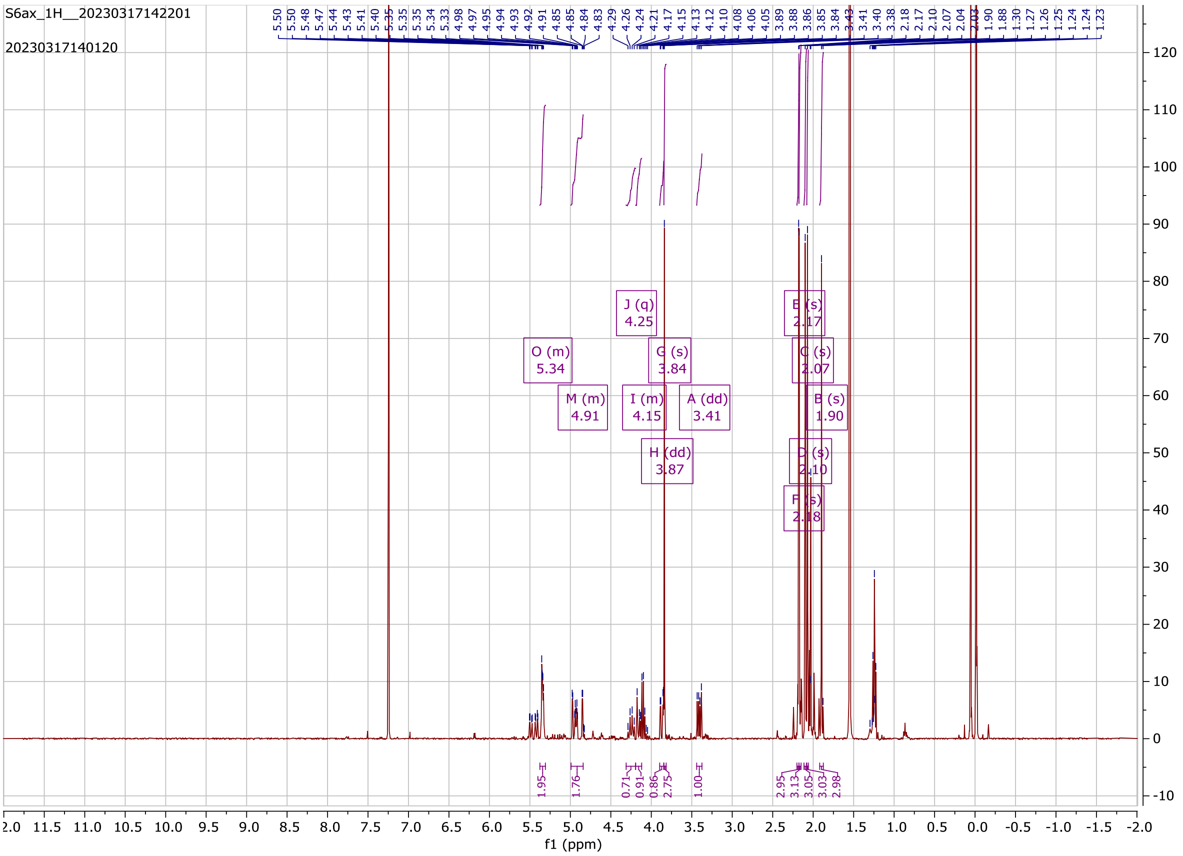

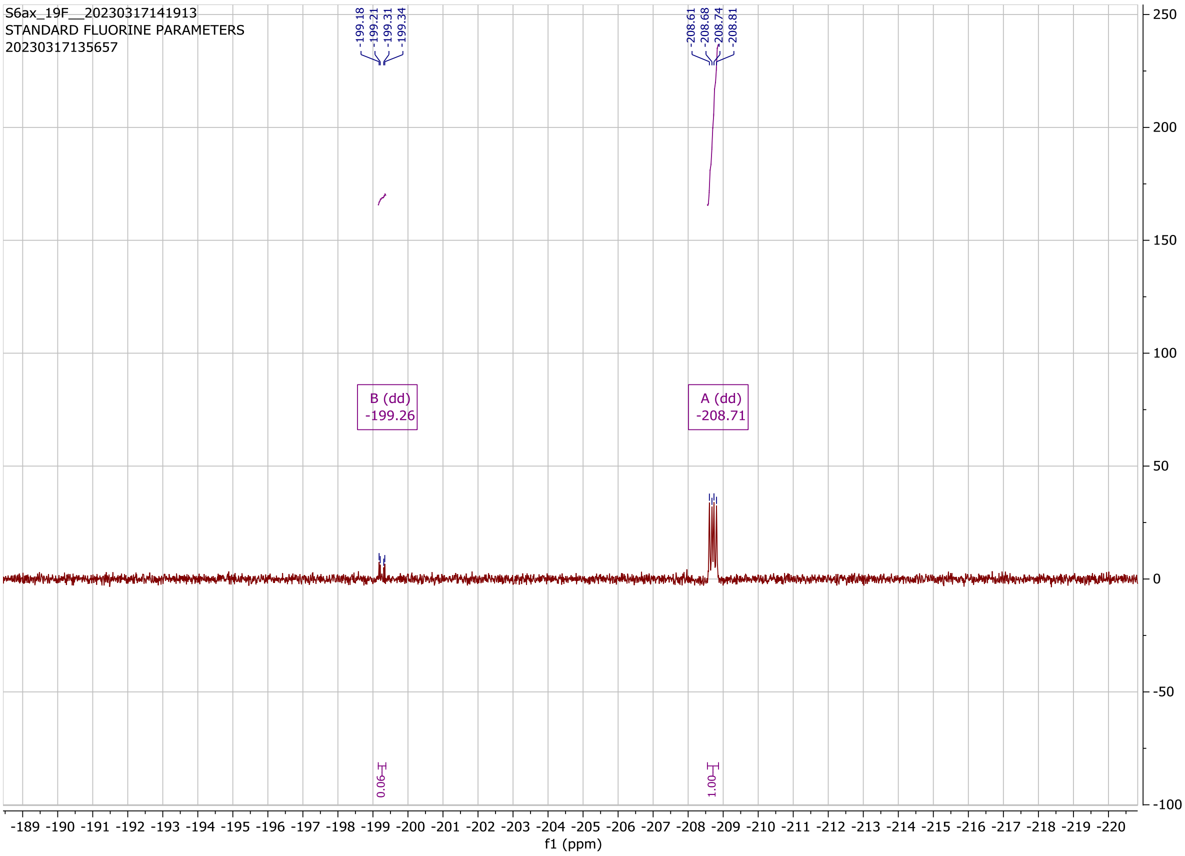

[S5e] *Methyl 5-acetamido-2,4,7,8-tetra-O-acetyl-9-azido-3,5,9-trideoxy-3-fluoro-D-erythro-α-L-gluco-non-2-ulopyranosonate*

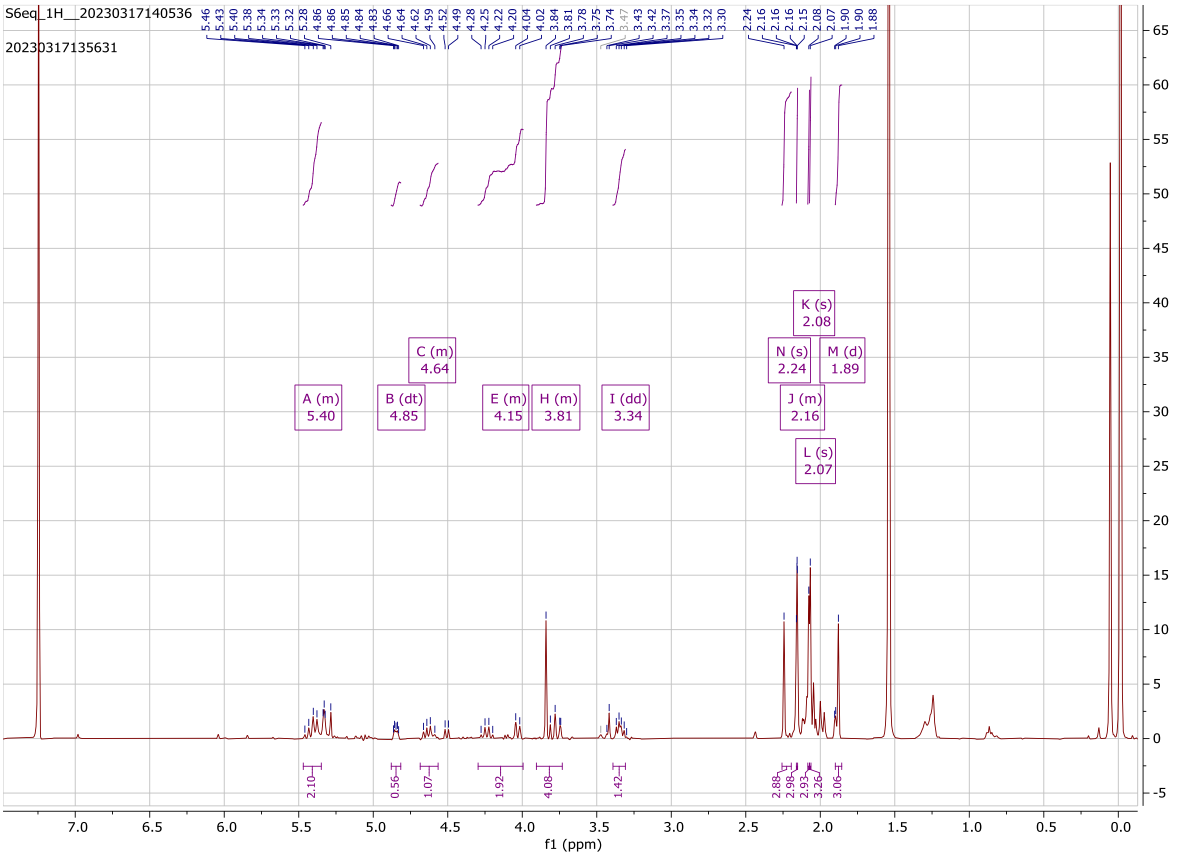

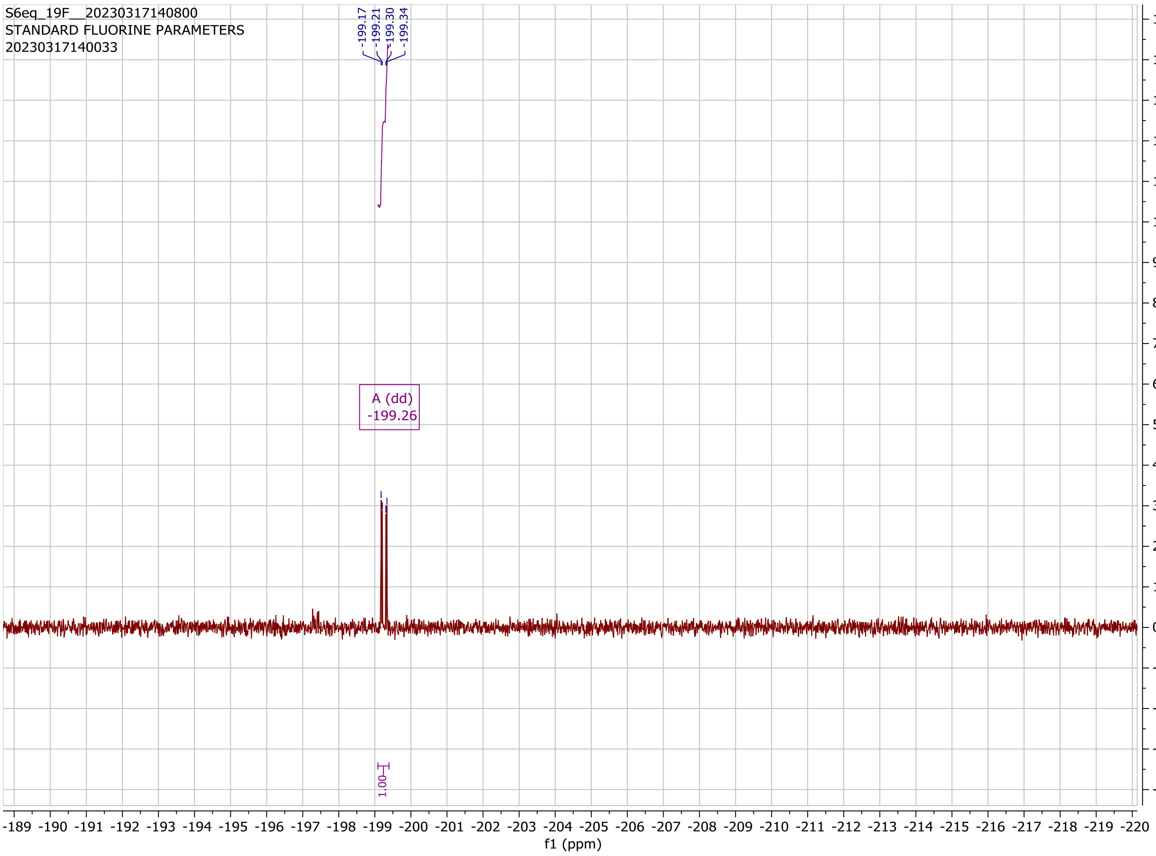

[S6a] *Methyl 5-acetamido-4,7,8-tri-O-acetyl-9-azido-3,5,9-trideoxy-3-fluoro-D-erythro-α-L-manno-2-non-2-ulopyranosonate*

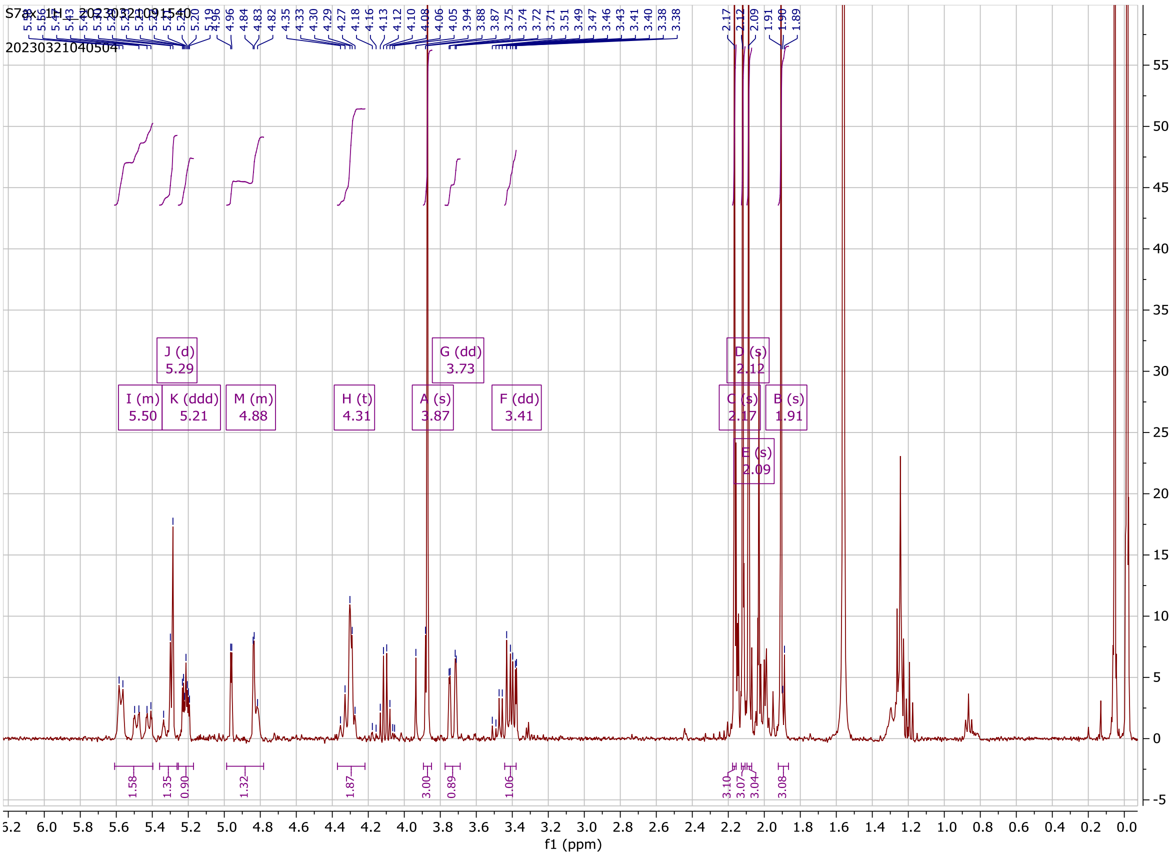

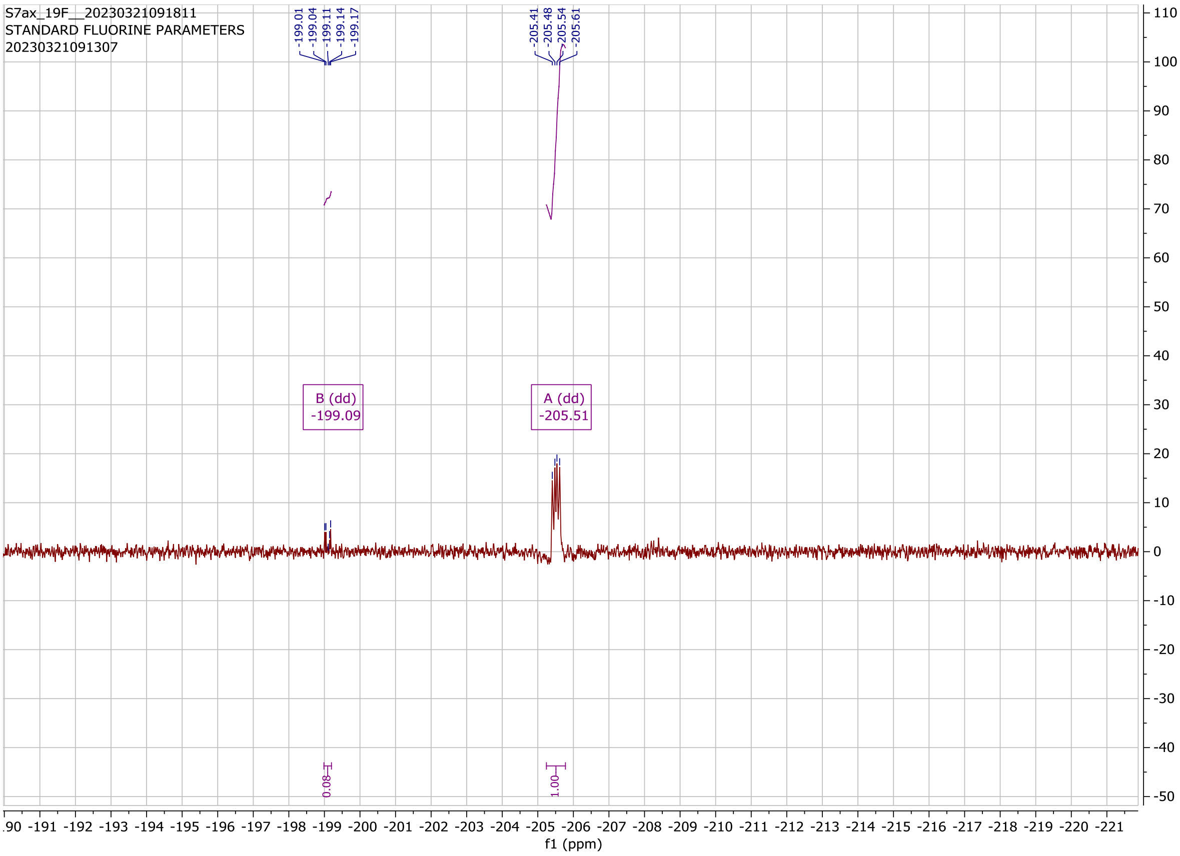

[S6e] *Methyl 5-acetamido-4,7,8-tri-O-acetyl-9-azido-3,5,9-trideoxy-3-fluoro-D-erythro-α-L-gluco-2-non-2-ulopyranosonate*

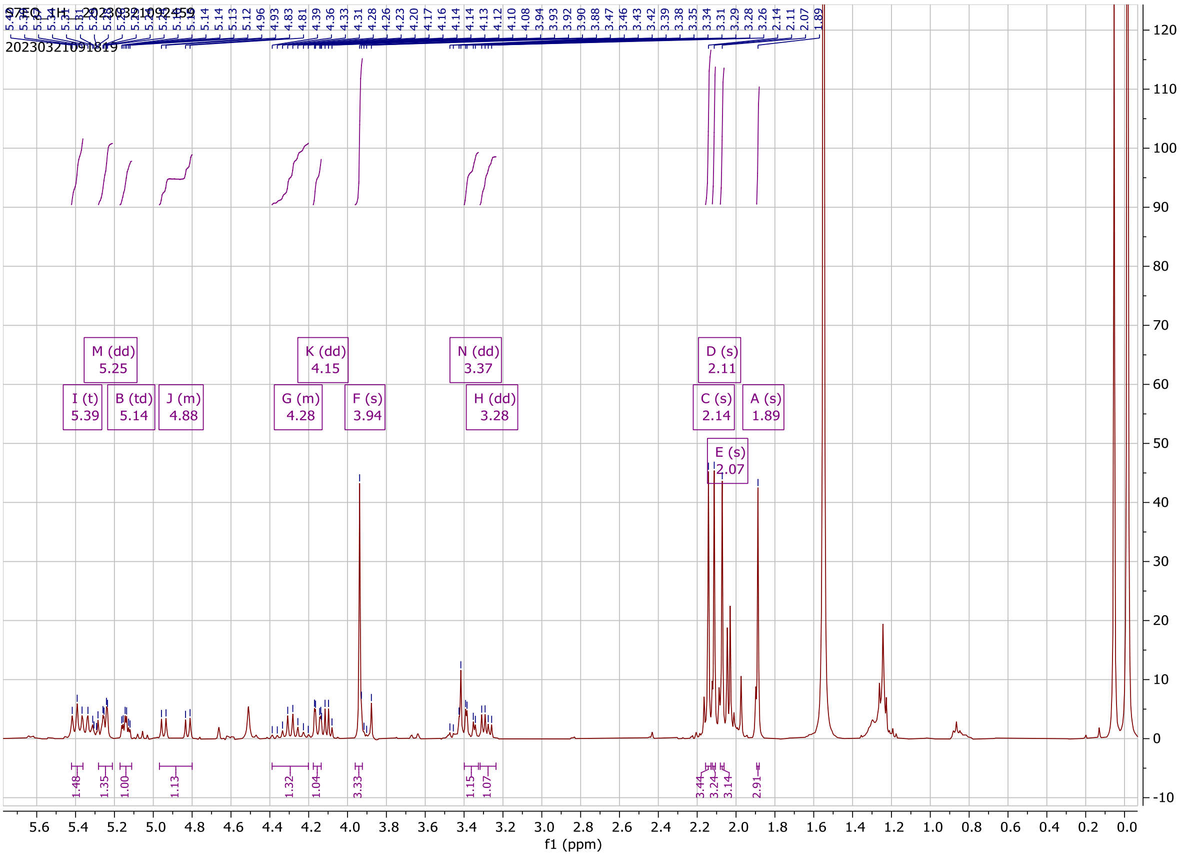

[S7ae]Methyl 5-acetamido-4,7,8-tri-O-acetyl-9-azido-2,3,5,9-tetradeoxy-3-fluoro-D-erythro-β-L-manno-non-2-ulopyranosylonate fluoride

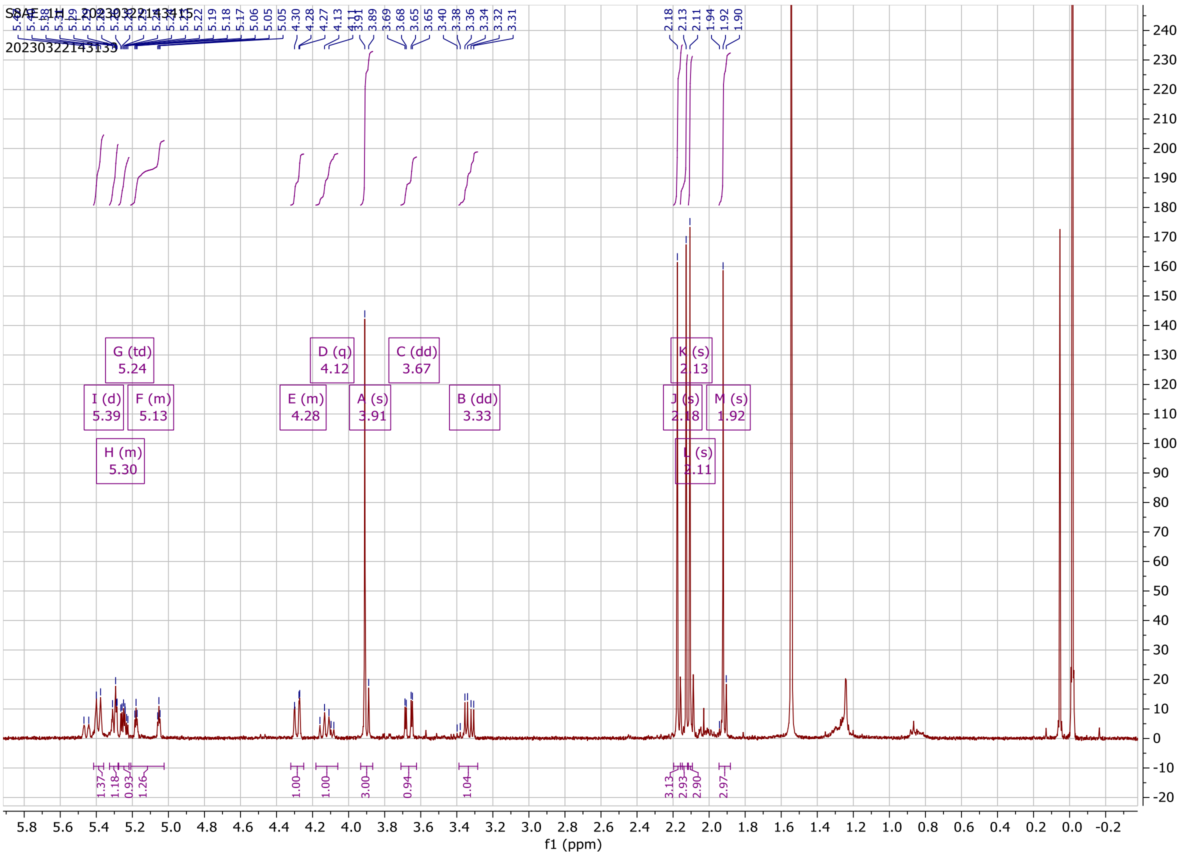

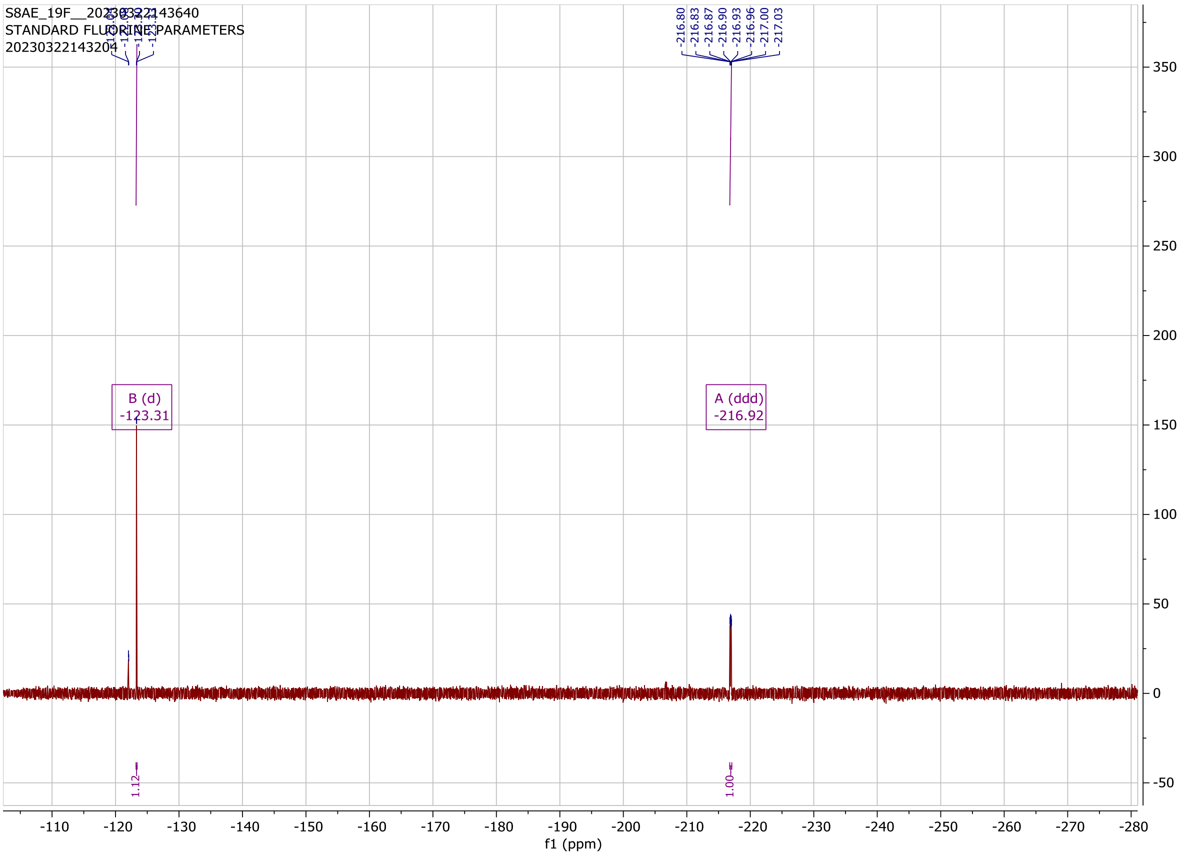

[S7aa+ea] *Methyl 5-acetamido-4,7,8-tri-O-acetyl-9-azido-2,3,5,9-tetradeoxy-3-fluoro-D-erythro-α-L-manno-non-2-ulopyranosylonate fluoride*

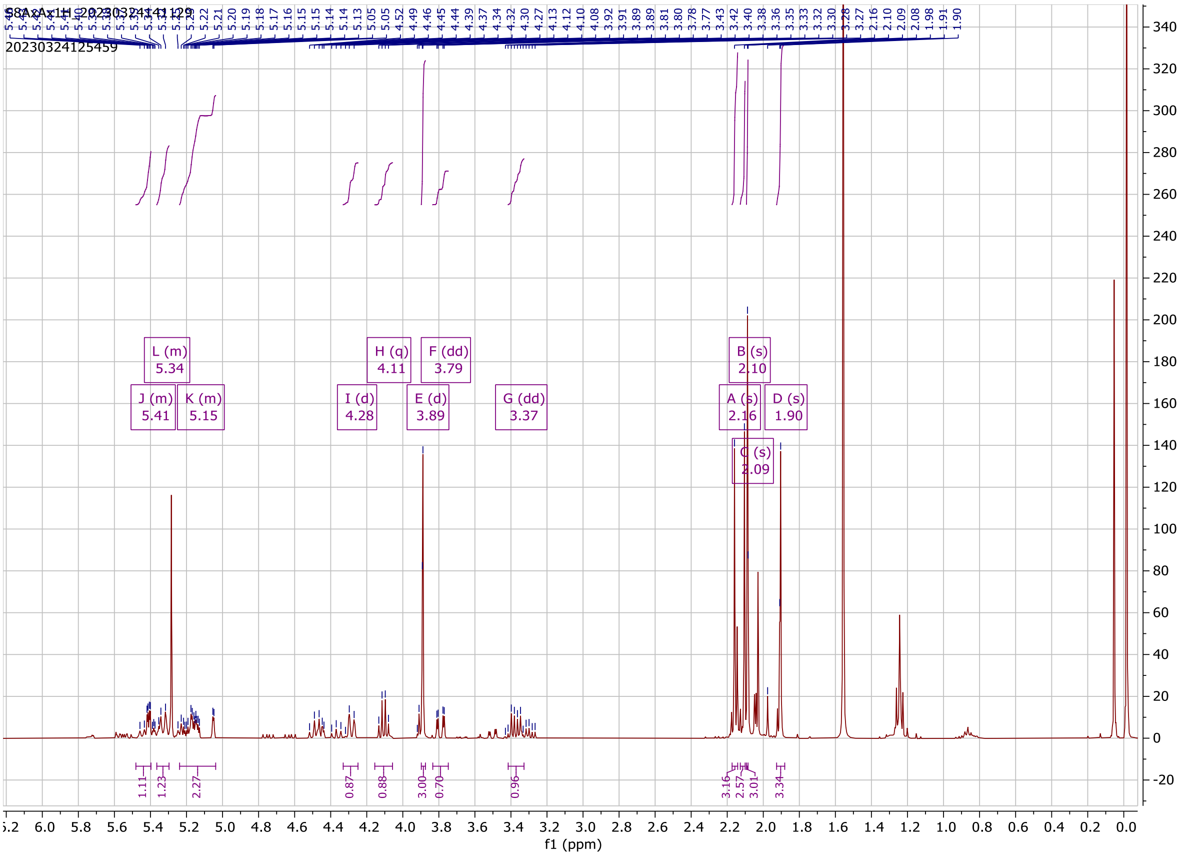

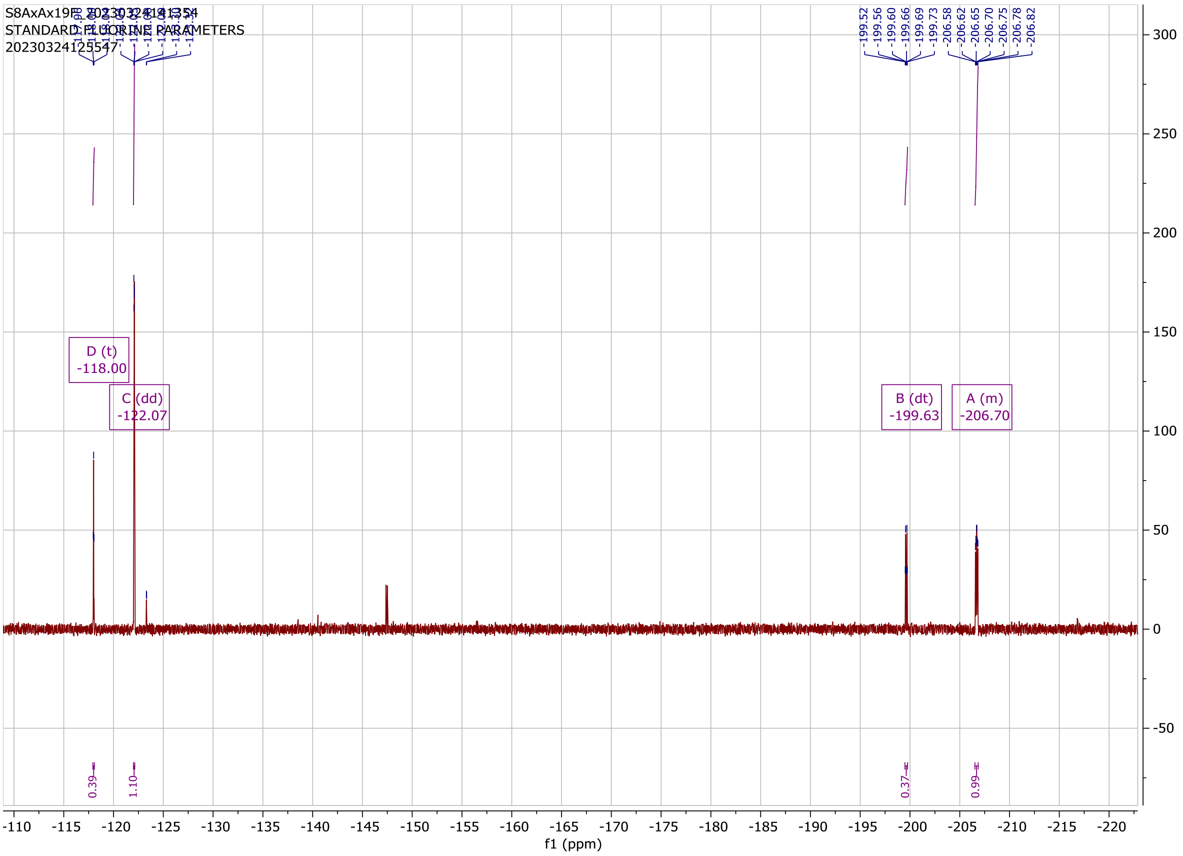

[S7ea] *Methyl 5-acetamido-4,7,8-tri-O-acetyl-9-azido-2,3,5,9-tetradeoxy-3-fluoro-D-erythro-α-L-gluco-non-2-ulopyranosylonate fluoride*

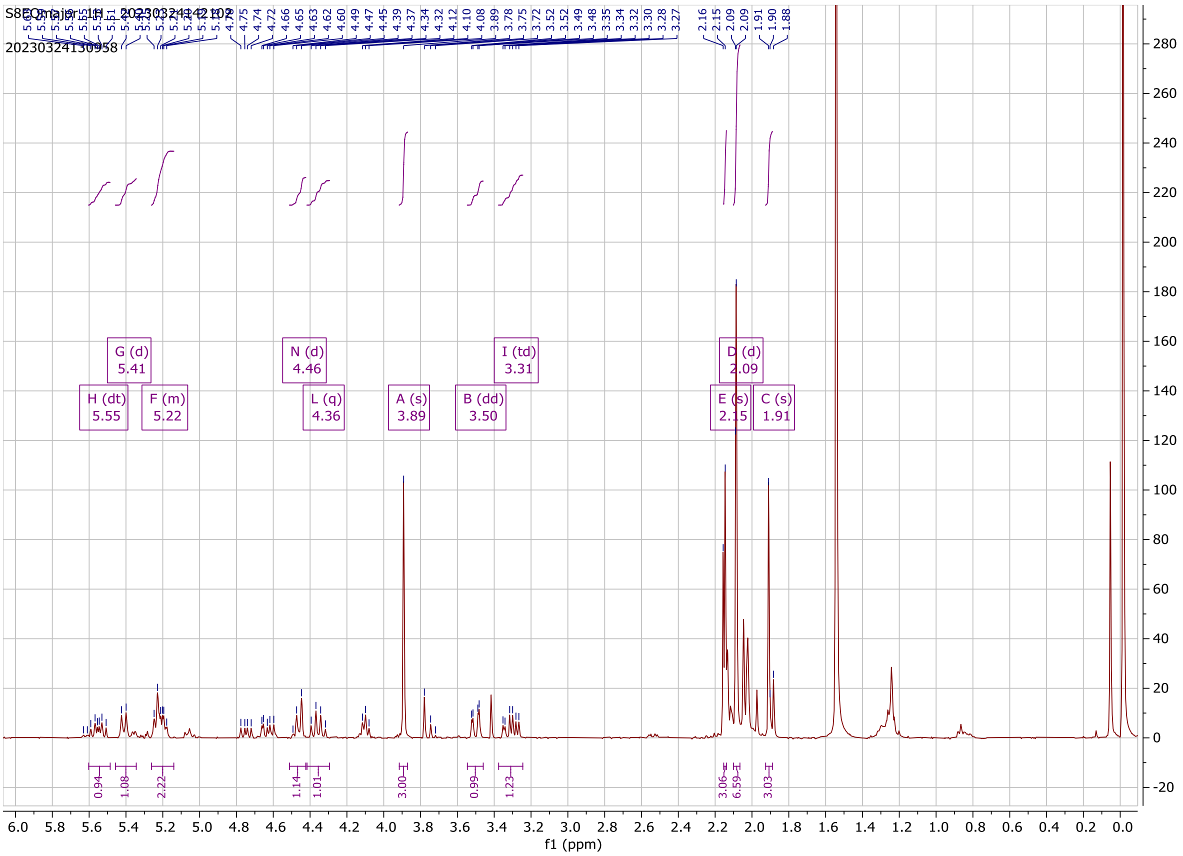

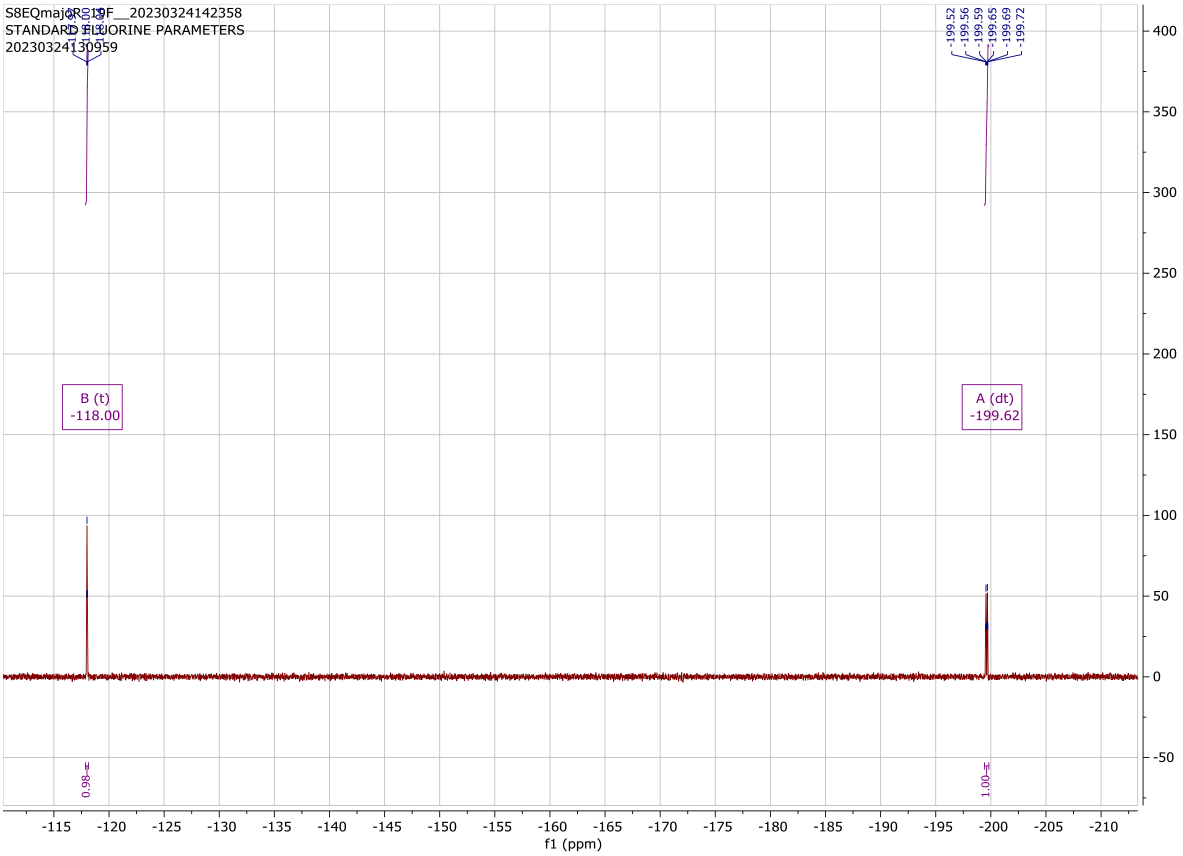

[A1] *Diethyl 4,4'-[(Z/E)-diazenediyl]bis(3,5-difluorobenzoate)*

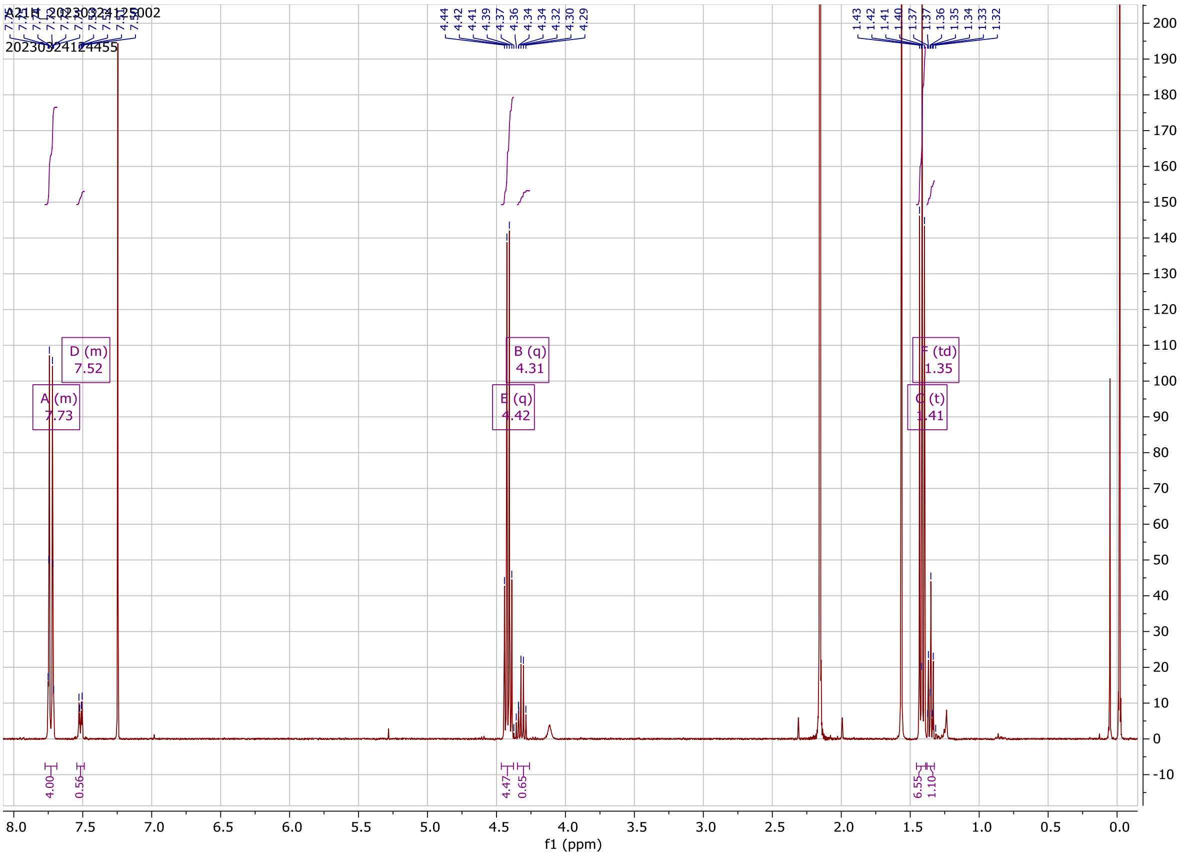

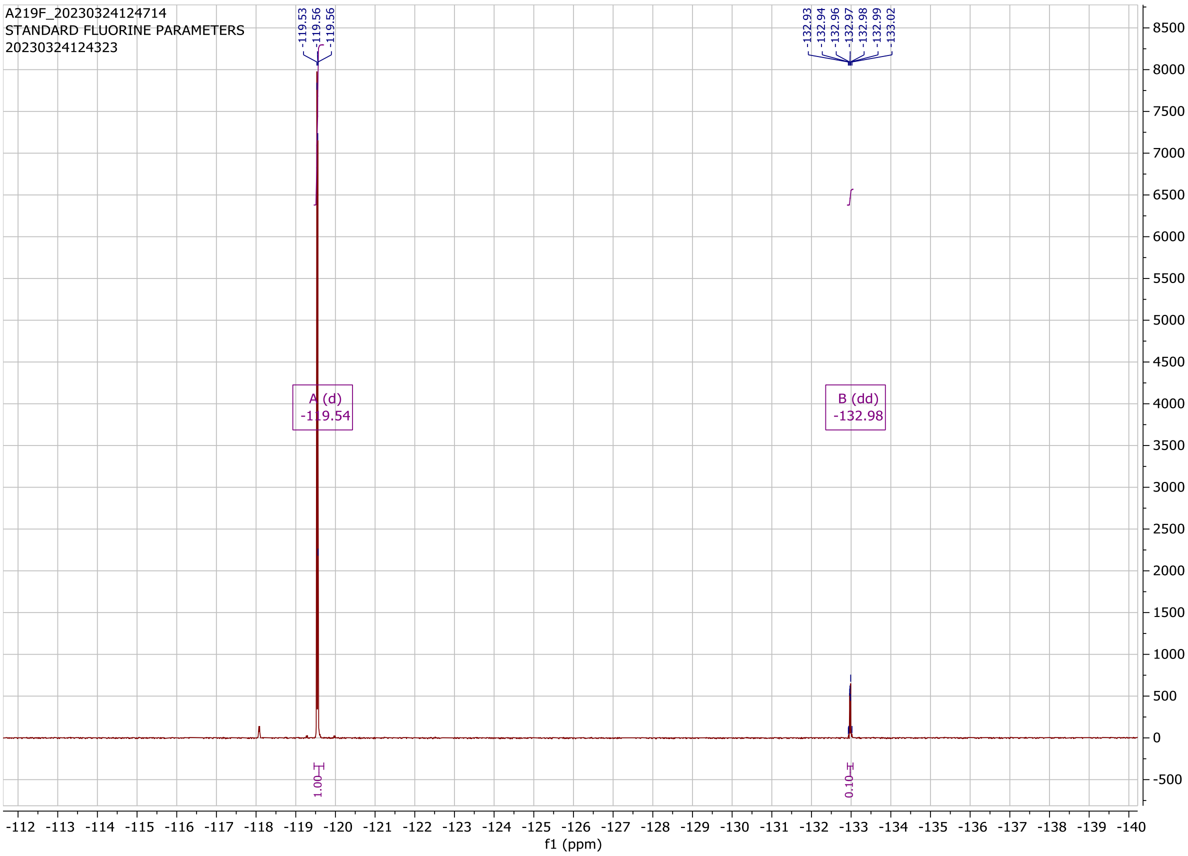

[A2] *4,4'-[(Z/E)-diazenediyl]bis(3,5-difluorobenzoic acid)*

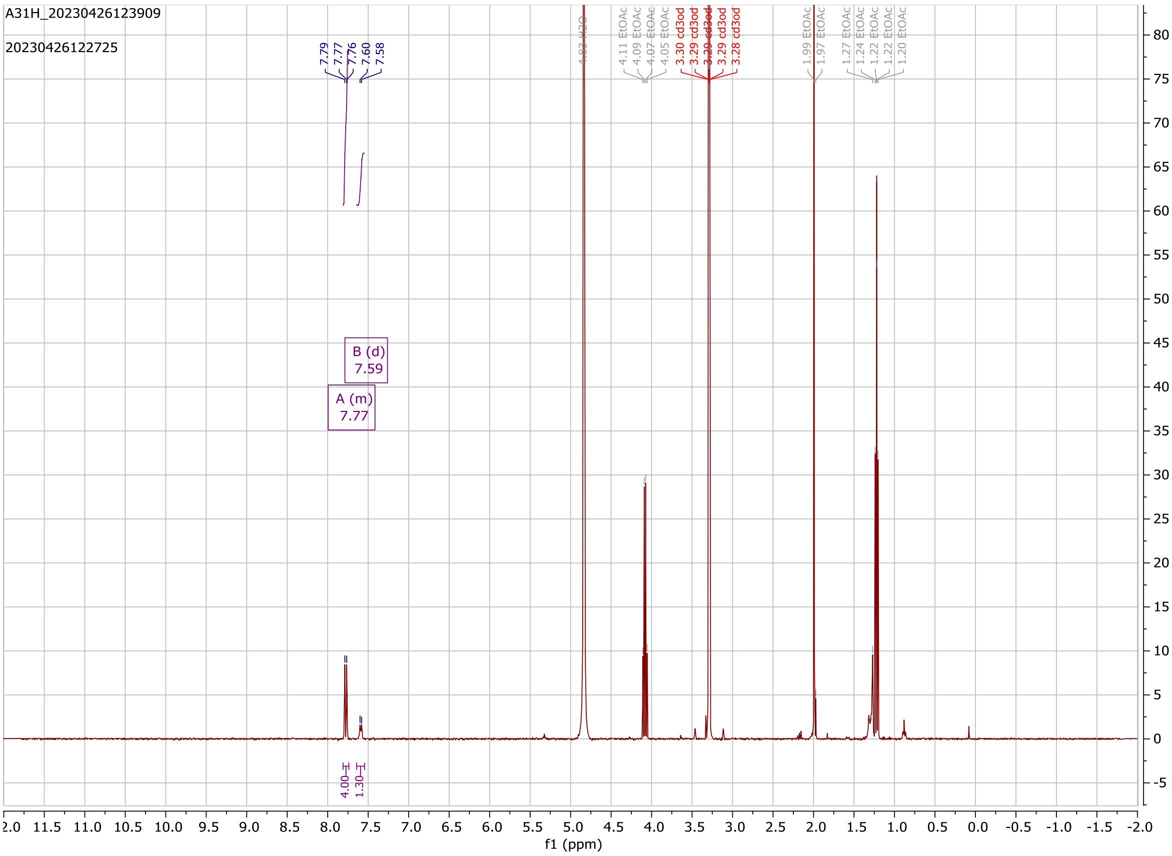

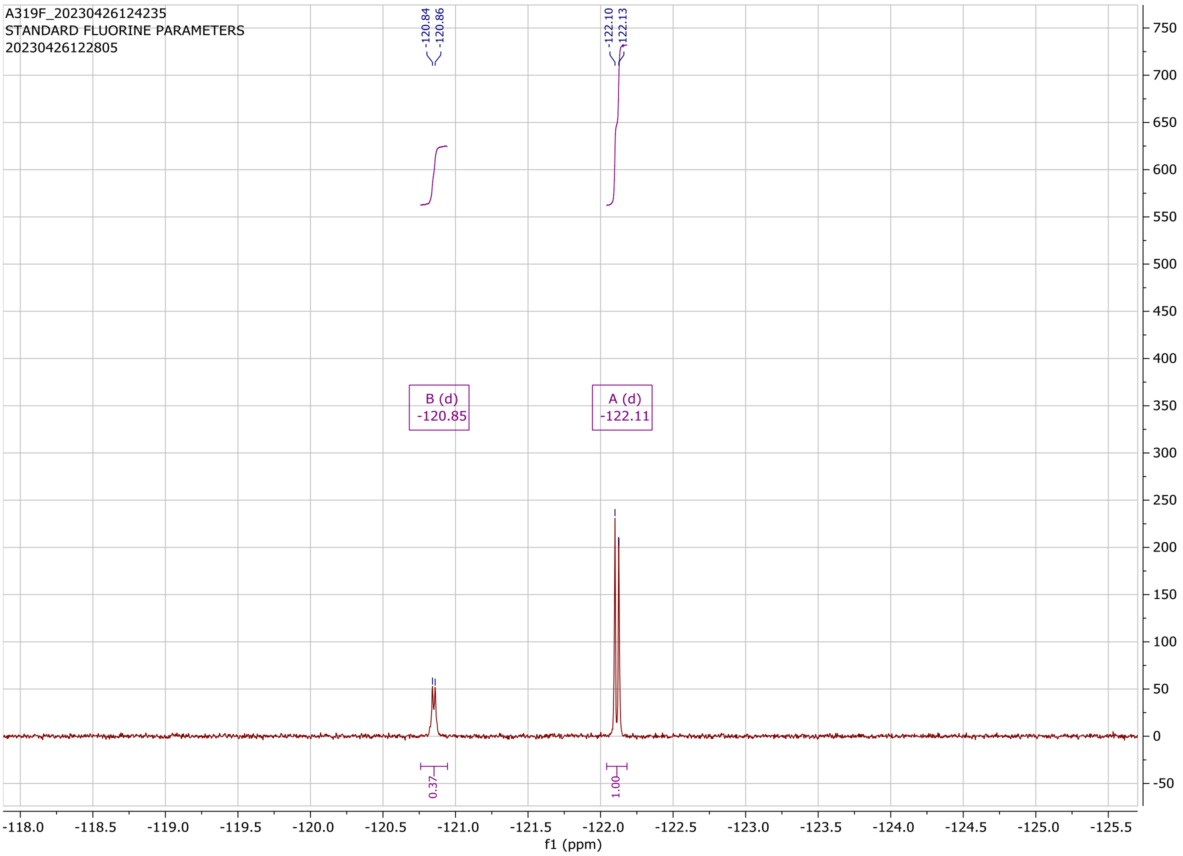

[E1] *3-Amino-1-methyl-1H-indazole*

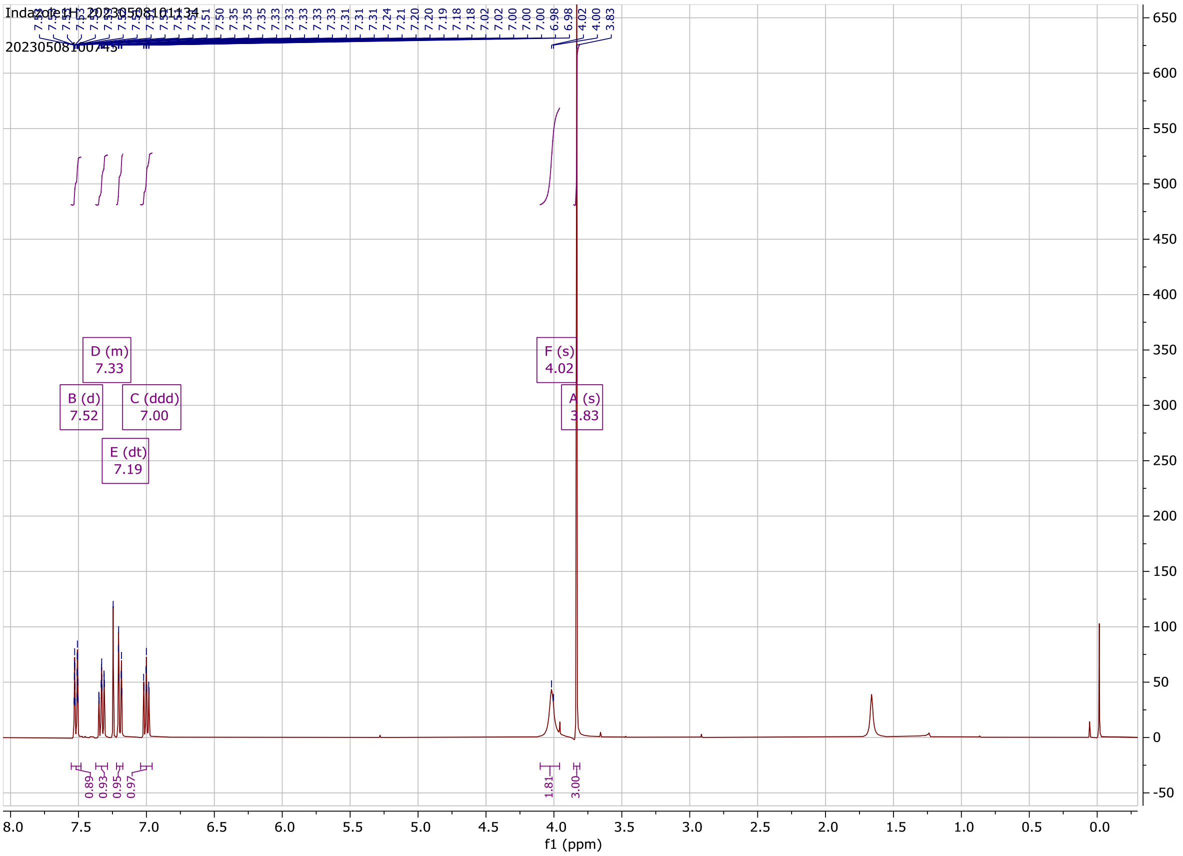

[E3] *(E)-1-methyl-3-(((triisopropylsilyl) ethynyl)diazenyl)-1H-indazole*

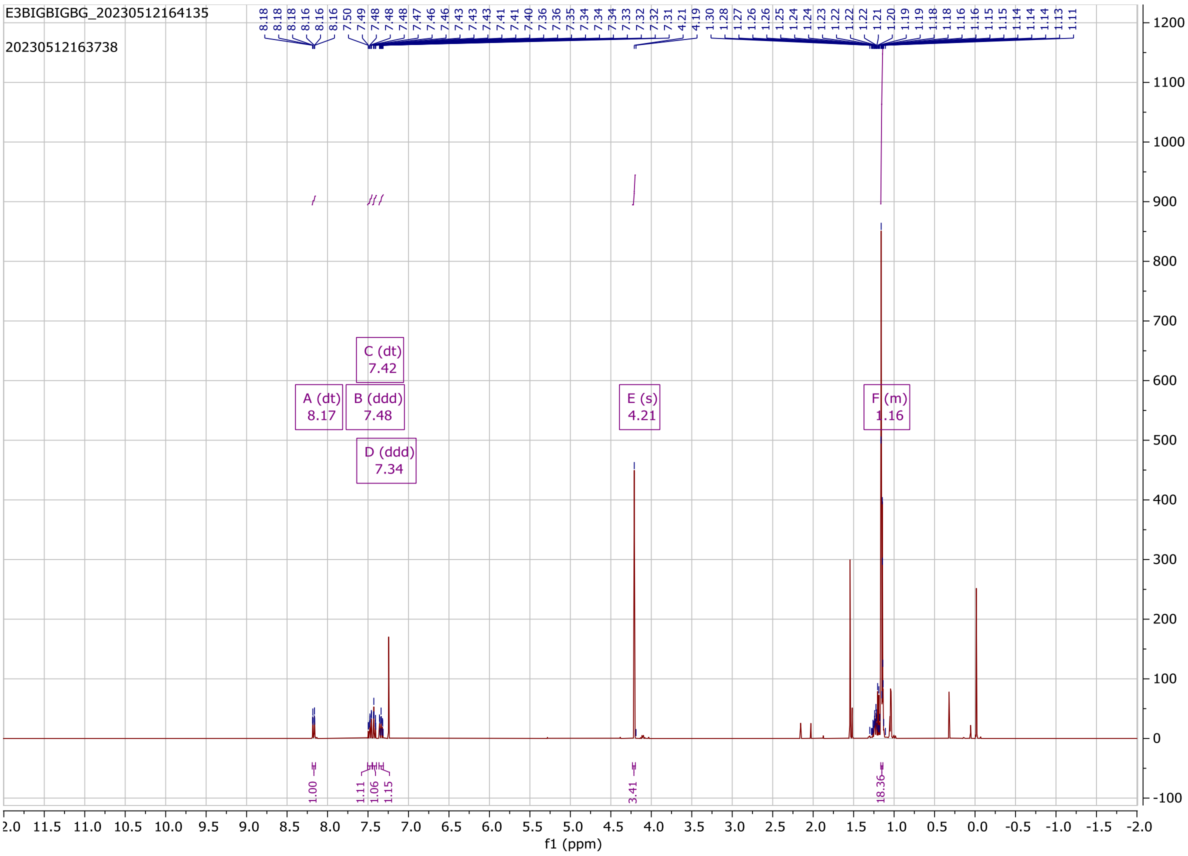

[$\Gamma_{1\varepsilon\alpha}$] *Methyl 5-acetamido-4,7,8-tri-O-acetyl-9-((4-(E)-(1-methyl-1H-indazol-3-yl) diazenyl)-1H-1,2,3-triazol-1-yl)-2,3,5,9-tetradeoxy-3-fluoro-D-erythro-α-L-gluco-non-2-ulopyranosylonate fluoride*

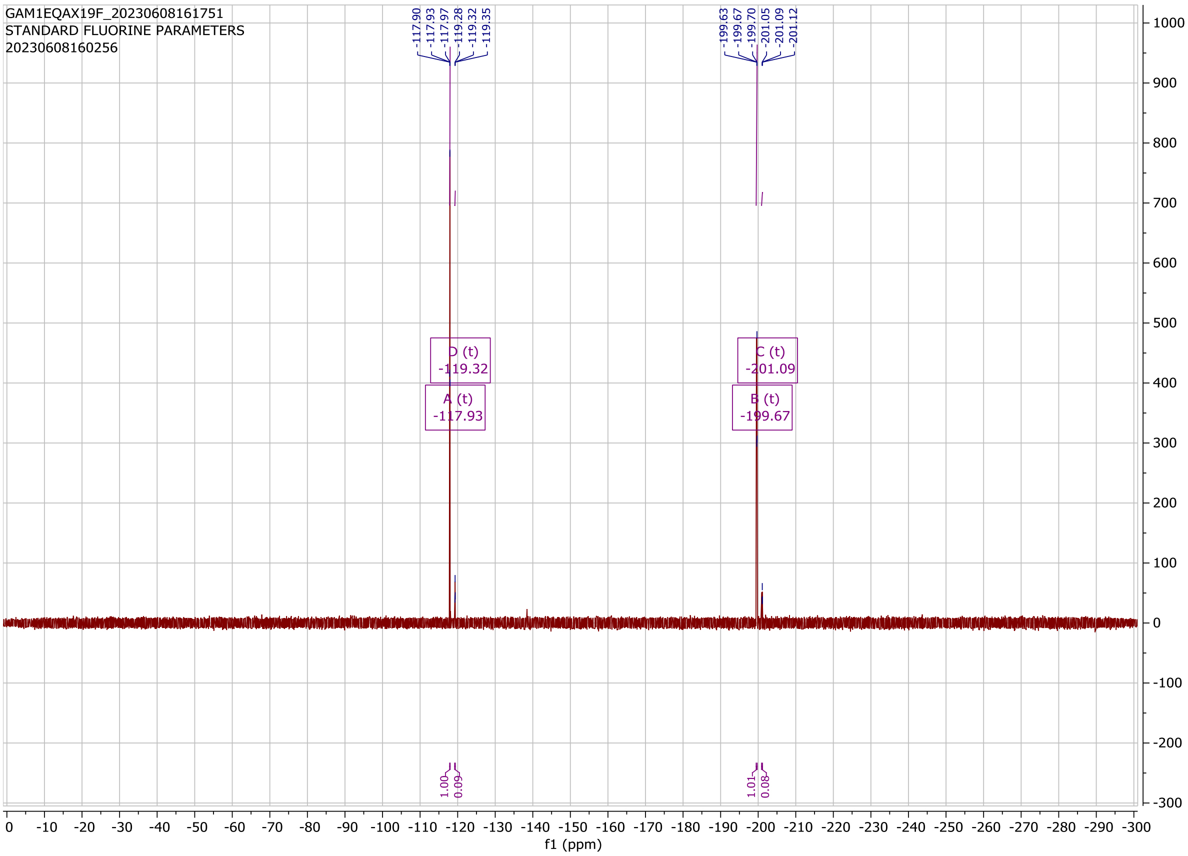

5.2 Cartesian Coordinates for the Optimized Geometry of $\Gamma_{\alpha\varepsilon}$

E-isomer

Units in Angstrom (Å)

N	17.6249900000	-13.5820900000	-1.7316700000
N	16.8530300000	-14.4382100000	-2.2083700000
C	17.3026900000	-10.0467500000	-1.5528800000
C	17.8118400000	-8.7605600000	-1.3674400000
C	18.0947600000	-11.1569000000	-1.4507500000
C	19.1831700000	-8.6389300000	-1.0725300000
C	19.4541700000	-11.0732100000	-1.1567500000
C	19.9999300000	-9.7888700000	-0.9671600000
N	16.0440600000	-10.4304500000	-1.8495600000
N	16.0079600000	-11.7553400000	-1.9514100000
C	17.2567800000	-12.2189200000	-1.7068000000
C	14.8850100000	-9.5677100000	-2.0392100000
C	17.1891700000	-15.8104800000	-2.1958200000
C	18.2104600000	-16.4067300000	-1.4966000000
N	16.5288300000	-16.7551800000	-2.8910700000
N	18.1412000000	-17.7160900000	-1.7880900000
N	17.1355000000	-17.9056900000	-2.6310200000
C	18.4643000000	-24.3139800000	-1.5499600000
C	17.2326400000	-24.9925700000	-2.2380700000
O	18.1681500000	-23.0164500000	-1.0259600000
C	15.9662700000	-24.4349700000	-1.5863900000
C	17.3127900000	-22.2708200000	-1.8681000000
C	15.8799300000	-22.9143300000	-1.8936000000
F	19.5172100000	-24.2315400000	-2.4469400000
F	17.2019500000	-24.6937000000	-3.5927000000
O	14.8278100000	-25.0991900000	-2.0674900000
N	14.9235400000	-22.2968800000	-0.9826900000
C	13.7315500000	-21.7808900000	-1.4078800000
C	18.9396200000	-25.1673200000	-0.3969800000
O	18.9679600000	-24.7212200000	0.7415300000

O	19.3785400000	-26.4223500000	-0.6345900000
C	17.3836300000	-20.7730500000	-1.4689800000
C	18.8017100000	-20.1768100000	-1.7533300000
C	19.0376000000	-18.7342900000	-1.2427900000
O	17.0738500000	-20.6449000000	-0.1038600000
O	19.8113300000	-20.9935900000	-1.2107800000
O	13.4142400000	-21.8258300000	-2.5883100000
C	12.7655600000	-21.1667400000	-0.4400300000
H	17.2974500000	-26.0999400000	-2.1589900000
H	16.0723300000	-24.6177700000	-0.4893300000
H	17.7126800000	-22.3309700000	-2.9093300000
H	15.5338900000	-22.7885300000	-2.9443800000
H	16.6283200000	-20.2388700000	-2.0861000000
H	18.9469600000	-20.1774800000	-2.8557500000
H	17.1811400000	-7.8853200000	-1.4521500000
H	19.6155100000	-7.6573900000	-0.9276000000
H	20.0707400000	-11.9596300000	-1.0821400000
H	21.0529500000	-9.6803900000	-0.7419300000
H	15.0710000000	-8.8700800000	-2.8820500000
H	13.9860600000	-10.1787900000	-2.2679100000
H	14.6962100000	-8.9862700000	-1.1123000000
H	18.9307000000	-15.9416400000	-0.8344300000
H	14.0930100000	-24.9035000000	-1.4287600000
H	15.1439400000	-22.2847700000	0.0243300000
H	19.7219200000	-26.9813500000	0.0765800000
H	20.0802800000	-18.4511300000	-1.5076300000
H	18.9551200000	-18.7202400000	-0.1340700000
H	16.6202500000	-19.7693100000	0.0119300000
H	19.6988700000	-21.0021100000	-0.2238700000
H	12.5510200000	-20.1218900000	-0.7490600000
H	11.8168500000	-21.7448600000	-0.4471800000
H	13.1720100000	-21.1585500000	0.5918300000

Z-isomer

Units in Angstrom (Å)

N	24.4118100000	-30.2290400000	-3.7528100000
N	24.9922000000	-31.2229800000	-4.2559600000
C	22.4069600000	-30.0425300000	-0.8039100000
C	22.1106100000	-29.5558200000	0.4769900000
C	23.5342500000	-29.6336000000	-1.5147000000
C	22.9931700000	-28.6216400000	1.0309700000
C	24.4103900000	-28.6941200000	-0.9394900000
C	24.1244900000	-28.1950700000	0.3360500000
N	21.7665900000	-30.9364000000	-1.6302500000
N	22.3798400000	-31.1311900000	-2.8129900000
C	23.4651700000	-30.3596900000	-2.7249000000
C	20.5525300000	-31.6601300000	-1.3375800000
C	24.8431400000	-32.5105600000	-3.7216600000
C	25.2709900000	-32.9182900000	-2.4774400000
N	24.3404800000	-33.5873800000	-4.4037900000
N	24.9184400000	-34.2325200000	-2.4319700000
N	24.3898800000	-34.6424100000	-3.6021600000
C	21.8035000000	-39.8565000000	-1.4719600000
C	20.5834000000	-39.7898100000	-2.3889500000
O	22.2183400000	-38.5868400000	-0.9508100000
C	19.6427600000	-38.6947600000	-1.8929600000
C	21.8967300000	-37.4867100000	-1.8179900000
C	20.3436800000	-37.3073700000	-1.9585700000
F	22.8728900000	-40.3268200000	-2.1782500000
F	20.9975300000	-39.4379200000	-3.6505100000
O	18.4555900000	-38.7232400000	-2.6940200000
N	19.8066300000	-36.3422600000	-0.9738700000
C	18.4673000000	-36.0553600000	-0.8401600000
C	21.4637000000	-40.8302900000	-0.3271400000
O	21.6477100000	-42.0382700000	-0.3178600000
O	20.8667100000	-40.2452700000	0.7373300000
C	22.6610000000	-36.2374900000	-1.2981000000

C	24.1998000000	-36.4278200000	-1.4327500000
C	25.0065900000	-35.1282000000	-1.3009500000
O	22.1562700000	-35.0536900000	-1.9130400000
O	24.6625400000	-37.3291500000	-0.4121400000
O	17.5707500000	-36.6987400000	-1.3737800000
C	18.1847500000	-34.8498600000	0.0166400000
H	20.0751800000	-40.7539300000	-2.4933000000
H	19.3274500000	-38.9148700000	-0.8670100000
H	22.2947500000	-37.7128000000	-2.8167500000
H	20.1382000000	-36.8419300000	-2.9317900000
H	22.4512500000	-36.1421700000	-0.2242100000
H	24.4354700000	-36.9030200000	-2.3924200000
H	21.2293800000	-29.8764100000	1.0230200000
H	22.7902700000	-28.2161900000	2.0204800000
H	25.2918500000	-28.3575000000	-1.4782400000
H	24.7916900000	-27.4637800000	0.7873000000
H	20.1622300000	-32.1064800000	-2.2559400000
H	20.7893600000	-32.4423400000	-0.6120000000
H	19.8168500000	-30.9640000000	-0.9274800000
H	25.7363000000	-32.3973300000	-1.6553500000
H	17.8724800000	-38.0075100000	-2.3499600000
H	20.3986000000	-35.5232000000	-0.8524200000
H	20.7374900000	-40.9788600000	1.3775700000
H	26.0712700000	-35.3605500000	-1.1758000000
H	24.6937600000	-34.5734100000	-0.4082200000
H	22.5353400000	-34.9751100000	-2.8185600000
H	24.1135900000	-38.1375000000	-0.4692200000
H	17.9879600000	-33.9902100000	-0.6293400000
H	17.3103300000	-35.0499800000	0.6418600000
H	19.0287600000	-34.6202700000	0.6733500000

5.3 TD-DFT/TDA Excited States (Singlets) Calculated for $\Gamma_{\alpha\varepsilon}$

[Low-lying excited state singlets of the trans-conformer]

```
STATE  1:  E=   0.068719 au      1.870 eV    15082.0 cm**-1
           139a -> 140a  :    0.976377 (c=  0.98811783)
           139a -> 142a  :    0.011836 (c= -0.10879195)

STATE  2:  E=   0.086111 au      2.343 eV    18899.2 cm**-1
           138a -> 140a  :    0.999996 (c=  0.99999794)

STATE  3:  E=   0.094397 au      2.569 eV    20717.7 cm**-1
           136a -> 140a  :    0.940787 (c= -0.96994167)
           137a -> 140a  :    0.058602 (c=  0.24207914)

STATE  4:  E=   0.099011 au      2.694 eV    21730.4 cm**-1
           139a -> 141a  :    0.999996 (c=  0.99999810)

STATE  5:  E=   0.103383 au      2.813 eV    22689.9 cm**-1
           137a -> 140a  :    0.010530 (c= -0.10261714)
           139a -> 140a  :    0.012789 (c= -0.11308968)
           139a -> 142a  :    0.970157 (c= -0.98496543)

STATE  6:  E=   0.115223 au      3.135 eV    25288.5 cm**-1
           135a -> 140a  :    0.987846 (c=  0.99390464)

STATE  7:  E=   0.117371 au      3.194 eV    25759.9 cm**-1
           137a -> 140a  :    0.013259 (c=  0.11514759)
           139a -> 143a  :    0.977610 (c=  0.98874158)

STATE  8:  E=   0.119623 au      3.255 eV    26254.3 cm**-1
           124a -> 140a  :    0.023065 (c=  0.15187266)
           127a -> 140a  :    0.028573 (c=  0.16903629)
           131a -> 140a  :    0.069416 (c= -0.26346838)
           132a -> 140a  :    0.019886 (c= -0.14101645)
```

```
   134a -> 140a  :     0.060244 (c=  0.24544618)
   135a -> 140a  :     0.010005 (c=  0.10002498)
   136a -> 140a  :     0.043476 (c= -0.20850985)
   137a -> 140a  :     0.663799 (c= -0.81473846)
   137a -> 142a  :     0.017175 (c= -0.13105427)
   139a -> 142a  :     0.010627 (c=  0.10308616)
   139a -> 143a  :     0.014518 (c=  0.12049196)

STATE  9:  E=   0.122179 au      3.325 eV    26815.1 cm**-1
   134a -> 140a  :     0.931552 (c=  0.96516921)
   137a -> 140a  :     0.041174 (c=  0.20291312)

STATE 10:  E=   0.124199 au      3.380 eV    27258.5 cm**-1
   133a -> 140a  :     0.999237 (c=  0.99961830)
```

[Low-lying excited state singlets of the cis-conformer]

```
STATE  1:  E=   0.087502 au      2.381 eV    19204.4 cm**-1
   138a -> 140a  :     0.013413 (c=  0.11581299)
   139a -> 140a  :     0.951804 (c=  0.97560430)

STATE  2:  E=   0.088584 au      2.410 eV    19442.0 cm**-1
   138a -> 140a  :     0.986536 (c= -0.99324516)
   139a -> 140a  :     0.012814 (c=  0.11320065)

STATE  3:  E=   0.105380 au      2.868 eV    23128.3 cm**-1
   137a -> 140a  :     0.446667 (c= -0.66833144)
   139a -> 141a  :     0.518162 (c= -0.71983478)

STATE  4:  E=   0.108162 au      2.943 eV    23738.8 cm**-1
   136a -> 140a  :     0.983041 (c= -0.99148424)
   139a -> 141a  :     0.014701 (c= -0.12124619)

STATE  5:  E=   0.108777 au      2.960 eV    23873.7 cm**-1
   135a -> 140a  :     0.962053 (c=  0.98084315)
```

```
     139a -> 141a  :     0.031284 (c= -0.17687306)


STATE  6:  E=   0.110839 au      3.016 eV    24326.4 cm**-1

     139a -> 142a  :     0.999594 (c= -0.99979678)


STATE  7:  E=   0.116494 au      3.170 eV    25567.4 cm**-1

     126a -> 140a  :     0.013248 (c=  0.11509810)

     132a -> 140a  :     0.043494 (c= -0.20855164)

     133a -> 140a  :     0.039134 (c= -0.19782260)

     134a -> 140a  :     0.013661 (c=  0.11688014)

     135a -> 140a  :     0.023681 (c=  0.15388476)

     137a -> 140a  :     0.436239 (c= -0.66048392)

     137a -> 141a  :     0.036608 (c= -0.19133136)

     139a -> 141a  :     0.343088 (c=  0.58573698)


STATE  8:  E=   0.122061 au      3.321 eV    26789.4 cm**-1

     133a -> 140a  :     0.355852 (c= -0.59653358)

     134a -> 140a  :     0.640473 (c= -0.80029551)


STATE  9:  E=   0.125388 au      3.412 eV    27519.6 cm**-1

     138a -> 141a  :     0.999593 (c= -0.99979641)


STATE 10:  E=   0.125781 au      3.423 eV    27605.8 cm**-1

     131a -> 143a  :     0.010269 (c= -0.10133680)

     132a -> 140a  :     0.027960 (c=  0.16721158)

     133a -> 140a  :     0.045318 (c=  0.21288140)

     134a -> 140a  :     0.027165 (c= -0.16481920)

     139a -> 143a  :     0.826459 (c=  0.90909767)
```

Literature & Citations

1.) Colli, W. (1993). Trans-sialidase: a unique enzyme activity discovered in the protozoan Trypanosoma cruzi. The FASEB Journal, 7(13), 1257–1264. doi:10.1096/fasebj.7.13.8405811

2.) Amaya, M. F., Watts, A. G., Damager, I., Wehenkel, A., Nguyen, T., Buschiazzo, A., … Alzari, P. M. (2004). Structural Insights into the Catalytic Mechanism of Trypanosoma cruzi trans-Sialidase. Structure, 12(5), 775–784. doi:10.1016/j.str.2004.02.036

3.) Amaya, M. F., Watts, A. G., Damager, I., Wehenkel, A., Nguyen, T., Buschiazzo, A., … Alzari, P. M. Trypanosoma cruzi trans-sialidase in complex with 2,3-difluorosialic acid (covalent intermediate). 27 July 2005 *https://doi.org/10.2210/pdb2ah2/pdb*

4.) UCSF ChimeraX: Structure visualization for researchers, educators, and developers. Pettersen EF, Goddard TD, Huang CC, Meng EC, Couch GS, Croll TI, Morris JH, Ferrin TE. Protein Sci. 2021 Jan;30(1):70-82.

5.) Burgos, J. M., Risso, M. G., Brenière, S. F., Barnabé, C., Campetella, O., & Leguizamón, M. S. (2013). Differential Distribution of Genes Encoding the Virulence Factor Trans-Sialidase along Trypanosoma cruzi Discrete Typing Units. PLoS ONE, 8(3), e58967. doi:10.1371/journal.pone.0058967

6.) Buchini, S., Buschiazzo, A., & Withers, S. G. (2008). A New Generation of Specific Trypanosoma cruzi trans-Sialidase Inhibitors. Angewandte Chemie International Edition, 47(14), 2700–2703. doi:10.1002/anie.200705435

7.) Li, W., Santra, A., Yu, H., Slack, T. J., Muthana, M. M., Shi, D., … Chen, X. (2019). 9-Azido-9-deoxy-2,3-difluoro-sialic Acid as a Subnanomolar Inhibitor against Bacterial Sialidases. The Journal of Organic Chemistry, 84(11), 6697–6708. doi:10.1021/acs.joc.9b00385

8.) Cheng, B., Dong, L., Zhu, Y., Huang, R., Sun, Y., You, Q., … Chen, X. (2019). 9-Azido Analogues of Three Sialic Acid Forms for Metabolic Remodeling of Cell-Surface Sialoglycans. ACS Chemical Biology. doi:10.1021/acschembio.9b00556

9.) Neese, F., Wennmohs, F., Becker, U., & Riplinger, C. (2020). The ORCA quantum chemistry program package. The Journal of Chemical Physics, 152(22), 224108. doi:10.1063/5.0004608

10.) Marcus D Hanwell, Donald E Curtis, David C Lonie, Tim Vandermeersch, Eva Zurek and Geoffrey R Hutchison; “Avogadro: An advanced semantic chemical editor, visualization, and analysis platform” Journal of Cheminformatics 2012, 4:17.

11.) Mart, R. J., & Allemann, R. K. (2016). Azobenzene photocontrol of peptides and proteins. Chemical Communications, 52(83), 12262–12277. doi:10.1039/c6cc04004g

12.) Moreno, M.; Lluch, J.M.; Gelabert, R. On the Computational Design of Azobenzene-Based Multi-State Photoswitches. Int. J. Mol. Sci. 2022, 23, 8690. https://doi.org/10.3390/ijms23158690

13.) Mitscherlich, E. (1834). "Ueber das Stickstoffbenzid". Ann. Pharm. 12 (2–3): 311–314. Bibcode:1834AnP...108..225M. doi:10.1002/jlac.18340120282

14.) Yager, K. G., & Barrett, C. J. (2006). Novel photo-switching using azobenzene functional materials. Journal of Photochemistry and Photobiology A: Chemistry, 182(3), 250–261. doi:10.1016/j.jphotochem.2006.04.

15.) Schultz, T., Quenneville, J., Levine, B., Toniolo, A., Martínez, T. J., Lochbrunner, S., … Stolow, A. (2003). Mechanism and Dynamics of Azobenzene Photoisomerization. Journal of the American Chemical Society, 125(27), 8098–8099. doi:10.1021/ja021363x

16.) Muždalo, A., Saalfrank, P., Vreede, J., & Santer, M. (2018). Cis-to-Trans Isomerization of Azobenzene Derivatives Studied with Transition Path Sampling and Quantum Mechanical/Molecular Mechanical Molecular Dynamics. Journal of

Chemical Theory and Computation, 14(4), 2042–2051. doi:10.1021/acs.jctc.7b01120

17.) Titov, E. On the Low-Lying Electronically Excited States of Azobenzene Dimers: Transition Density Matrix Analysis. Molecules 2021, 26, 4245. https://doi.org/ 10.3390/molecules26144245

18.) Wörner, Hans Jakob; Merkt, Frédéric. Fundamentals of Electronic Spectroscopy; ETH Zurich, 2011. https://doi.org/10.3929/ETHZ-A-010782748.

19.) Ciminelli, C., Granucci, G., & Persico, M. (2004). The Photoisomerization Mechanism of Azobenzene: A Semiclassical Simulation of Nonadiabatic Dynamics. Chemistry - A European Journal, 10(9), 2327–2341. doi:10.1002/chem.200305415

20.) Sun, S.; Liang, S.; Xu, W.-C.; Xu, G.; Wu, S. Photoresponsive Polymers with Multi-Azobenzene Groups. Polymer Chemistry, 2019, 10, 4389–4401. https://doi.org/10.1039/c9py00793h.

21.) H. Rau, in: J. Rebek (Ed.), Photochemistry and Photophysics, vol. 2, CRC Press, Boca Raton, FL, 1990, p. 119

22.) H. M. D. Bandara and S. C. Burdette, Chem. Soc. Rev., 2012, 41, 1809-1825.

23.) Brzozowski, L.; Sargent, E. H. Journal of Materials Science: Materials in Electronics, 2001, 12, 483–489. https://doi.org/10.1023/a:1012446007088.

24.) (Hetero)arylazo-1,2,3-triazoles: “Clicked” Photoswitches for Versatile Functionalization and Electronic Decoupling, Dong Fang, Zhao-Yang Zhang, Zhichun Shangguan, Yixin He, Chunyang Yu, and Tao Li. Journal of the American Chemical Society 2021 143 (36), 14502-14510 doi: 10.1021/ jacs.1c08704

25.) Jana Volarić, Jeffrey Buter, Albert M. Schulte, Keimpe-Oeds van den Berg, Eduardo Santamaría-Aranda, Wiktor Szymanski, and Ben L. Feringa, The Journal of Organic Chemistry 2022 87 (21), 14319-14333 doi: 10.1021/ acs.joc.2c01777

26.) Kobauri, P.; Dekker, F. J.; Szymanski, W.; Feringa, B. L. Rational Design in Photopharmacology with Molecular Photoswitches. Angewandte Chemie International Edition, 2023, 62. https://doi.org/10.1002/anie.202300681.

27.) Szymański, W.; Beierle, J. M.; Kistemaker, H. A. V.; Velema, W. A.; Feringa, B. L. Reversible Photocontrol of Biological Systems by the Incorporation of Molecular Photoswitches. Chemical Reviews, 2013, 113, 6114–6178. https://doi.org/10.1021/cr300179f.

28.) Mart, R. J.; Allemann, R. K. Azobenzene Photocontrol of Peptides and Proteins. Chemical Communications, 2016, 52, 12262–12277. https://doi.org/10.1039/c6cc04004g

29.) Morris, G. M., Huey, R., Lindstrom, W., Sanner, M. F., Belew, R. K., Goodsell, D. S. and Olson, A. J. (2009) Autodock4 and AutoDockTools4: automated docking with selective receptor flexiblity. J. Computational Chemistry 2009, 16: 2785-91.

30.) Tian Lu, Feiwu Chen, Multiwfn: A Multifunctional Wavefunction Analyzer, J. Comput. Chem. 33, 580-592 (2012) DOI: 10.1002/jcc.22885

31.) A. J. Schaefer, V. M. Ingman, and S. E. Wheeler, "SEQCROW: A ChimeraX Bundle to Facilitate Quantum Chemical Applications to Complex Molecular Systems" J. Comp. Chem. 42, 1750 (2021).

32.) V. M. Ingman, A. J. Schaefer, L. R. Andreola, and S. E. Wheeler, "QChASM: Quantum Chemistry Automation and Structure Manipulation" WIREs Comp. Mol. Sci. 11, e1510 (2021)

33.) Baptista, L., Bauerfeldt, G. F., Arbilla, G., & Silva, E. C. (2006). Theoretical study of fluorination reaction by diethylaminosulfur trifluoride (DAST). Journal of Molecular Structure: THEOCHEM, 761(1-3), 73–81. doi:10.1016/j.theochem.2006.01.002

34.) Miljković, M., Yeagley, D., Deslongchamps, P., & Dory, Y. L. (1997). Experimental and Theoretical Evidence of Through-Space Electrostatic Stabilization of the Incipient Oxocarbenium Ion by an Axially Oriented Electronegative

Substituent During Glycopyranoside Acetolysis. The Journal of Organic Chemistry, 62(22), 7597–7604. doi:10.1021/jo970677d

35.) Liu, H.-J., Hung, S.-F., Chen, C.-L., & Lin, M.-H. (2013). A method for the regioselective synthesis of 1-alkyl-1H-indazoles. Tetrahedron, 69(19), 3907–3912. doi:10.1016/j.tet.2013.03.042

36.) Huisgen, Rolf; Szeimies, Gunter; Mobius, Leander (1967). "K1.3-Dipolare Cycloadditionen, XXXII. Kinetik der Additionen organischer Azide an CC-Mehrfachbindungen". Chemische Berichte. 100 (8): 2494–2507. doi:10.1002/cber.19671000806

37.) Yu, H., Chokhawala, H., Karpel, R., Yu, H., Wu, B., Zhang, J., … Chen, X. (2005). A Multifunctional Pasteurella multocida Sialyltransferase: A Powerful Tool for the Synthesis of Sialoside Libraries. Journal of the American Chemical Society, 127(50), 17618–17619. doi:10.1021/ja0561690

38.) Han, S., Collins, B. E., Bengtson, P., & Paulson, J. C. (2005). Homomultimeric complexes of CD22 in B cells revealed by protein-glycan cross-linking. Nature Chemical Biology, 1(2), 93–97. doi:10.1038/nchembio71

39.) J. Am. Chem. Soc. 2022, 144, 14, 6143–6147, Publication Date: March 31, 2022

40.) Nowrouzi, N., & Zareh Jonaghani, M. (2011). Nitration of aromatic compounds under neutral conditions using the Ph2PCl/I2/AgNO3 reagent system. Tetrahedron Letters, 52(39), 5081–5082. doi:10.1016/j.tetlet.2011.07.097

41.) Bracher, F., & Popp, T. (2015). N-Methylation of Aromatic Amines and N-Heterocycles under Acidic Conditions with the TTT (1,3,5-Trioxane–Triethylsilane–Trifluoroacetic Acid) System. Synthesis, 47(21), 3333–3338. doi:10.1055/s-0034-1381049

42.) Heller, S. T., Schultz, E. E., & Sarpong, R. (2012). Chemoselective N-Acylation of Indoles and Oxazolidinones with Carbonylazoles. Angewandte Chemie International Edition, 51(33), 8304–8308. doi:10.1002/anie.201203976

43.) Chenot, E., Bernardi, D., Comel, A., & Kirsch, G. (2007). Preparation of Monoalkyl Terephthalates: An Overview. Synthetic Communications, 37(3), 483–490. doi:10.1080/00397910601039226

44.) Harada, J., Ogawa, K., & Tomoda, S. (1997). Molecular Motion and Conformational Interconversion of Azobenzenes in Crystals as Studied by X-ray Diffraction. Acta Crystallographica Section B Structural Science, 53(4), 662–672. doi:10.1107/s0108768197002772